AD-A126 717 A NUMERICAL MODEL FOR GAS-DROPLET FLOW APPLICATION TO LIQUID SPRAY AND CO..(U) VON KARMAN INST FOR FLUID DYNAMICS RHODE-SAINT-GENESE (BELGIU..

UNCLASSIFIED P WEINACHT ET AL. FEB 83 EOARD-TR-83-5 F/G 20/4 NL

1/2

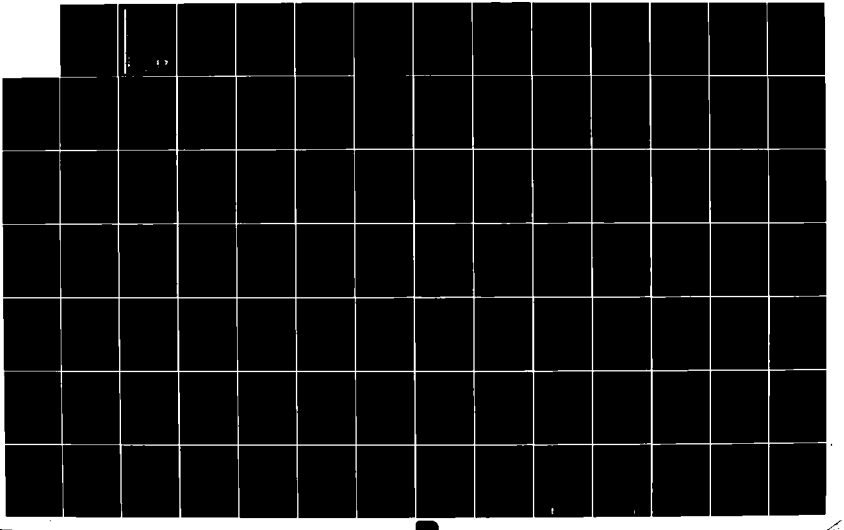

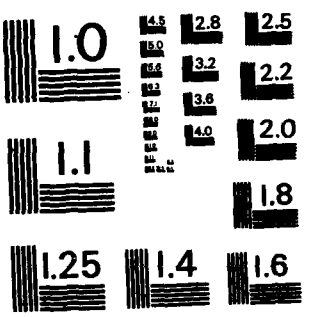

EOARD-TR-83-5

GRANT AFOSR 82-0202

A NUMERICAL MODEL FOR GAS-DROPLET FLOW APPLICATION TO LIQUID SPRAY AND COOLING TOWERS

PAUL WEINACHT AND J-M. BUCHLIN
VON KARMAN INSTITUTE FOR FLUID DYNAMICS
CHAUSSÉE DE WATERLOO, 72
B - 1640 RHODE SAINT GENÈSE, BELGIUM

FEBRUARY 1983

FINAL SCIENTIFIC REPORT, 15 MAY 1982 - 14 FEBRUARY 1983

APPROVED FOR PUBLIC RELEASE; DISTRIBUTION UNLIMITED

PREPARED FOR

AIR FORCE OFFICE OF SCIENTIFIC RESEARCH
BOLLING AF BASE, DC 20332

AND

EUROPEAN OFFICE OF AEROSPACE RESEARCH AND DEVELOPMENT
LONDON, UK

EOARD-TR-83-5-

This report has been reviewed by the EOARD Information Office and is releasable to the National Technical Information Service (NTIS). At NTIS it will be releasable to the general public, including foreign nations.

This technical report has been reviewed and is approved for publication.

CARY A. FISHER
Colonel, USAF
Chief Scientist

JERRY R. BETTIS
Lt Colonel, USAF
Deputy Commander

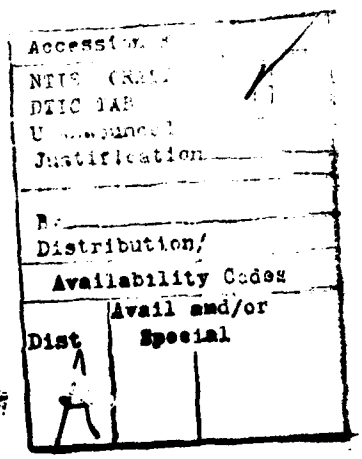

SECURITY CLASSIFICATION OF THIS PAGE (When Data Entered)

REPORT DOCUMENTATION PAGE		READ INSTRUCTIONS BEFORE COMPLETING FORM
1. REPORT NUMBER EOARD-TR-83-35	2. GOVT ACCESSION NO. AD-A126 419	3. RECIPIENT'S CATALOG NUMBER
4. TITLE (and Subtitle) A NUMERICAL MODEL FOR GAS-DROPLET FLOW APPLICATION TO LIQUID SPRAY AND COOLING TOWERS		5. TYPE OF REPORT & PERIOD COVERED Final Scient Rep., 15 May 82 - 14 Feb 83 6. PERFORMING ORG. REPORT NUMBER
7. AUTHOR(s) Paul WEINACHT & Jean-Marie BUCHLIN		8. CONTRACT OR GRANT NUMBER(s) AFOSR 82-0202
9. PERFORMING ORGANIZATION NAME AND ADDRESS von Karman Institute for Fluid Dynamics, Chaussée de Waterloo, 72, B-1649 Rhode-Saint-Genèse, Belgium.		10. PROGRAM ELEMENT, PROJECT, TASK AREA & WORK UNIT NUMBERS P.E. 61102F Proj/Task 2301/D1
11. CONTROLLING OFFICE NAME AND ADDRESS European Office of Aerospace R&D/CA Box 14 FPO New York 09510		12. REPORT DATE February 1983 13. NUMBER OF PAGES 113
14. MONITORING AGENCY NAME & ADDRESS(if different from Controlling Office) European Office of Aerospace Research and Development/CA Box 14 FPO New York 09510		15. SECURITY CLASS. (of this report) UNCLASSIFIED 15a. DECLASSIFICATION/DOWNGRADING SCHEDULE

16. DISTRIBUTION STATEMENT (of this Report)

Approved for public release; distribution unlimited

17. DISTRIBUTION STATEMENT (of the abstract entered in Block 20, if different from Report)

Approved for public release; distribution unlimited

18. SUPPLEMENTARY NOTES

19. KEY WORDS (Continue on reverse side if necessary and identify by block number)

GAS-LIQUID FLOW;NUMERICAL SOLVERS (MAC METHOD); EULER-LAGRANGIAN APPROACHES; 2D FLOW FIELD IN LIQUID SPRAYS AND WETTED NATURAL DRAFT COOLING TOWER

20. ABSTRACT (Continue on reverse side if necessary and identify by block number)

A two dimensional model (axisymmetric or planar) has been implemented to study the gas-droplet flow due to water sprays or in cooling towers.

The model consists of coupled sets of equations governing the gas and liquid phases. Modelling the gas phase as a continuum allows use of the Navier-Stokes equations with momentum source terms included. The liquid phase, represented by a finite number of droplet trajectories is governed by the equations of motion of falling spherical droplets subject to gravitational and drag forces. The particle-gas momentum exchange and the influence of the gas flow on the droplet trajectories results in a coupling of both of these sets of equations.

Numerical solution of these equations is made in an iterative fashion by solving first the liquid phase equations and then the gas

DD FORM 1 JAN 73 1473 EDITION OF 1 NOV 65 IS OBSOLETE

SECURITY CLASSIFICATION OF THIS PAGE (When Data Entered)

20. ABSTRACT (contd.)

phase equations until a steady state solution is reached. Solution of the liquid phase equations by a fourth order Runge-Kutta method, allows subsequent determination of the droplet-gas momentum exchange field. Solution of the gas phase equations by the simplified MAC (SMAC) method then completed a single cycle of the iterative procedure.

Calculations of the flow field due to an axisymmetric spray shows good agreement with experiment. The degrading effect of wind on a spray curtain is demonstrated, though calculations show that curtain performance may be improved by tilting the nozzle into the wind. The flow inside a cooling tower and the resulting pressure losses are seen to be reasonably predicted.

TABLE OF CONTENTS

Abstract i
List of symbols ii
List of figures v
List of Tables vii

1. INTRODUCTION 1

2. THE GAS-DROPLET MODEL 3
   2.1 Introduction 3
   2.2 The gas phase model 3
   2.3 The droplet phase model 7

3. THE NUMERICAL METHOD 10
   3.1 Numerical solution of the gas phase equations . . . 10
      3.1.1 Equations for the first step 11
      3.1.2 Equations for the second step 14
      3.1.3 Equations for the third step 15
      3.1.4 Equations for the fourth step 17
   3.2 Numerical solution at the droplet equations 19
   3.3 Calculation of the droplet to gas momentum source term 19
   3.4 The solution procedure 22

4. APPLICATIONS AND RESULTS 23
   4.1 Axisymmetric spray 23
      4.1.1 Modelling of an axisymmetric spray 23
      4.1.2 Results 26
         4.1.2.1 Comparsion and experiments 27
         4.1.2.2 Evaluation of ceiling effect 29
         4.1.2.3 Influence of pressure terms momentum equations. 29
      4.1.3 Conclusions 30
   4.2 Wind effects on a planar spray curtain 32
      4.2.1 Modelling of a planar representation of a spray curtain. 32
      4.2.2 Results 35
         4.2.2.1 Effect of wind speed 35
         4.2.2.2 Effect of nozzle spacing 35
         4.2.2.3 Effect of tilting nozzle 36
         4.2.2.4 Effect of decreasing cone angle . . . 37
         4.2.2.5 Effect of height of spray 37
         4.2.2.6 Sensitivity of the calculation to drop size and injection velocity . 38

4.2.3 Conclusions 38
4.3 Calculation of the flow inside a cooling tower . . 39
4.3.1 Modelling of the cooling tower 39
4.3.2 Results 42
4.3.2.1 Velocity field 42
4.3.2.2 Pressure field 43
4.3.3 Conclusions 46
5. CONCLUSIONS 47
REFERENCES 48
FIGURES 51

ABSTRACT

A two dimensional model (axisymmetric or planar) has been implemented to study the gas-droplet flow due to water sprays or in cooling towers.

The model consists of coupled sets of equations governing the gas and liquid phases. Modelling the gas phase as a continuum allows use of the Navier-Stokes equations with momentum source terms included. The liquid phase, represented by a finite number of droplet trajectories is governed by the equations of motion of falling spherical droplets subject to gravitational and drag forces. The particle-gas momentum exchange and the influence of the gas flow on the droplet trajectories results in a coupling of both of these sets of equations.

Numerical solution of these equations is made in an iterative fashion by solving first the liquid phase equations and then the gas phase equations until a steady state solution is reached. Solution of the liquid phase equations by a fourth order Runge-Kutta method, allows subsequent determination of the droplet-gas momentum exchange field. Solution of the gas phase equations by the simplified MAC (SMAC) method then completed a single cycle of the iterative procedure.

Calculations of the flow field due to an axisymmetric spray shows good agreement with experiment. The degrading effect of wind on a spray curtain is demonstrated, though calculations show that curtain performance may be improved by tilting the nozzle into the wind. The flow inside a cooling tower and the resulting pressure losses are seen to be reasonably predicted.

LIST OF SYMBOLS

C_D	drag coefficient at a sphere	
C_N	nozzle design parameter	($Kg^{1/3}/sec^{2/3}$)
d_0	inside diameter of nozzle	(mm)
D	droplet diameter	(mm), (m)
D_{ij}	divergence of cell i,j	(1/sec)
D_m	mean droplet diameter	(mm); (m)
D_t	diameter of spray envelope	(m)
f_{ij}	flag for velocity i,j	
f_{Qw}	fractional volume flow of liquid	(m^3/s); (m^2/s)
f_r	radial component of drag force acting on droplet	(N)
f_{TOT}	sum of flags at each cell	
f_z	axial component of drag force acting on droplet	(N)
F(D)	Rossin-Rammler distribution function	
F_r	radial momentum source term	(N/m^3)
F_z	axial momentum source term	(N/m^3)
g	gravitational acceleration	(m/s^2)
H	height of injection point	(m)
H_{inlet}	height of inlet	(m)
i	subscript in the radial direction	
j	subscript in the axial direction	
K_1	axial packing coefficient	
K_2	radial packing coefficient	
ℓ_m	subsegment length	(m)
ℓ_{TOT}	total segment length	(m)
$\bar{L}$	characteristic length	(m)

L_c	length of curtain	(m)
L_p	packing thickness	(m)
L_R	radial length of computational domain	(m)
L_z	axial length of computational domain	(m)
m	mass of droplet	(kg)
N	unit normal to boundary	(m)
N_{noz}	number of nozzles	
N_{traj}	number of trajectories	
NX	number of cells in radial direction	
NY	number of cells in axial direction	
P	pressure	(N/m^2)
ΔP_N	water delivery pressure	(N/m^2)
P_{t_1}	total pressure outside tower	(N/m^2)
P_{t_2}	total pressure above packing	(N/m^2)
q_w	liquid volume flow per unit length	(m^2/s)
Q_a	volume flow of air	(m^3/s)
Q_w	volume flow of water	(m^3/s), ($\ell t/min$)
r	radial coordinate	(m)
R	radial position of droplet trajectories	(m)
Re	Reynolds number	
Res	residual	(m^2/s^2)
R_ℓ	radial position of droplet injection point	(m)
R_{tower}	tower radius	(m)
t	time	(sec)
$\tilde{t}$	artificial time	(sec)
u_r	axial velocity of droplet	(m/s)
u_z	radial velocity of droplet	(m/s)

$\bar{U}$	characteristic velocity	(m/s)
U_0	injection velocity of droplet	(m/s)
V_N	gas velocity normal to boundary	(m/s)
V_r	radial gas velocity	(m/s)
V_t	gas velocity tangent to boundary	(m/s)
V_z	axial gas velocity	(m/s)
ΔV	source cell volume	(m^3)
V_{rel}	velocity at droplet relative to gas	(m/s)
z	axial coordinate	(m)
Z	axial position of droplet trajectory	(m)
α	switch for axisymmetric or planar case	
α_{TILT}	tilt angle of spray	(degrees)
β	relaxation coefficient	
ρ	gas density	(kg/m^3)
ρ_w	liquid density	(kg/m^3)
θ	initial angle of injection of droplet	(degrees)
θ_{MAX}	maximum injection angle at droplet	(degrees)
η	spray efficiency	($m^3/\ell t$)
ν	molecular viscosity of gas	(m^2/s)
ν_{EFF}	effective viscosity of gas	(m^2/s)
χ	inverse nondimensional spray diameter squared	($\ell t/m^3$)
Δ	indicates incremental quantity	

LIST OF FIGURES

2.1 Domain of interest

3.1 SMAC cell structure for the gas phase computation

3.2 Particle trajectory crossing momentum source cells

3.3 Computational procedure

4.1.1 Computational domain for axisymmetric sprays

4.1.2 Flow field due to a spray (Q_w = 6.6 ℓt/min H = 2. m)

4.1.3 Flow field due to a spray (Q_w = 13.3 ℓt/min H = 2. m)

4.1.4 Flow field due to a spray (Q_w = 21.1 ℓt/min H = 2. m)

4.1.5 Flow field due to a spray (Q_w = 6.6 ℓt/min H = 0 m)

4.1.6 Flow field due to a spray (Q_w = 13.3 ℓt/min H = 0. m)

4.1.7 Flow field due to a spray (Q_w = 21.1 ℓt/min H = 0. m)

4.1.8 Performances data for sprays

4.1.9 Spray efficiency versus inverse spray diameter squared SZ1 nozzle θ_{MAX} = 30. degrees

4.1.10 Spray efficiency versus inverse spray diameter squared SZ1 nozzle θ_{MAX} = 22.5 degrees

4.1.11 Spray efficiency versus inverse spray diameter squared SZ2 nozzle θ_{MAX} = 30. degrees

4.1.12 Predicted and measured velocities inside the spray Z = 50. cm

4.1.13 Predicted and measured velocities inside the spray Z = 40. cm

4.1.14 Predicted and measured velocities inside the spray Z = 30. cm

4.1.15 Determination of ceiling effects on nozzle performance

4.1.16 Comparison of results with and without pressure terms

4.2.1 Computational domain for planar spray curtain

4.2.2 Effect of wind on the performance of a spray curtain V_∞ = 2.0 m/s Q_w = 3. ℓt/s.m

4.2.3 Effect of wind on the performance of a spray curtain V_∞ = 2.5 m/s Q_w = 3. ℓt/s.m

4.2.4 Effect of wind on the performance of a spray curtain V_∞ = 3.0 m/s Q_w = 3. ℓt/s.m

4.2.5 Effect of wind on the performance of a spray curtain V_∞ = 4.5 m/s Q_w = 3. ℓt/s.m

4.2.6 Effect of wind on the performance of a spray curtain V_∞ = 1.5 m/s Q_w = 1.5 ℓt/s.m U_0 = 23.68 m/s

4.2.7 Effect of wind on the performance of a spray curtain V_∞ = 3.0 m/s Q_w = 1.5 ℓt/s.m U_0 = 23.68 m/s

4.2.8 Effect of wind on the performance of a spray curtain $V_{\emptyset}$ = 1.5 m/s Q_w = 1.5 ℓt/s.m U_0 = 11.85 m/s

4.2.9 Effect of wind on the performance of a spray curtain $V_{\emptyset}$ = 3.0 Q_w = 1.5 ℓt/s.m U_0 = 11.85 m/s

4.2.10 Effect of tilt angle on the performance of a spray curtain α_{TILT} = 0

4.2.11 Effect of tilt angle on the performance of a spray curtain α_{TILT} = - 7.5 degrees

4.2.12 Effect of tilt angle on the performance of a spray curtain α_{TILT} = -15 degrees

4.2.13 Effect of tilt angle on the performance of a spray curtain α_{TILT} = -30 degrees

4.2.14 Effect of tilt angle on the performance of a spray curtain α_{TILT} = +15 degrees

4.2.15 Effect of tilt angle on the performance of a spray curtain α_{TILT} = +30 degrees

4.2.16 Effect of wind on the performance of a spray curtain θ_{MAX} = 30 degrees

4.2.17 Effect of wind on the performance of a spray curtain H = 3.5 m

4.2.18 Effect of wind on the performance of a spray curtain H = 1.5 m

4.2.19 Effect of wind on the performance of a spray curtain D = .88 mm

4.2.20 Effect of wind on the performance of a spray curtain D = .66 mm

4.2.21 Effect of wind on the performance of a spray curtain U_0 = 28.42 m/s

4.2.22 Effect of wind on the performance of a spray curtain U_0 = 33.15 m/s

4.3.1 Computational domain for cooling tower

4.3.2 Flow field in a cooling tower - No droplets

4.3.3 Static pressure isobars for flow through cooling tower - No droplets

4.3.4 Flow field in a cooling tower - D = 3 mm

4.3.5 Static pressure isobars for flow through a cooling tower D = 3 mm

4.3.6 Flow field in a cooling tower D = 4 mm

4.3.7 Static pressure isobars for flow through a cooling tower D = 4 mm

4.3.8 Flow field in a cooling tower D = 6 mm

4.3.9 Static pressure isobars for flow through a cooling tower D = 6 mm

4.3.10 Comparison of velocity profiles at inlet and after packing D = 3 mm

4.3.11 Comparison of velocity profiles at inlet and after packing D = 6 mm

4.3 12 Flow field in a cooling tower - No droplets ν_{EFF} = .1 m^2/s

4.3.13 Static pressure isobars for flow through a cooling tower - No droplets ν_{EFF} = .1 m^2/s

4.3.14 Flow field in a cooling tower D = 4 mm ν_{EFF} = .1 m^2/s

4.3.15 Static pressure isobars for flow through a cooling tower D = 4 mm ν_{EFF} = .1 m^2/s

4.3.16 Comparison of velocity profiles at inlet and after packing ν_{EFF} = .1m^2/s

LIST OF TABLES

4.1.1 Properties of Lechler SZ1 nozzle p. 31

4.1.2 Properties of Lechler SZ2 nozzle 31

4.2.1 Hypothetical nozzle characteristics 34

4.3.1 Tower dimensions and test conditions 42

4.3.2 Total pressure losses in domain of interest ν_{EFF} = 1.0 m^2/s 45

4.3.3 Total pressure losses in domain of interest ν_{EFF} = 0.1 m^2/s 45

1. INTRODUCTION

Liquid sprays and cooling towers represent just a few typical examples of applications of gas-droplet flows. Optimizing the performance in these applications requires that the fluid dynamics be understood. Difficulties in modelling such flows experimentally at below full-scale levels and the expense of full scale tests has mandated a need for the development of numerical models.

The presence of droplets in these flow fields introduces additional complications in their physical descriptions and subsequent calculation. Often the primary effect of the droplets, due to the aerodynamic drag they experience, is to transfer momentum to the gas, a consequence of the conservation of momentum. This results in a modification of the gas flow field. The complications arise in that the droplet motion and resulting momentum exchange is a function gas motion which the droplets influence. Thus the complete description of the phenomenon involves coupling between the two phases.

The droplets may also modify other properties of the gas, such as its turbulence level, density and viscosity, though these effects are treated only very superficially in this report.

Modelling of gas-droplet flows has been made in the past. A one dimensional axisymmetric spray model has been developed at VKI (Ref. 13) and has shown good results, though its applicability for the inclusion of boundary effects is limited. Two dimensional spray and cooling tower models existing in the literature (Refs. 1,2,3,8,16) are better able to handle the effects of boundaries. In this light, it is of interest to develop a two dimensional model at the VKI to complement the range of applicability of the one dimensional axisymmetric spray model, to examine a planar representation of spray curtain, and to investigate flow in a cooling tower.

In this report the model used is outlined, the numerical method used for its solution is described, and finally the results for the three applications mentioned above are presented and discussed.

2. THE GAS-DROPLET MODEL

2.1 Introduction

The gas-droplet model consists of two distinct sets of equations, one set governing the gas phase and another governing the liquid phase. Linkage between these two sets of equations accounts for the following mode of gas-droplet interaction. The viscous nature of the gas causes droplets moving relative to the gas to experience an aerodynamic drag. Because momentum must be conserved, this aerodynamic drag, acting to change the momentum of the droplets, also changes the momentum of the gas in a signwise opposite manner. The result is that the motion of the droplets is influenced by the local gas velocity and visa versa. It should be noted that the effect of turbulence on the droplets is not taken into account and the turbulence induced by the droplets or by other sources is only crudely accounted for.

2.2 The gas phase model

The gas phase, occupying the most significant portion of the flow, is treated as a continuum. Making the standard assumptions of incompressible, isothermal, Newtonian fluid, and assuming the volume occupied by the droplets is negligible allows the following form of the Navier-Stokes equations to be applied. The possibility of considering planar or axisymmetric cases is provided.

Continuity

$$\frac{1}{r^{\alpha}} \frac{\partial}{\partial r} \left(r^{\alpha} V_r \right) + \frac{\partial V_z}{\partial z} = 0 \qquad (2.1)$$

Momentum

Horizontal direction

$$\frac{\partial V_r}{\partial \tilde{t}} + \frac{1}{r^\alpha}\frac{\partial}{\partial r}\left(r^\alpha V_r^2\right) + \frac{\partial}{\partial z}\left(V_r V_z\right) = -\frac{\partial (P/\rho)}{\partial r}$$

$$+ \nu_{EFF}\left\{\frac{1}{r^\alpha}\frac{\partial}{\partial r}\left(r^\alpha \frac{\partial V_z}{\partial r}\right) - \frac{1}{r^\alpha}\frac{\partial^2}{\partial z \partial r}\left(r^\alpha V_r\right)\right\} + \frac{F_r}{\rho} \qquad (2.2)$$

Vertical direction

$$\frac{\partial V_z}{\partial \tilde{t}} + \frac{\partial (V_z^2)}{\partial z} + \frac{1}{r^\alpha}\frac{\partial}{\partial r}\left(r^\alpha V_z V_r\right) = -\frac{\partial (P/\rho)}{\partial z}$$

$$+ \nu_{EFF}\left\{\frac{1}{r^\alpha}\frac{\partial}{\partial r}\left(r^\alpha \frac{\partial V_z}{\partial r}\right) - \frac{1}{r^\alpha}\frac{\partial^2}{\partial z \partial r}\left(r^\alpha V_r\right)\right\} + \frac{F_z}{\rho} \qquad (2.3)$$

Here V_r, V_z, P are the horizontal and vertical components of velocity and pressure respectively, and r, z are the horizontal and vertical coordinates. ρ and ν_{EFF} represent the gas density, and the effective viscosity of the gas which could crudely account for the turbulence induced by the droplets. α is the switch for the axisymmetric (α=1) or planar (α=0) cases.

F_r and F_z are the horizontal and vertical momentum source terms which represent external sources (sinks) of gas momentum per unit volume such as that due to the droplets. They are defined as the sum of the external contributions to the horizontal or vertical components of gas momentum inside a volume ΔV divided by the volume ΔV, expressed symbolically below.

$$F_r = \frac{\sum \frac{f_r}{\Delta V}}{\Delta V} \tag{2.4}$$

$$F_z = \frac{\sum \frac{f_z}{\Delta V}}{\Delta V} \tag{2.5}$$

The horizontal and vertical momentum source terms due to the presence of droplets may be obtained by summing respectively the horizontal and vertical components of aerodynamic drag acting at each droplet inside a volume ΔV and dividing by the volume ΔV.

These equations and appropriate boundary conditions are applied inside a representative domain (see Fig. 2.1).

Four sets of boundary conditions are considered here corresponding to the following types of boundaries; no-slip walls, slip walls, specified inflow/outflow boundaries, and unspecified inflow/outflow boundaries.

A no-slip boundary condition is applied in the presence of a rigid wall where the friction effects of such a boundary are important. The component of velocity tangent to the wall is set equal to zero satisfying the no-slip condition while the normal component is set to zero to satisfy the condition of zero mass flow across the rigid wall. The pressure boundary condition follows by applying the momentum equation in the direction normal to the wall. These conditions are expressed below. Here the subscript N denotes the normal coordinate while t denotes the tangential coordinate.

$$V_t = 0$$

$$V_N = 0 \tag{2.6}$$

$$\frac{\partial P}{\partial N} = \nu_{eff} \left\{ \left[\frac{1}{r^\alpha} \frac{\partial}{\partial r} \left(r^\alpha \frac{V_N}{\partial r} \right) + \frac{\partial^2 V_N}{\partial z^2} \right] \right.$$

The slip wall boundary condition is applied at an axis of symmetry or at a rigid wall where the friction effects of such a boundary are not important or not desired. The component of velocity normal to the wall is set equal to zero to again satisfy the condition of zero mass flow across the rigid wall. The slip condition is satisfied by requiring the gradient of the tangential component to be zero at the wall. Again the pressure boundary condition follows from the momentum equation in the direction normal to the wall.

$$V_N = 0$$

$$\frac{\partial V_t}{\partial N} = 0 \qquad (2.7)$$

$$\frac{\partial P}{\partial N} = 0$$

The boundary conditions for the velocity at a specified inflow/outflow boundary follows by definition, while the pressure boundary conditions may be obtained by substituting the specified velocities into the momentum equation in the direction normal to the boundary.

$$V_r = V_r(r,z)$$

$$V_z = V_z(r,z) \qquad (2.8)$$

$$\frac{\partial P}{\partial N} \rightarrow \text{obtained from momentum equation.}$$

At the unspecified inflow/outflow boundary the applied boundary conditions reflect the porous nature of such a boundary.

$$\frac{\partial (rV_r)}{\partial N} = 0$$

$$\frac{\partial V_z}{\partial N} = 0 \qquad (2.9)$$

$$\frac{\partial P}{\partial N} \rightarrow \text{obtained from momentum equation}$$

It should be noted that since the pressure boundary conditions are all von Neumann type, the pressure needs to be specified at one point in the domain.

2.3 The droplet phase model

The droplet phase is modelled by considering a finite and discrete distribution of droplets of varying diameter, injection velocity, and injection angle. Using a Lagrangian approach individual droplets are followed from injection until hitting the ground. Appropriately assigning a portion of the total number of droplets injected by nozzle per unit time to each of the trajectories and determining the drag force along each trajectory allows representation of the droplet-gas momentum exchange. This approach assumes no droplet-droplet interactions such as collisions or droplet break-up occur.

Thus the equations of motion of the droplet need to be considered. Forces acting on the droplet other than aerodynamic drag and gravitational force are neglected. Further assuming that the droplets are spherical and non-evaporating allows the following equations of motion to be written :

$$m \frac{du_r}{dt} = - f_r \qquad (2.10)$$

$$m \frac{du_z}{dt} = - f_z \pm mg \qquad (2.11)$$

$$\frac{dR}{dt} = u_r \tag{2.12}$$

$$\frac{dZ}{dt} = u_z \tag{2.13}$$

Here u_r, u_z are the horizontal and vertical components of droplet velocity and R,Z are the horizontal and vertical coordinates of the droplet trajectory. The mass of the droplet, "m", is simply defined.

$$m = \rho_w \frac{\pi}{6} D^3 \tag{2.14}$$

where D is the droplet diameter and ρ_w is the droplet density.

The horizontal and vertical components of aerodynamic drag force f_r, f_z needed for the calculation of F_r and F_z may be written as follows

$$f_r = C_D Re \frac{\pi D \nu \rho}{8} (u_r - v_r) \tag{2.15}$$

$$f_z = C_D Re \frac{\pi D \nu \rho}{8} (u_z - v_z) \tag{2.16}$$

The Reynolds number of the droplet, Re, is defined.

$$Re = \frac{\sqrt{(u_z - v_z)^2 + (u_r - v_r)^2}\, D}{\nu} \tag{2.17}$$

The drag coefficient of the droplet is assumed equivalent to that of a sphere and is described by the following standard form fit (Ref. 9)

$$C_D = \frac{24}{Re} + \frac{6.}{1+\sqrt{Re}} + .4 \qquad 0. < Re < 10^5 \qquad (2.18)$$

Initial conditions:

The initial conditions for the droplet injection are obtained by considering the initial position, injection velocity, and injection angle (see Fig. 2.1). These variables are dependent on the particular phenomenon being studied such as sprays where the droplets are injected by a nozzle or cooling towers where the droplets drip from the packing.

$$\begin{aligned} R(t=0) &= R_\ell \\ Z(t=0) &= L_z - H \\ u_r(t=0) &= U_0 \sin\theta \\ u_z(t=0) &= U_0 \cos\theta \end{aligned} \qquad (2.19)$$

Here R_ℓ is the horizontal distance from the left boundary of the domain to the injection point, L_z is the vertical domain length, H is the height from the ground to the injection point, U_0 is the injection velocity and θ is the injection angle.

3. THE NUMERICAL METHOD

It is difficult indeed to conceptualize a numerical method for the simultaneous solution of both sets of equations. A more natural approach involves a two-step iterative procedure where, in the first step, the solution of the gas phase equations is made using the most updated solution of the droplet equations and, in the second step, the solution of the droplet equations is made using the newest gas phase solution. This process continues until convergence of both sets of equations is reached.

Such a procedure, common in the literature for gas-droplet flows (Refs. 1,2,3), is used here for the solution of the gas-droplet model equations. The numerical methods used to solve each set of equations reflect the different nature of the equations themselves and are discussed separately in the following two sections. The third section describes the calculation of the source terms and finally in a fourth section the details of the two-step procedure used here are discussed.

3.1 Numerical solution of the gas phase equations

The numerical scheme for the solution of the gas phase equations is based on the Simplified Marker and Cell (SMAC) method (Refs. 4,5). The SMAC method, used for the solution of the primitive variable (u,v,P) form of the Navier-Stokes equations, is a finite-difference time-marching procedure characterized by a cell structure shown in figure 3.1.

Pressure is defined at the center of each cell, horizontal components of velocity defined at the vertical cell boundaries, and vertical components of velocity defined at the horizontal boundaries of the cell. The vertical and horizontal momentum source cells are rectangular, of dimension $\Delta r \times \Delta z$, and centered at the positions where the corresponding vertical and horizontal velocity components are defined.

The method is an iterative procedure involving four steps at each cycle. During the first step the velocity components inside the domain are explicitly updated using a discretized form of the momentum equations. Using the values of velocity inside the domain, the unspecified normal velocities on the domain boundary are calculated to complete the second step. In the third step sweeps are made through the grid checking to make sure that the divergence (mass conservation) of each cell is below some tolerable level. If the divergence is greater than this value then the pressure inside the cell is modified appropriately and the velocities are redistributed so that continuity is satisfied. The sweeps through the grid continue until the divergence of each cell is below the tolerence level.

Finally in the fourth step the boundary conditions necessary to specify the velocity components tangent to the boundaries in the "fictitious" cells surrounding domain are applied.

This four-step procedure is applied iteratively until convergence is obtained.

3.1.1 Equations for the first step

As mentioned the equations used in the first step are finite difference forms of the momentum equations (2.2, 2.3). Here forward differencing in time, upwind differencing on the advection terms and central differencing of the other spatial derivatives is used to obtain explicit equations for the velocity components inside the domain. The form of these equations is similar to that used by Viecelli (Ref. 5), and are given as follows. Here the tilde (~) represents the updated velocities.

Radial momentum equation

$$\tilde{V}_{r_{i+1/2,j}} = V_{r_{i+1/2,j}} + \Delta t \cdot f_{i+1/2,j} \Bigg\{$$

$$- \frac{1}{r^{\alpha}_{i+1/2}\Delta r} \Bigg[r^{\alpha}_{i+1} V_{r_{i+1,j}} \begin{cases} V_{r_{i+3/2,j}} & \text{if } V_{r_{i+1,j}} < 0 \\ V_{r_{i+1/2,j}} & \text{if } V_{r_{i+1,j}} > 0 \end{cases}$$

$$- r^{\alpha}_{i} V_{r_{i,j}} \begin{cases} V_{r_{i+1/2,j}} & \text{if } V_{r_{i,j}} < 0 \\ V_{r_{i-1/2,j}} & \text{if } V_{r_{i,j}} > 0 \end{cases} \Bigg]$$

$$- \frac{1}{\Delta z} \Bigg[V_{z_{i+1/2,j+1/2}} \begin{cases} V_{r_{i+1/2,j+1}} & \text{if } V_{z_{i+1/2,j+1/2}} < 0 \\ V_{r_{i+1/2,j}} & \text{if } V_{z_{i+1/2,j+1/2}} > 0 \end{cases}$$

$$- V_{z_{i+1/2,i-1/2}} \begin{cases} V_{r_{i+1/2,j}} & \text{if } V_{z_{i+1/2,j-1/2}} < 0 \\ V_{r_{i+1/2,j-1}} & \text{if } V_{z_{i+1/2,j-1+2}} > 0 \end{cases} \Bigg]$$

$$- \frac{1}{\Delta r} \left[\frac{P}{\rho}_{i+1,j} - \frac{P}{\rho}_{i,j} \right] + \frac{\nu_{eff}}{\Delta z^2} \left[V_{r_{i+1/2,j+1}} - 2V_{r_{i+1/2,j}} + V_{r_{i+1/2,j-1}} \right]$$

$$- \frac{\nu_{eff}}{\Delta r \Delta z} \left[V_{z_{i+1,j+1/2}} - V_{z_{i+1,j-1/2}} - V_{z_{i,j+1/2}} + V_{z_{i,j-1/2}} \right]$$

$$+ \frac{F_r}{\rho}_{i+1/2,j} \Bigg\} \qquad (3.1)$$

Axial momentum equation

$$\tilde{V}_{z_{i,j+1/2}} = V_{z_{i,j+1/2}} = \Delta t \cdot f_{i,j+1/2} \Bigg\{$$

$$- \frac{1}{\Delta z} \Bigg[V_{z_{i,j+1}} \begin{cases} V_{z_{i,j+3/2}} & \text{if } V_{z_{i,j+1}} < 0 \\ V_{z_{i,j+1/2}} & \text{if } V_{z_{i,j+1}} > 0 \end{cases}$$

$$- V_{z_{i,j}} \begin{cases} V_{z_{i,j+1/2}} & \text{if } V_{z_{i,j}} < 0 \\ V_{z_{i,j-1/2}} & \text{if } V_{z_{i,j}} > 0 \end{cases} \Bigg]$$

$$- \frac{1}{r_i^{\alpha} \Delta r} \Bigg[r_{i+1/2}^{\alpha} V_{r_{i+1/2,j+1/2}} \begin{cases} V_{z_{i+1,j+1/2}} & \text{if } V_{r_{i+1/2,j+1/2}} < 0 \\ V_{z_{i,j+1/2}} & \text{if } V_{r_{i+1/2,j+1/2}} > 0 \end{cases}$$

$$- r_{i-1/2}^{\alpha} V_{r_{i-1/2,j+1/2}} \begin{cases} V_{z_{i,j+1/2}} & \text{if } V_{r_{i-1/2,j+1/2}} < 0 \\ V_{z_{i-1,j+1/2}} & \text{if } V_{r_{i-1+2,j+1/2}} > 0 \end{cases} \Bigg]$$

$$- \frac{\nu_{eff}}{r_i^{\alpha} \Delta r \Delta z} \Big[\left(V_{r_{i+1/2,j+1}} - V_{r_{i+1/2,j}} \right) r_{i+1/2}^{\alpha}$$

$$- \left(V_{r_{i-1/2,j+1}} - V_{r_{i-1/2,j}} \right) r_{i-1/2}^{\alpha} \Big]$$

$$- \frac{\nu_{eff}}{r_i^{\alpha} \Delta r^2} \Big[\left(V_{z_{i,j+1/2}} - V_{z_{i-1,j+1/2}} \right) r_{i-1/2}^{\alpha}$$

$$- \left(V_{z_{i+1,j+1/2}} - V_{r_{i,j+1/2}} \right) r_{i+1/2}^{\alpha} \Big] - \frac{1}{\Delta z} \left[\frac{P}{\rho}_{i,j+1} - \frac{P_{i,j}}{\rho} \right]$$

$$+ \frac{F_z}{\rho}_{i,j+1/2} \Bigg\} \qquad (3.2)$$

Discretized velocities not explicitly available are obtained by a simple averaging such as

$$V_{r_{i,j}} = \frac{1}{2}\left(V_{r_{i+1/2,j}} + V_{r_{i-1/2,j}}\right) \tag{3.3}$$

$$V_{z_{i+1/2,j+1/2}} = \frac{1}{2}\left(V_{z_{i,j+1/2}} + V_{z_{i+1,j+1/2}}\right) \tag{3.4}$$

A flagging scheme is used to allow the possibility of obstacles inside the domain. The flags $f_{i,j+1/2}$ and $f_{i+1/2,j}$ in equations (3.1, 3.2) are set equal to zero inside or on the boundary of an obstacle and equal to one elsewhere in the flow domain. This causes the components of velocity on or inside obstacles to be unchanged during the first step, while allowing the other velocity components inside the domain to be updated according to the discretized momentum equations.

3.1.2 Equations for the second step

After completing the first step, the velocity components inside the flow domain will have been updated. In the second step, the unspecified normal velocity components on the boundary are updated by requiring that the volume flow through the boundary be the same as that on the cell face just inside the domain. Normal velocity components on boundaries which have specified inflow/outflow, such as non-porous walls, symmetry boundaries, or boundaries where the inflow/outflow is known, are left unchanged by this step. Again making use of the flagging scheme the equations of the second step may be written. Here only the equations for the top and right boundaries are given because extension to the bottom and left boundaries is straightforward.

Top boundary

$$V_{z_{i,3/2}} = V_{z_{i,5/2}} * f_{i,3/2} + V_{z_{i,3/2}} * \left(1.-f_{i,3/2}\right) \qquad (3.5)$$

Right boundary

$$V_{r_{NX-1/2,j}} = V_{r_{NX-3/2,j}} * \left(\frac{NX-3}{NX-2}\right)^{\alpha} * f_{NX-1/2,j} + V_{r_{NX-1/2,j}} * \left(1-f_{NX-1/2,j}\right) \qquad (3.6)$$

where NX is the number of cells in the horizontal direction including the two fictitious cells.

3.1.3 The equations for the third step

Arriving at the third step, all the velocity components inside the domain and on the domain boundaries have been updated. Now the divergence of each cell is checked and the pressure modified and velocities reapportioned if the divergence is greater than a specified value.

Divergence equation

A finite differencing of the divergence equation yields the following.

$$D_{i,j} = \frac{1}{\Delta z}\left(V_{z_{i,j+1/2}} - V_{z_{i,j-1/2}}\right) + \frac{1}{r_i^{\alpha}\Delta r}\left(r_{i+1/2}^{\alpha} V_{r_{i+1/2,j}} - r_{i-1/2} V_{r_{i-1/2,j}}\right) \qquad (3.7)$$

Pressure and velocity modification

If D_{ij} is greater than a specified tolerance then the following operations, similar to that used by Hirt and Cook (Ref. 4), are applied to update the pressure and velocity in the cell. Updated quantities are devoted by a tile (~).

If $D_{ij} > \epsilon$, then

$$\delta P_{ij} = - \frac{\beta D_{i,j}}{2\Delta t \left(\frac{1}{\Delta z^2} + \frac{1}{\Delta r^2} \right)} \tag{3.8}$$

$$\tilde{P}_{ij} = P_{ij} + \delta P_{ij} \tag{3.9}$$

β is the relaxation coefficient and varies between 0. and 2.

$$\tilde{V}_{r_{i+1/2,j}} = V_{r_{i+1/2,j}} + \frac{\Delta t}{\Delta z} \delta P_{ij} \frac{f_{i+1/2,j}}{f_{TOT}} \tag{3.10}$$

$$\tilde{V}_{r_{i-1/2,j}} = V_{r_{i-1/2,j}} - \frac{\Delta t}{\Delta z} \cdot \delta P_{ij} \frac{f_{i-1/2,j}}{f_{TOT}} \tag{3.11}$$

$$\tilde{V}_{z_{i,j+1/2}} = V_{z_{i,j+1/2}} + \frac{\Delta t}{\Delta r} \delta P_{ij} \frac{f_{i,j+1/2}}{f_{TOT}} \tag{3.12}$$

$$\tilde{V}_{z_{i,j-1+2}} = V_{z_{i,j-1+2}} - \frac{\Delta t}{\Delta r} \delta P_{ij} \frac{f_{i,j-1+2}}{f_{TOT}} \tag{3.13}$$

$$f_{TOT} = f_{i+1/2,j} + f_{i-1/2,j} + f_{i,j+1/2} + f_{i,j-1/2} \tag{3.14}$$

The process of checking the divergence continues cell by cell through the mesh until a complete sweep is made without any cell having a divergence greater than the tolerence.

This tolerance, ϵ, is typically .0001-.001 $\frac{\bar{U}}{\bar{L}}$ where $\bar{U}$ is a characteristic velocity and $\bar{L}$ a length scale of the flow.

3.1.4 Equations for the fourth step

The fourth step consists of specifying the velocity components tangent to the boundary in the ficittious cells which surround the domain and inside the cells which represent obstacles in order to satisfy the remaining boundary conditions. Two types of boundary conditions for velocity components tangent to the boundaries are considered; those involving slip walls and those involving no-slip walls.

No-slip walls

The no-slip wall is a rigid wall where there is no tangential component of velocity at the wall and is often used to represent ceilings, ground etc., where the friction effects of such boundaries are important. Because the boundary of the domain coincides with the cell boundaries and because of the staggered grid used, averaging of the velocity components tangential to the wall, located a half cell width inside and outside the boundary, is required to satisfy the no-slip conditions

$$V_{w-1+2} + V_{w+1/2} = V_w = 0$$

$$V_{w-1/2} = - V_{w+1/2} \qquad (3.15)$$

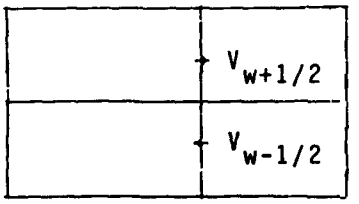

Slip-walls

The slip-wall condition may be applied when no tangential velocity gradient at the boundary is desired, as for the cases of axis of symmetry boundaries, unspecified inflow-outflow boundaries, or rigid walls where the friction effects are not of interest.

Again averaging across the boundary is used to obtain the following.

$$\frac{V_{w+1/2}-V_{w-1/2}}{\Delta z} = 0$$

$$V_{w-1+2} = V_{w+1/2} \tag{3.16}$$

Convergence criteria

The test for convergence of the gas phase is made by examining the residual of the velocities defined below and by examining the velocities and pressure at two points in the flow field.

$$R = \sum_{ij}\sum \left(V_{z}^{N}{}_{ij+1/2} - V_{z}^{N-1}{}_{ij+1/2}\right)^2 + \sum_{ij}\sum \left(V_{r}^{N}{}_{i+1/2,j} - V_{r}^{N-1}{}_{i+1,j}\right)^2 \tag{3.17}$$

A typical value of the residual at convergence is on the order of $1. \times 10^{-7} * \bar{U}^2$ where $\bar{U}$ is a characteristic velocity.

Numerical stability

From references 4 and 5 the following two stability criteria are deduced.

First criteria is a result of the finite difference approximation of viscous terms in the momentum equations.

$$\Delta t < \frac{1}{2\nu_{eff}\left(\frac{1}{\Delta z^2} + \frac{1}{\Delta r^2}\right)} \tag{3.18}$$

The second criteria requires that a fluid particle not cross a cell in a single time step.

$$\Delta t < \min\left[\frac{\Delta r}{V_r}, \frac{\Delta z}{V_z}\right] \tag{3.19}$$

3.2 Numerical solution at the droplet equations

The droplet equations are solved simultaneously using a fourth-order Runge-Kutta technique for each different set of initial conditions. Such techniques are well documented in the literature (Ref. 6) and thus the details are not considered here.

One detail that needs to be clarified concerns the interpolation of the gas velocities which are not always available at the same position in the flow field as the droplet. A bi-variate linear interpolation, similar to that used in MAC codes to calculate the marker particle positions, is applied here (Ref. 7). Thus, the marker particles of the original MAC method can be thought of as merely massless "droplets" which do not interact with the gas as opposed to the droplets in the method discussed here which do.

Once the droplet equations have been solved, the solution, the droplet position and velocity along the trajectories as a function of time, may then be used to calculate the droplet to gas momentum source terms.

3.3 Calculation of the droplet to gas momentum source term

Once a droplet trajectory has been calculated the contribution of the droplets along the trajectory to the

droplet-gas momentum exchange may be evaluated. The trajectory consists of a number of segments the location of whose end points have been computed. The horizontal and vertical components of the droplet velocity are also known at these end points and allow the aerodynamic drag which acts on the droplets along the trajectory to be determined.

The horizontal and vertical droplet to gas momentum source terms may be determined from the sum of the respective components of the aerodynamic drag acting on the droplets in the source cells, divided by the volume of the source cells as defined below.

$$F_{z_{i,j+1/2}} = \frac{\sum_{k}^{N_{i,j+1/2}} f_z^k}{V_{ij+1/2}}$$

or equivalently

$$F_{z_{i,j+1/2}} = \frac{f_{z_{ave}} N_{i,j+1/2}}{\Delta V_{i,j+1/2}}$$

$$F_{r_{i+1/2,j}} = \frac{f_{r_{ave}} N_{i+1/2,j}}{\Delta V_{i+1/2,j}}$$

where $f_{r_{ave}}$ and $f_{z_{ave}}$ are the average horizontal and vertical aerodynamic drig force acting on the $N_{i+1/2,j}$ and $N_{i,j+1/2}$ droplets in the source cells of volume $\Delta V_{i+1/2,j}$ and $\Delta V_{i,j+1/2}$ respectively.

The evaluation of the droplet to gas momentum source proceeds segment by segment along each trajectory from the injection point until the droplet reaches the ground. The

droplet to gas momentum source evaluation due to droplets along a single segment (R_t,Z_t)-$(R_{t+\Delta t},Z_{t+\Delta t})$ begins by determining which of the source cells the segment is contained in (see Fig. 3.2). The segment is divided into subsegments if the segment crosses any source cell boundaries. The number of droplets along each subsegment is calculated as follows :

$$N = \frac{f_{qw} \cdot \Delta t \cdot \frac{\ell m}{\ell_{tot}}}{\frac{\pi}{6} D^3}$$

where Δt is the time step of the droplet integration, ℓ_{tot} is the length of the segment (R_t,Z_t)-$(R_{t+\Delta t},Z_{t+\Delta t})$ and ℓm is the subsegment length. f_{qw} is the volume flow of liquid assigned to the trajectory of interest, and is calculated such that the distribution of droplet quantity summed over all the trajectories in the domain represents the physical phenomenon being studied.

The calculation of the average force is made by simply averaging the aerodynamic drag force acting on the droplet at both of the segmant endpoints.

With the simple determination of the source cell volume the evaluation of the droplet to gas momentum source contribution from this segmant is complete.

If two or more segments are contained in the same source cell the contributions of each to the momentum source are simply added.

It is to be noted that the time step for the integration of the droplet equation should be small so that the distance travelled by the droplet is small compared with the cell sizes, ensuring accuracy in the evaluation of the momentum source terms.

3.4 The solution procedure

A solution procedure similar to the one discussed in the beginning of this section was adopted and is outlined in figure 3.3.

The procedure begins with a "guessed" initial gas flow field. The initial droplet trajectories and droplet to gas momentum source are calculated using this initial flow field.

The gas phase computations are then made using the newly obtained momentum source terms. Because the changes in the gas flow field from cycle to cycle are small, ten cycles of the SMAC procedure are made before resolving the droplet equations.

After updating the droplet trajectories and droplet to gas momentum source terms based on the most updated gas flow field, the gas flow computations continue with 10 more cycles.

The process is repeated until convergence of the gas flow field is obtained.

4. APPLICATIONS AND RESULTS

The method is applied to three typical problems involving gas-droplet flows; calculation of the flow field induced by an axisymmetric spray, determination of the wind effects on a spray curtain, and examination of the flow in the lower portion of a cooling tower.

4.1 Axisymmetric spray

The first application made is in the prediction of the flow induced by an axisymmetric spray.

4.1.1 Modelling of an axisymmetric spray

The axisymmetric spray is represented by a discrete and finite distribution of droplets of varying sizes and initial injection angles injected into the gas from a single point along the axis of symmetry.

A distribution of droplet sizes is considered using an approach taken by Alpert and Mathews (Ref. 10). They attribute Dundas (Ref. 11) with having shown that the range of droplet sizes produced by a deflector type nozzle is represented by the Rassin-Rammler distribution function given below.

$$F(D) = 1-\exp\left[-(\ell n 2)\,\frac{D^2}{D_m^2}\right] \qquad (4.1.1)$$

where F(D) is the mass fraction of droplets having diameters less than D and D_m is the mean droplet size. Five classes of droplet sizes are considered, each having the same proportion of the liquid volume flow. Thus, the representation diameters of each class are .39, .72, 1.0, 1.32 and 1.82 times the mean droplet diameter, calculated using the simple approach given by Heskested et al. (Ref. 12) as follows :

$$D_m = C_N \frac{d_0^{2/3}}{\Delta P_N^{1/3}} \qquad (4.1.2)$$

where d_0 is the inside diameter of the nozzle and ΔP_N is the water delivery pressure. Due to the lack of data, the nozzle design parameter, C_N, is taken as 1.0.

Each class of droplet sizes is further discretized by considering a distribution of initial injection angles in order to represent a full cone spray. The initial injection angles are chosen such that a line perpendicular to the axis of symmetry is cut into the number of trajectories per class minus one (N_{traj}-1) segments of equal length by a set of lines tangent to the initial droplet trajectories. This is expressed by the following

$$\theta_i = \tan^{-1}\left\{\frac{(i-1)}{(N_{traj}-1)} \tan\theta_{MAX}\right\} \qquad i=1,\ldots,N_{traj} \qquad (4.1.3)$$

where θ_{MAX} is the half angle of the spray.

It is desired to have a mass flow of droplets per unit area which is fairly constant throughout the spray near the nozzle. The following formula are used to assign the volume flow of liquid to each trajectory.

$$f_{Qw_1} = \frac{1}{5} Qw \frac{1}{2(N_{traj}-1)^2}$$

$$f_{Qw_i} = \frac{1}{5} Qw \frac{2i-2}{(N_{traj}-1)} \qquad i=2,\ldots,N_{traj}-1$$

$$f_{Qw_{N_{traj}}} = \frac{1}{5} Q_w \frac{N_{traj}-5/4}{(N_{traj}-1)^2} \qquad (4.1.4)$$

The one-fifth factor represents the equal share of the total volume flow of water assigned to the five droplet size classes. The ratio on the right hand side of these equations represents the area of the i^{th} ring formed by circles drawn at the midpoint of the segments discussed above, divided by the total area of a circle drawn at the endpoint of the outermost segment. This ratio gives a fairly constant mass flow per unit area for moderate half angles of the spray.

A constant droplet injection velocity is chosen due to the lack of data concerning this parameter, and is calculated by assuming that the injection velocity of the droplet is equal to the velocity of the liquid at the outlet of the nozzle. Such an approach is used by Buchlin (Ref. 13) and Botterrud (Ref. 11).

$$U_0 = \frac{Q_w}{\frac{\pi}{4} d_0^2} \qquad (4.1.5)$$

Expressing the condition that the droplets are injected from a single point along the axis of symmetry completes the specification of the inlet conditions for the droplet phase.

$$R_{\ell_i} = 0$$

$$H_i = \text{height of spray} \qquad (4.1.6)$$

Computations are made on a rectangular domain shown in figure 4.1.1 using a 20 × 20 to 20 × 40 cell mesh. The boundary conditions which are applied are also shown in figure 4.1.1.

Optimization of the relaxation coefficient, β, for the pressure-velocity modification step of the numerical method yielded a value of 1.4.

The value of the viscosity is taken as the molecular viscosity of air.

4.1.2 Results

Calculation of the flow fields due to an axisymmetric spray for several different nozzles is made.

The flow fields due to a Lechler SZ1 nozzle with the characteristics shown in Table 4.1.1 are displayed in figures 4.1.2-4.1.7. Here calculations are performed in a square domain using a 20 × 20 cell mesh with the nozzle located on the ceiling. The first three figures display the flow field with the nozzle two meters above the ground for increasing mass flow through the nozzle, from 6.6 to 21.1 liters per minute. These figures represent typical nozzle operating modes for use in spray curtains or for fire extingtion. The second three figures display the flow fields for the same corresponding mass flows but with the nozzle located 0.4 meters above the ground allowing the near field behaviour of the nozzle to be evaluated. To be noted in all six of these figures is the manner in which the air enters the spray. Outside the spray the velocity vectors are nearly perpendicular to the axis of symmetry but are quickly deflected parallel to this axis after entering the spray. The entrained air then leaves the spray in a thin layer after impinging on the wall. These results are observable in both experiment and in other numerical calculations (Refs. 10,15).

Also seen in these figures is the increase in the magnitudes of the velocities inside the spray, or equivalently, an increase in the volume of air entrained into the spray with increasing volume flow through the nozzle.

The continuous lines shown in these figures represent the outermost trajectory of each of the five droplet size classes, with the trajectory closest to the axis of symmetry representing the smallest droplet size and the furthest, the largest droplet size.

For the two meter high spray the radial distribution of droplets inside the spray is highly dependent on the droplet diameter with the smallest droplets concentrated near the axis of symmetry for the bulk of the spray. The reason for the decrease in the penetration of the smaller droplets is due to their higher drag to weight ratio and to the fact that their terminal velocities are well below the injection velocity.

It should be noted that droplet transport due to the turbulence within the spray and droplet break-up are not con i-dered in the model, both of which could allow smaller droplets to migrate further out from the axis of symmetry.

For the 0.4 meter high spray and close to the nozzle for the two meter spray the droplets are fairly well distributed radially, particularly for the larger droplet sizes.

4.1.2.1 Comparison and experiment

Comparison of the calculated amount of air entrained into the spray is obtained by plotting the entrainment efficiency versus the nondimensional spray envelope diameter squared. The entrainment efficiency, η, is defined as the ratio of the volume flow of air entrained into the spray, Q_a, to the volume flow of liquid through the nozzle, Q_w, while the inverse spray envelope diameter, D_t, squared is nondimensionalized as given below

$$\eta = \frac{Q_a}{Q_w}$$

$$Q_a = 2\pi \int_0^{D_{t/2}} r\, V_z(r)\, dr$$

$$x = \frac{Q_w}{D_t^2} \sqrt{\frac{\rho_w}{\Delta P_N}}$$

Typical results of experimental investigations carried out at VKI (Ref. 15) are plotted in figure 4.1.8. Superimposed on the experimental data is the McQuaid correlation and the ±20% limits between which much of the data is located.

The calculated values for the cases discussed above are shown in figure 4.1.9. Fair to good agreement is seen, particularly further away from the nozzle. Near the nozzle the entrainment seems to be slightly underpredicted.

Slightly better agreement is seen in figure 4.1.10. Here the results of the calculations are displayed for the same nozzle characteristics except that the half angle of the spray is reduced from 30 degrees to 22.5 degrees. The 30 degree half angle represents the value given by the manufacturer, while the 22.5 degree half angle was the value measured by Buchlin (Ref. 15).

Similar calculations are made for the SZ2 nozzle with characteristics shown in Table 4.1.2. Again the nozzle is located on the ceiling and a squared domain with a 20 × 20 mesh is used. The values of the entrainment efficiency are shown plotted in figure 4.1.11. Good agreement is depicted.

Interestingly the overlap of the calculations made on three different size domains shows little variation in the efficiency indicating first, that the boundaries have little influence and secondly, that there is sufficient resolution near the nozzle to calculate the efficiency correctly.

Comparison between the calculated and experimentally measured axial velocity profiles within the spray are shown in Figs. 4.1.12-4.1.14 for three different locations in the spray. The numerical values are taken from the calculations made on the one meter by one meter domain. Fair agreement is seen, though the velocity profile seems to be more underestimated close to the nozzle and further from the axis of symmetry.

The slight underestimation of air entrained into the spray noted previously is consistent with these results. Possible improvements could be attained through the use of a turbulence model which might further encourage entrainment of air into the spray.

4.1.2.2 Evaluation of ceiling effect

The model is used to evaluate the effect of the ceiling on the performance of the spray. Calculations are made for the SZ1 nozzle with a volume flow of 21.1 liters per minute located halfway below the ceiling and the ground. Rectangular domains are used, of dimensions two meters wide by 4 meters high and 0.4 meters wide by 0.8 meters high with a 20 × 40 cell mesh. Results are compared with the corresponding calculations with the nozzle located on the ceiling and are shown in figure 4.1.15.

Only very slight improvement in the efficiency of the spray is seen as the ceiling is displaced from the nozzle, with the largest differences observed near the nozzle though these differences may be exaggerated by the lack of mesh resolution near the nozzle. It is clear, however, that the bulk of the flow inside the spray is only slightly effected by the presence of the ceiling. This is confirmed by Botterrud (Ref. 14) and Weinacht (Ref. 16).

4.1.2.3 Influence of pressure terms momentum equations

The influence of the pressure terms in the momentum equations may be examined by computing the flow field with the pressure terms eliminated from the momentum equations and comparing the results with the corresponding calculations discussed previously. The results of the computations for the SZ1 nozzle with 30 degree half angle and 21.1 liter per minute volume are shown in figure 4.1.16. The results show little difference in

the amount of air entrained into the spray for the calculations with and without pressure terms.

This result is significant in that it confirms the validity of neglecting the pressure gradient in the approach taken by Buchlin (Ref. 13).

4.1.3 Conclusions

The results show fair to good prediction of the flow inside the spray demonstrating the adequacy of the model. Though entrainment is slightly underestimated improvement may be possible with the addition of a turbulence model.

The lack of influence of the ceiling on the entrainment efficiency over the bulk of the spray is demonstrated by the calculations.

Results also indicate that the pressure terms in the momentum equations are of little importance over the majority of the flow field.

d_0 mm	Q_w ℓt/min	ΔP_N KPa	θ_{MAX} degrees
4.4	6.6	34.3	30
4.4	13.3	176.5	30
4.4	21.1	617.8	30

Table 4.1.1 Properties of Lechler SZ1 nozzle

d_0 mm	Q_w ℓt/min	ΔP_N KPa	θ_{MAX} degrees
5.6	36.0	588.6	30
5.6	44.5	981.	30

Table 4.1.2 Properties of Lechler SZ2 nozzle

4.2 Wind effects on a planar spray curtain

As a second application of the method, the wind effects on a planar representation of a spray curtain are examined.

Spray curtains are currently used for the dispersion of heavy, sometimes toxic or flammable, gases. As a step toward evaluating the effectiveness of the spray curtain for gas dispersal, the flow field produced by the interaction of the wind with the spray is predicted.

4.2.1 Modelling of a planar representation of a spray curtain

A spray curtain is formed by distributing a series of spray nozzles along a certain orientation, often forming a straight line, and ideally situated normal to the wind direction.

In this orientation, a planar model of the spray curtain is applied to predict the global behaviour of the flow field under the influence of the curtain. Nozzles of similar type and massflow are assumed to be equally distributed along a straight line parallel to the ground. The length of the curtain should be large compared with the height of the nozzles so that three dimensional effects are suppressed.

In the planar formulation the discrete spacing of the nozzles is represented as a constant uniform distribution of injected liquid along the length of a curtain. The distributed volume flow of the curtain per unit length, q_w, is calculated by multiplying the volume flow of the individual nozzles by the number of nozzles and dividing by the length of the curtain, expressed by the following

$$q_w = \frac{N_{noz} \times Q_w}{L_c} \qquad (4.2.1)$$

Here N_{noz} is the number of nozzles, Q_w is the volume flow of the individual nozzles, and L_c is the length of the curtain.

The spray in the plane of symmetry is represented by five to fifteen trajectories of varying injection angle of constant increment. The possibility of allowing the nozzle to be tilted relative to the vertically downwards position by α_{TILT} degrees is accounted for. This is expressed below as

$$\theta_i = 2\theta_{MAX} \left(\frac{1}{2} - \frac{i-1}{N_{traj}-1} \right) + \alpha_{TILT} \qquad i=1,\ldots,N_{traf} \qquad (4.2.2)$$

Here θ_{MAX} is the half angle of the spray and N_{traj} is the number of trajectories.

The fractional volume flow of liquid assigned to each trajectory is a constant, being equally divided between the N_{traj} trajectories. This may be expressed below

$$f_{Q_w} = \frac{1}{N_{traj}} \; q_w \qquad (4.2.3)$$

Only constant droplet injection velocities and droplet sizes are considered, and may be calculated as before using equations (4.1.5) and (4.1.2).

The particular curtain configuration presented here is modelled after typical configurations used in the Buxton full-scale trials (Ref. 17). In these trials a Protectospray nozzle was used, but due to the lack of data on the nozzle the following hypothetical nozzle characteristics are used.

Inside diameter	Nozzle design parameter	Half angle of spray
d_0	C_N	θ_{MAX}
mm	$Kg^{1/3}/sec^{2/3}$	degrees
12.7	.75	45

Table 4.2.1 Hypothetical nozzle characteristics

The volume flow through each nozzle is assumed to obey the following relationship to the delivery pressure.

$$Q_w = .1334 \sqrt{\Delta P_N} \qquad (4.2.4)$$

where ΔP_N is given in kP_a and Q_w in liters per second. Typical overpressures of 127 and 650 kP_a yield volume flows at 1.5 to 3.4 liters per second through each nozzle.

In the Buxton trials, curtain heights ranged from two to three meters with a nozzle spacing of 0.5 to 3 nozzles per meter covering distances at 16 to 32 meters. These typical values serve as inputs for the calculations made here.

The computations are made in a domain similar to that shown in figure 4.2.1. The nozzle is located approximately in the middle of the domain.

The applied boundary conditions are also shown in figure 4.2.1. At the specified inflow boundary a constant horizontal velocity and zero vertical velocity are applied.

Optimization of the relaxation coefficient for these calculations yields a value of 1.7.

The effective viscosity is taken as the molecular viscosity of air.

4.2.2 Results

The method is applied to examine the effect of wind speed, nozzle spacing, and tilting the nozzle into or away from the wind on the performance of a spray curtain. The effect of curtain height and spray angle on the curtain performance as well as the sensitivity of the calculation to drop size and injection velocity are also examined.

4.2.2.1 Effect of wind speed

Examination of the effect of wind speed on spray curtain performance may be made by performing calculations on a particular curtain geometry for increasing wind speed.

The curtain examined here is of 2.5 meters height with the nozzles hypothetically spaced one per meter and operating at individual volume flow rates of three liters per second.

Figure 4.2.2-4.2.5 shows the resulting flow field for increasing wind speeds from 2 to 4.5 meters per second. To be noted is the decrease in the size of the recirculation region in front of the spray with increasing wind speed, and its complete disappearance at the higher wind speed. These results demonstrate well the degradation of curtain performance with increasing wind speed.

4.2.2.2 Effect of nozzle spacing

Some of the effects of nozzle spacing may be examined, though three dimensional effects, such as interaction between adjacent sprays and flow between adjacent sprays, are not considered.

Figures 4.2.6 and 4.2.7 show the curtain with the same height and nozzle operating conditions but with a spacing increased by a factor of two.

Again the decrease in curtain performance is observed with increasing wind speed. Also seen is the decrease in performance with increasing spacing when compared with the previous set of results. It must be stated, however, that this is true as long as the droplets from adjacent sprays do not interact.

Figure 4.2.8 and 4.2.9 show the curtain with the same height of 2.5 meters but with the nozzles spaced at one per meter and operating at a volume flow rate of 1.5 liters per second. Comparison between these two figures and the two previous ones yields the conclusion that better performances may be obtained for the same liquid volume flow per unit length by spacing the nozzles further apart and operating each nozzle at a higher massflow. This conclusion is valid to a limit where the spacing between nozzles becomes large enough that the gas slips through the gaps in the curtain. This limiting behaviour is not predictable with this two-dimensional model.

4.2.2.3 Effect of tilting nozzle

During the Buxton trials, it was observed that tilting the spray into the wind yielded better dispersion of a heavy gas compared with the dispersion with the nozzle positioned vertically downwards or tilted away from the wind.

Figures 4.2.10-4.2.13 show the changes in the flow field as the nozzle is tilted increasingly more into the wind. In the vertically downwards position there is little modification of the wind field due to the spray. As the tilt angle is increased into the wind a stagnation region behind the spray begins to appear. The flow upstream must then rise over the curtain or pass beneath the stagnation region where it seems to be mixed somewhat with the air entrained by the nozzle. The degree to which mixing between a heavy gas layer and surrounding air might occur is not immediately assessable without a dispersion model, but it is certainly clear that comparatively stronger modification to the flow field is obtainable by tilting the

nozzle into the wind. Efforts toward coupling a dispersion model with a flow field calculation are in progress (Ref. 18).

Figures 4.2.14 and 4.2.15 show the nozzle tilted away from the wind. Here it seems the flow is simply accelerated downstream with very little mixing occurring. This is cinsistent with the results of the Buxton trials where it was found that tilting the nozzle away from the wind led to decreased dispersion compared with the vertically downwards position or tilted into the wind. Though convergence difficulties prevented obtaining results for higher volume flow rates per unit length, indications of a strong recirculation downstream of the nozzles exist.

4.2.2.4 Effect of decreasing cone angle

Figure 4.2.16 shows the effect decreasing the cone angle of the spray when compared with figure 4.2.4. It appears locally that the effect of the spray is more concentrated for the smaller cone angle, though globally, there is not much difference between the two cases.

4.2.2.5 Effect of height of spray

Figure 4.2.17 and 4.2.18 when compared with figure 4.2.4 allow the effect of the height of the spray to be examined. It can be seen that raising the height of the spray extends its region of influence, though the increased spray height also causes the higher velocities near the nozzle, which might encourage more rapid mixing, to be displaced further from the ground level (and possible further from a heavy gas layer).

The optimal curtain height it seems should be large enough so that a heavy gas cloud would be contained by the curtain, but low enough so that more rapid mixing between the heavy gas and the surrounding air occurs.

4.2.2.6 Sensitivity of the calculation to drop size and injection velocity

Figure 4.2.19 and figure 4.2.20 show the flow fields when droplet size is decreased by 20% and 40% respectively compared to the results shown in figure 4.2.4. Small variations in the flow field are noticed. The perturbations introduced in the main flow field by the spray increase slightly with decreasing droplet size.

Figure 4.2.21 and 4.2.22 depict the effect of increasing the droplet injection velocity by 20% and 40% over the corresponding injection velocity used to obtain the results in figure 4.2.4. Seen here is the increase in the perturbation of the flow field with increasing injection velocity, with the reappearance of the recirculation region occurring for the higher injection velocity.

4.2.3 Conclusions

The model is shown to give qualitatively good results.

The predictions demonstrate the degradation of curtain performance with increasing wind speed and the improvements in performance with increased liquid massflow through the nozzles.

For the same liquid volume flow per unit length, the results predict better performance by spacing the nozzles further apart and operating each nozzle individually at a higher volume flow rate. This result is true to a limit where the gas begins to slip through adjacent sprays, which is not predictable with this model.

Quite significantly, the model indicates improved curtain performance can be obtained by tilting the nozzle into the wind direction, while tilting of the nozzle away from the wind is not advised.

Results also show that the height of the curtain can be optimized so that a heavy gas cloud does not roll over the curtain, while ensuring that entrained air has sufficient energy to mix with the heavy gas cloud.

Extension of the method to include a dispersion model is recommended and is currently proceeding.

4.3 Calculation of the flow inside a cooling tower

The method is applied to calculate the velocity and pressure fields inside and near the inlet of a cooling tower. Of particular interest is the effect of the droplets on the velocity and pressure fields.

4.3.1 Modelling of the cooling tower

The domain of interest is primarily the lower portion of the cooling tower below the packing which contains the water droplets. A computational domain (shown in Fig. 4.3.1) is constructed to allow the the investigation to be focussed in this region. The computational domain is equally divided between the inside and outside of the tower so that the flow entering the tower would not be greatly affected by the flow at the outer boundaries.

The shell of the tower is represented by a hollow cylinder of zero thickness and of radius R_{tower}, located at a distance H_{inlet} above the ground.

The packing, of thickness L_p, is located a distance of H_{inlet} above the ground and extended across the entire radius of the tower. The packing is modelled using an approach by Buffat et al. (Ref. 8) which treats the packing as a porous media that causes a loss of momentum to the gas passing through it. The momentum loss per unit volume may be expressed in the following manner :

$$F_r = - \frac{K_1}{L_p} |V_z(r,z)| V_r(r,z) \qquad (4.3.1)$$

$$F_z = - \frac{K_2}{L_p} |V_z(r,z)| V_z(r,z) \qquad (4.3.2)$$

These expressions when adapted to the SMAC cell structure may be written as follows :

$$F_{r_{i+1/2,j}} = \frac{K_1}{L_p} |V_{z_{i+1/2,j}}| V_{r_{i+1/2,j}} \qquad (4.3.3)$$

$$F_{z_{i,j+1/2}} = - \frac{K}{L_p} |V_{z_{i,j+1/2}}| V_{z_{i,j+1/2}} \qquad (4.3.4)$$

The velocity $V_{z_{i+1/2,j}}$, not explicitly available, is obtained by simple averaging of the four surrounding axial velocity components.

The values of the coefficients K_1, K_2 are both taken as equal to 6, as suggested in reference 8.

The boundary conditions applied at the edges of computational domain and along both sides of the tower shell are displayed in figure 4.3.1. Along the specified inflow boundary a constant normal velocity, proportional to the volume flow of air through the tower, is applied. The tangential velocity along the boundary is set equal to that just upstream. The details of the boundary conditions at the other boundaries have been dealt with in previous sections and are not discussed here.

Computations are made on a 20 × 20 mesh with the droplet phase represented by ten trajectories spaced at equal intervals across the packing. The volume flow of liquid assigned to each trajectory is such that the total volume flow per unit area leaving the packing is a constant (in a discrete sense).

This may be expressed as follows

$$H_i = H_{inlet}$$

$$R_{\ell_i} = \frac{R_{tower}}{N_{traj}} \quad (i-1) \qquad (4.3.5)$$

$$f_{Q_{w_i}} = Q_w \frac{2i-1}{N_{traj}^2} \qquad (i=1,\ldots,N)$$

where H_i and R_{ℓ_i} are the vertical and horizontal locations of droplet injection, $f_{Q_{w_i}}$ is the fractional volume flow of liquid assigned to the i^{th} trajectory of the total N_{traj} trajectories.

The droplet, of sizes varying from 3 to 6 millimeters, are assumed to drip from the lower edge of the packing with an initial vertical trajectory and a prescribed initial vertical velocity.

$$U_{0_i} = 0.2 \text{ m/s} \qquad (4.3.6)$$

$$\theta_i = 0$$

The effective viscosity of the fluid is taken as 1 m^2/s to account for the turbulence induced by the droplets (except where noted).

The relaxation coefficient for the pressure-velocity modification is chosen as 1.4, as used for computation of axisymmetric spray, though no optimization of this parameter is made for the case of a cooling tower.

4.3.2 Results

The method is applied to a cooling tower with dimensions shown in Table 4.3.1. Calculation of the velocity and pressure fields is made for the cases of no droplets and droplets of size 3, 4 and 6 millimeter diameter.

Tower radius	R_{tower}	60	m
Inlet height	H_{inlet}	10	m
Packing thickness	L_p	2	m
Volume flow of air through tower	Q_a	22619	m^3/s
Volume flow of water	Q_w	31.4	m^3/s

Table 4.3.1 Tower dimensions and test conditions

A volume flow of air inside the tower equal to 22619 m^3/s is used yielding a mean velocity through the packing of 2 m/s. For the cases considered with droplets, a volume flow of water equal to 31.4 m^3/s gives a constant volume flow per unit are of 10 $m^3/hr \cdot m^2$.

4.3.2.1 Velocity field

The computed velocity fields for the above conditions with no droplets, and droplets of 3, 4 and 6 millemeters are shown in figures 4.3.2, 4.3.4, 4.3.6 and 4.3.8, respectively.

The effect of the packing on the flow field is clear. The radial component of velocity is suppressed significantly as gas passes through the packing, while the axial component is caused to be fairly uniform (± 15% variation) across the radius of packing except very near the tower shell where the velocity goes to zero.

The effect of the droplets on the velocity field is to cause a retardation of penetration of the gas towards the axis of symmetry though this effect is somewhat dominated by the opposing effect of the packing which tends to cause the axial velocity to be radially uniform across the packing. The effect is somewhat more clearly shown in figures 4.3.10 and 4.3.11.

Additionally the effect of the droplets is to cause the profiles of the radial component of velocity below the packing to become slightly more uniform, thus decreasing the size of the stagnation region in the lower corner of the domain near the axis of symmetry.

4.3.2.2 Pressure field

The corresponding pressure fields for the above computations are shown in figures 4.3.3, 4.3.5, 4.3.7 and 4.3.9. Here non dimensional static pressure isobars are displayed in increments of 1.2. Pressure has been nondimensionalized by the gas density times the square of the mean axial velocity through the packing (2 m/s).

In these figures the pressure losses caused by the packing and the inlet are clearly shown by the crowding of isobars in these regions.

The pressure loss due to the droplets is shown to be quite significant and increases with decreasing droplet diameter. The physical validity of this trend can be demonstrated by the following argument. The pressure drop due to the droplets is proportional to the product of the number of droplets and the average droplet drag. The number of droplets inside the tower can be expressed in terms of the volume flow of water, the time for the droplet to fall from the packing to the ground and the droplet diameter, and the drag in terms of the drag

coefficient, droplet velocity relative to the air, and droplet diameter. Thus the pressure drop due to droplets may be expressed

$$\frac{dP}{dx} \propto \left[\frac{Q_w \cdot \Delta t}{\frac{\pi}{6} D^3}\right] C_D \frac{1}{2} V_{rel}^2 \frac{\pi}{4} D^2$$

Noting that the forces acting on the droplet are dominated by the gravitational force, the time for the droplet to reach the ground and the relative velocity of the droplet may be assumed to be mild functions of droplet diameter (decreasing and increasily respectively).

Further neglecting the small variations in the drag coefficient with droplet diameter, the pressure loss is seen to vary with the inverse of the droplet diameter for constant volume flow of water.

Calculation of the additional total pressure loss caused by the droplets, shown in table 4.3.2, is conventionally obtained by subtracting the total pressure loss with droplets from the total pressure loss in the absence of droplets. The total pressure loss in each case is obtained by subtracting the average total pressure above the packing, P_{t_2}, from the average total pressure outside the tower far from the inlet P_{t_1} (see figure 4.3.1).

Further assuming the pressure loss due to the packing to be equal to the coefficient K_2 times the average axial velocity through the packing squared, allows the approximate pressure loss due to the inlet to be extracted. These are also displayed in table 4.3.2.

The calculated pressure loss due to the droplets is reasonable though experimental data seem to indicate that these values slightly underestimate the actual pressure loss. Further experimental verification is warranted.

Overall total pressure losses (P_{t_2}-P_{t_1})		
No droplets		7.6 mm H_2O
D = 3 mm		10.7 mm H_2O
D = 4 mm		10.1 mm H_2O
D = 6 mm		9.4 mm H_2O
Individual total pressure losses		
Due to inlet		4.6 mm H_2O
Due to packing		∿3.0 mm H_2O
Due to droplets	D = 3 mm	3.1 mm H_2O
	D = 4 mm	2.5 mm H_2O
	D = 6 mm	1.8 mm H_2O

Table 4.3.2 Total pressure losses in domain of interest ν_{eff} = 1 m^2/s

Overall total pressure losses (P_{t_2}-P_{t_1})		
No droplets		5.8 mm H_2O
D = 4 mm		8.4 mm H_2O
Individual pressure losses		
Due to inlet		2.8 mm H_2O
Due to packing		∿3.0 mm H_2O
Due to droplets	D = 4 mm	2.65 mm H_2O

Table 4.3.3 Total pressure losses in domain of interest ν_{eff} = 0.1 m^2/s

The total pressure loss due to the inlet, however, is grossly overestimated. This is most probably due to the high effective viscosity chosen to represent the turbulence induced by the droplets, which may not model the effective viscosity outside the inlet where there are no droplets.

This is substantiated by the calculations shown in figures 4.3.12, 4.3.13, 4.3.14 and 4.3.15 in which an effective viscosity of 0.1 m^2/s was used. The overall and individual pressure losses shown in table 4.3.3 indicate a large reduction in the pressure drop due to the inlet, which demonstrates the sensitivity of this component of the pressure loss to the effective viscosity. This indicates that a variable effective viscosity may be required to properly simulate the different nature of the flow inside and outside the cooling tower.

Figure 4.3.16 also indicates differences in the velocity field. Compared here are the velocity profiles at the inlet and after the packing for the case of 4 mm droplets and effective viscosities of 1.0 and 0.1 m^2/s. The velocity profiles become flatter as the effective viscosity is decreased.

Because the velocity and pressure fields are sensitive to the effective viscosity, further work with regard to a turbulence modelling is recommended.

4.3.3 Conclusions

The results demonstrate the applicability of the method for the computation of flow through a cooling tower. Results are reasonable with the exception of the pressure drop due to the inlet. Improvement is expected with further work in the modelling of the turbulence.

Extension of the method to account for the true tower geometry is possible as the SMAC method is applicable to problems with curved boundaries (Ref. 5).

5. CONCLUSIONS

The results demonstrate the successful implementation of the model with good qualitative agreement being seen throughout. Comparison with experimental results indicated a slight underprediction of the effect of the droplets though results are quite reasonable and demonstrate the usefulness of the model.

Application of the model to axisymmetric sprays demonstrates the limited effect of the ceiling on spray performance, and the lack of influence of the pressure term on the flow field prediction validating some assumptions made in other investigations.

The calculations for the planar representation of a spray curtain demonstrate the degrading effect of wind on its performance, but indicate that this may be overcome by tilting the nozzle into the wind.

The modelling of the flow in a cooling tower demonstrates the reasonable prediction of the effects of the droplets on both the velocity and pressure fields.

Further development of the model is recommended, particularly in the areas of turbulence, dispersion and heat transfer modelling.

REFERENCES

1. CROWE, C.T.; SHARMA, M.P.; STOCK, D.E.: The particle-source-in-cell model for gas droplet flows. ASME Trans., Series I - J. Fluids Engineering, Vol. 99, No. 2, June 1977, pp 325-332.

2. BOYSAN, F. & BINARK, H.: Prediction of induced air flows in hollow cone sprays. ASME Trans., Series I - J. Fluids Engineering, Vol. 101, No. 3, Sept. 1979, pp 312-318.

3. ALPERT, R.L. & MATHEW, M.K.: Calculation of large-scale flow fields induced by droplet sprays. Factory Mutual Research Corp., Norwood, Massachusetts, OEOJ4 BU-RC79-BT-14, December 1971.

4. HIRT, C.W. & COOK, J.C.: Calculating three dimensional flows around structures and over rough terrain. J. Computational Physics, Vol. 10, 1972, pp 324-340.

5. VIECELLI, J.A.: Computing method for incompressible flows. J. Computational Physics, Vol. 8, 1971, pp 119-143.

6. KOLLMANN, W.: Basic numerical techniques. VKI CN 107, October 1979.

7. ROACHE, P.J.: Computational fluid dynamics. Hermosa Publishers, Albuquerque, New Mexico, 1976.

8. BUFFAT, M. et al.: Calcul de l'écoulement dans la zone de pluie d'un réfrigérant atmosphérique à contre-courant. Seizièmes Journées de l'Hydraulique "Rejets de Chaleur à l'Atmosphère", Paris 16-18 septembre, 1980.

9. WHITE, F.M.: Viscous fluid flow. McGraw-Hill, 1974, p 208.

10. ALPERT, R.L. & MATHEWS, M.K.: Calculation of large-scale flow fields induced by droplet sprays. Factory Mutual Research Corp., Norwood, Massachusetts, OEOJ4 BU-RC79-BT-14, December 1979.

11. DUNDAS, P.H.: The scaling of sprinkler discharge : prediction of drop size. Progress Report No. 10 in Optimization of Sprinkler Fire Protection, Technical Report RC73-T-40, Factory Mutual Research Corporation, Norwood, Massachusetts, June 1974.

12. HESKESTAD, G.; JUNG, H.C.; TODTENKOPF, N.F.: Air entrainment into water sprays and spray curtains. ASME P 76 WA/FE 40, 1976.

13. BUCHLIN, J-M.: Aerodynamic behaviour of liquid spray.
Part 1 - A mathematical model.
VKI TR 1979-162.

14. BOTTERUD, S.: Behaviour of liquid spray in air.
VKI PR 1980-06.

15. BUCHLIN, J-M.: Aerodynamic behaviour of liquid spray.
Part 2 - Experimental procedure.
VKI TR 1979-168.

16. WEINACHT, P.: A numerical investigation of the dynamics
of liquid spray.
VKI PR 1981-24.

17. MOODIE, K.; TAYLOR, G.; BECKETT, H.: private communication.
Health & Safety Executive, Research and Laboratory
Services Division.

18. SELMER-OLSEN, S.: Calculation of the quasi three dimensional
atmospheric dispersion of a pollutant of any density
in the presence of water spray curtains.
VKI PR 1982-13.

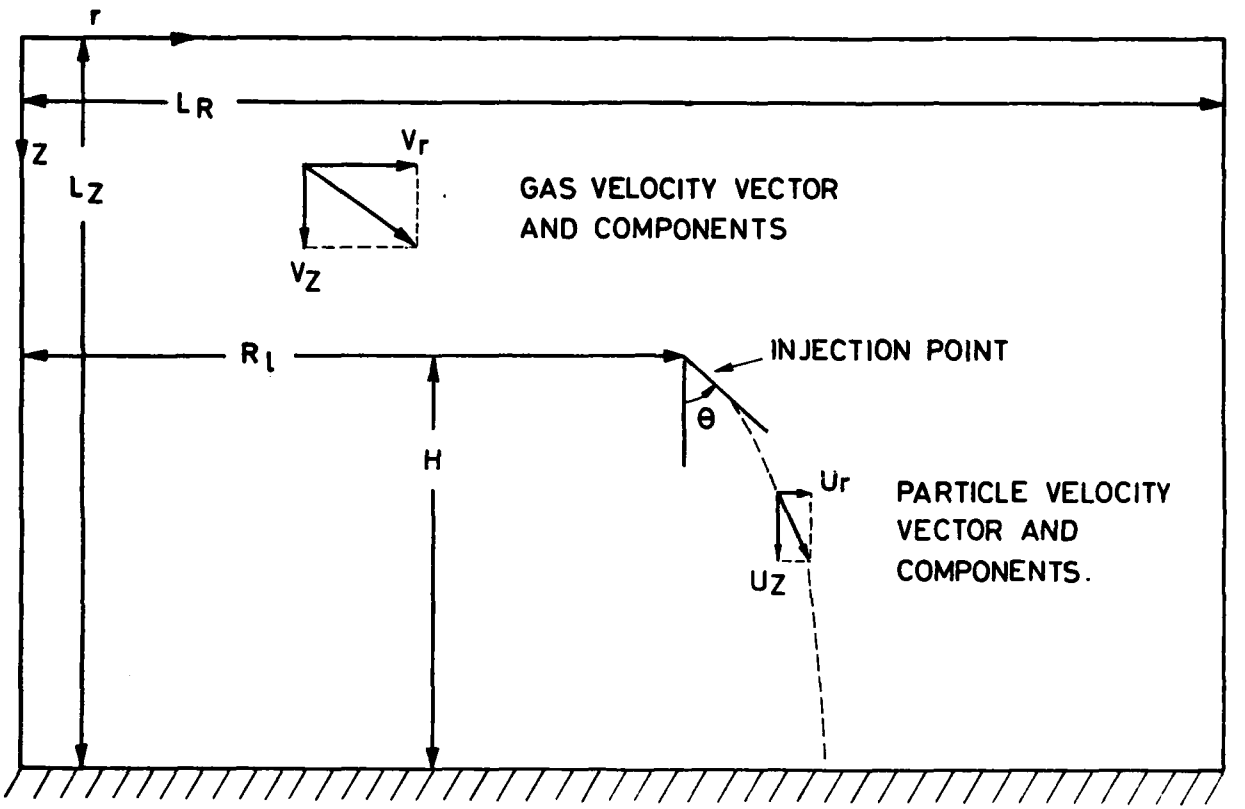

FIG. 2.1 - DOMAIN OF INTEREST

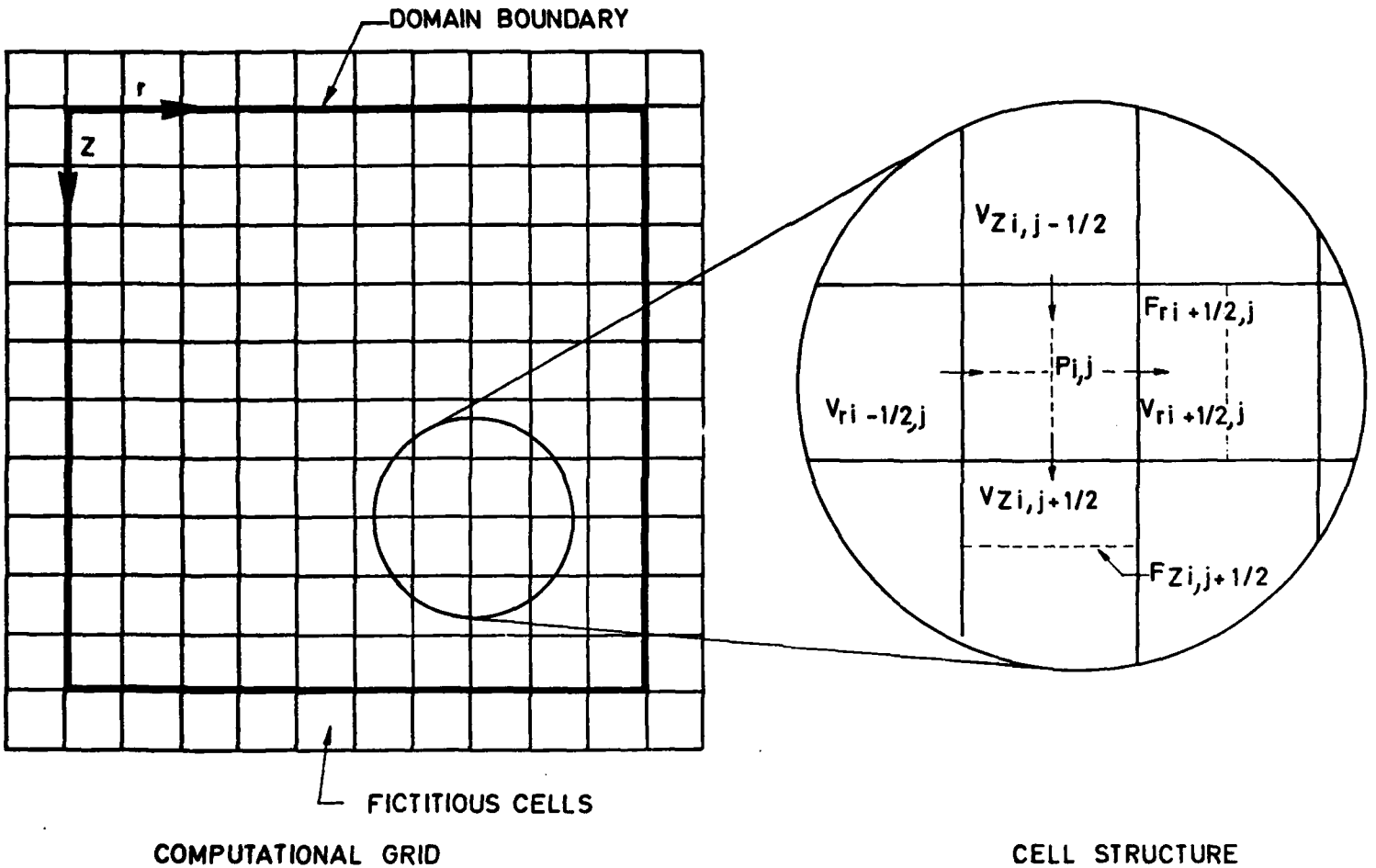

FIG. 3.1 - SMAC CELL STRUCTURE FOR THE GAS PHASE COMPUTATION.

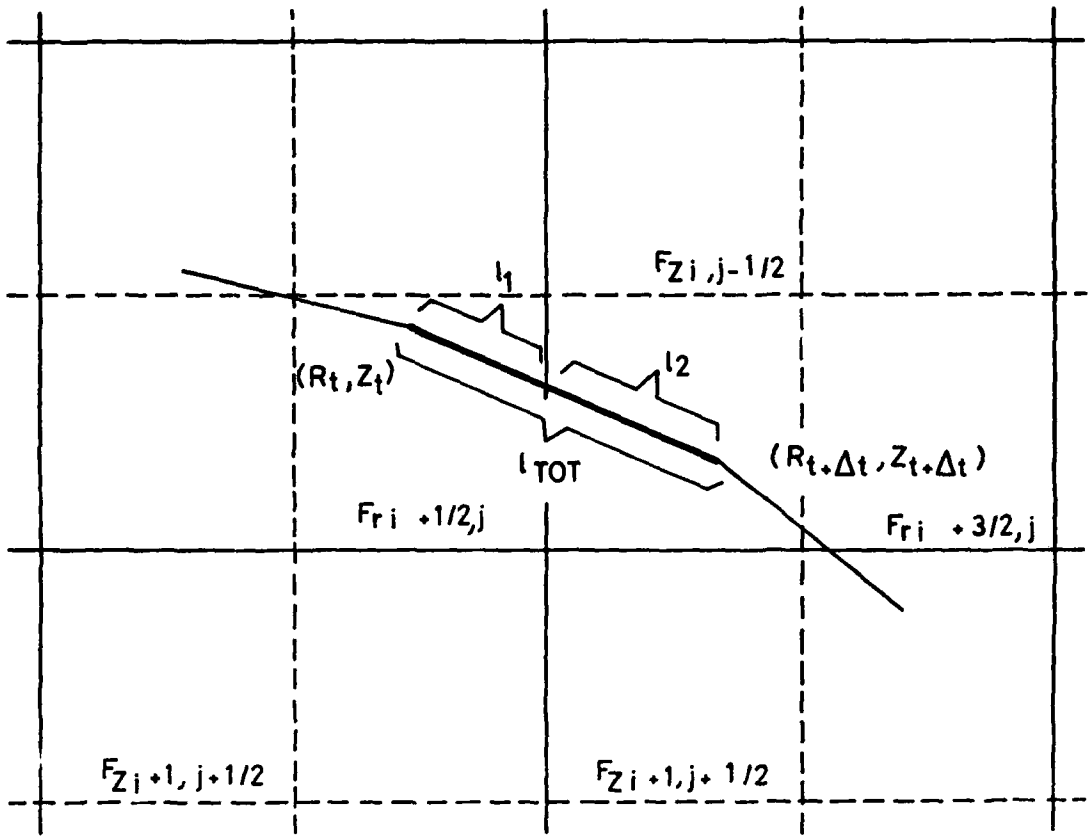

FIG. 3.2 - PARTICLE TRAJECTORY CROSSING MOMENTUM SOURCE CELLS.

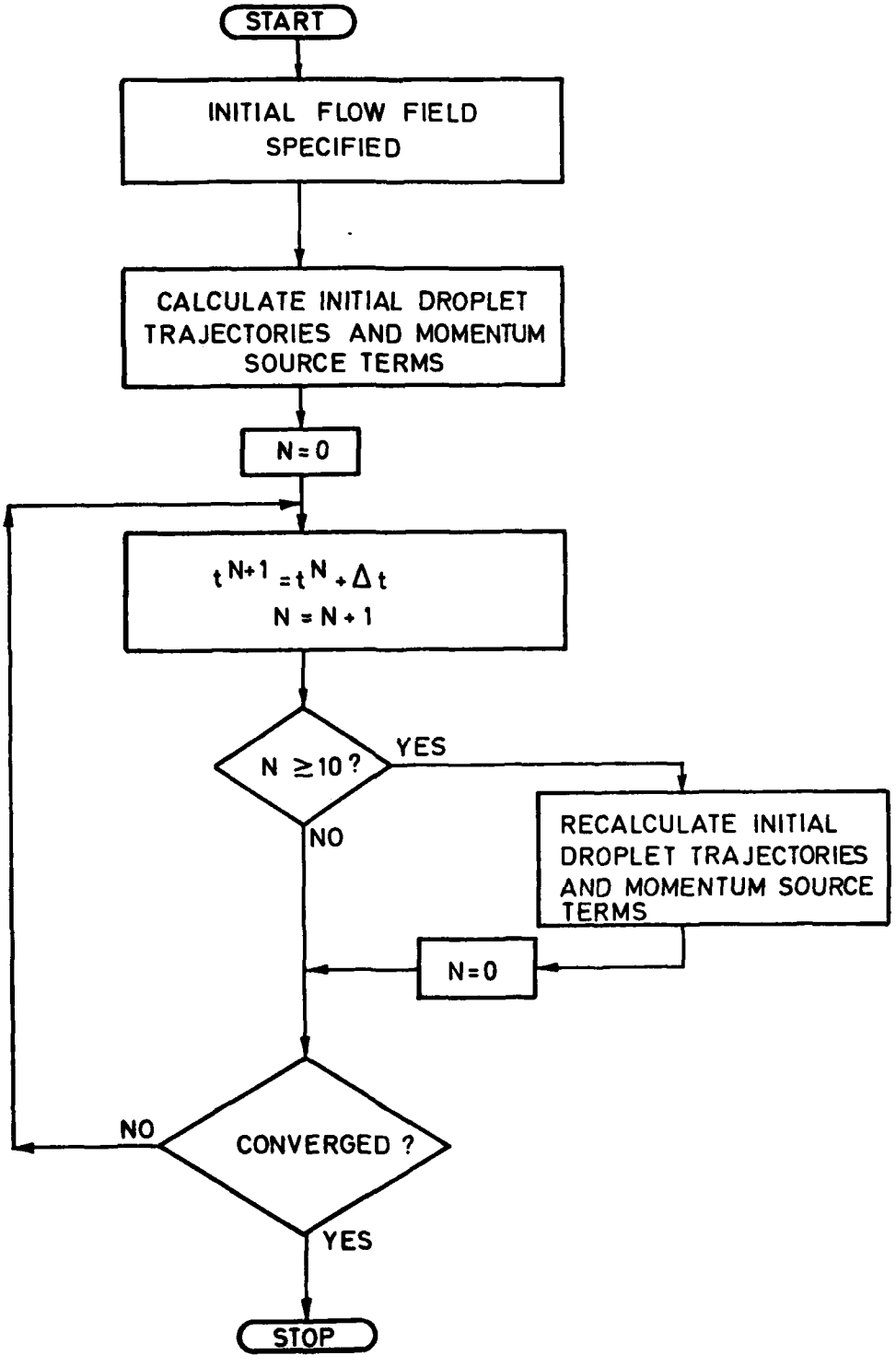

FIG. 3.3 - COMPUTATIONAL PROCEDURE

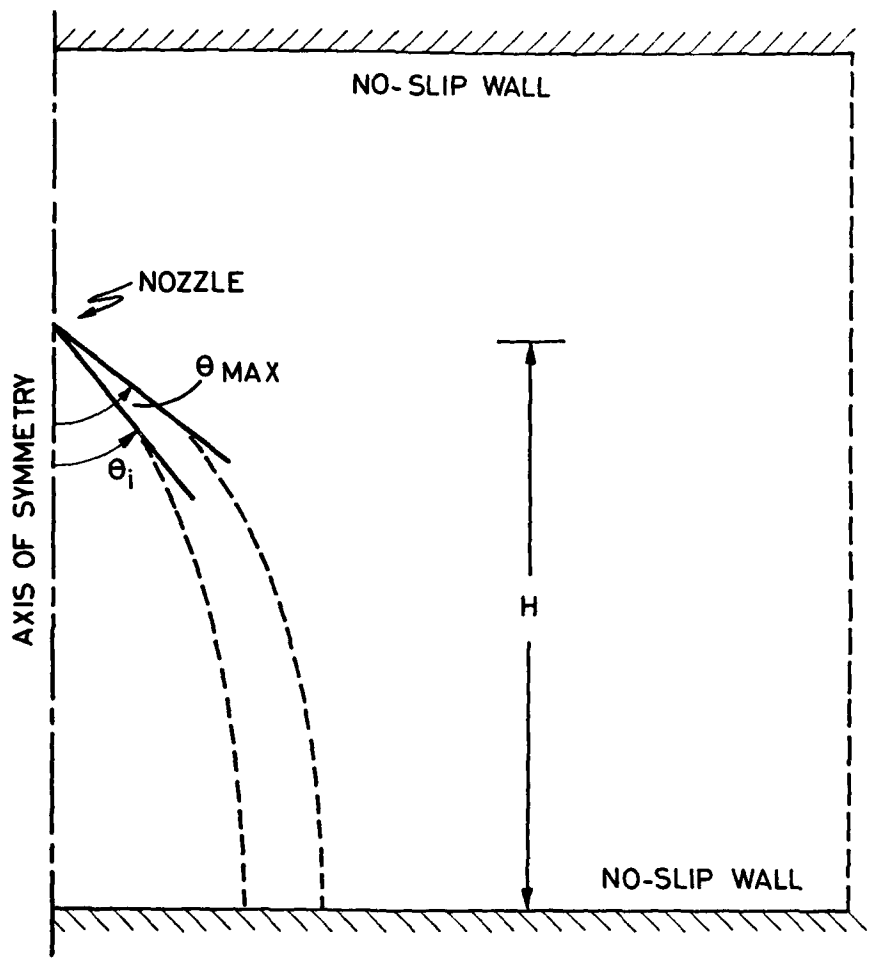

FIG. 4.1.1 – COMPUTATIONAL DOMAIN FOR AXISYMMETRIC SPRAYS.

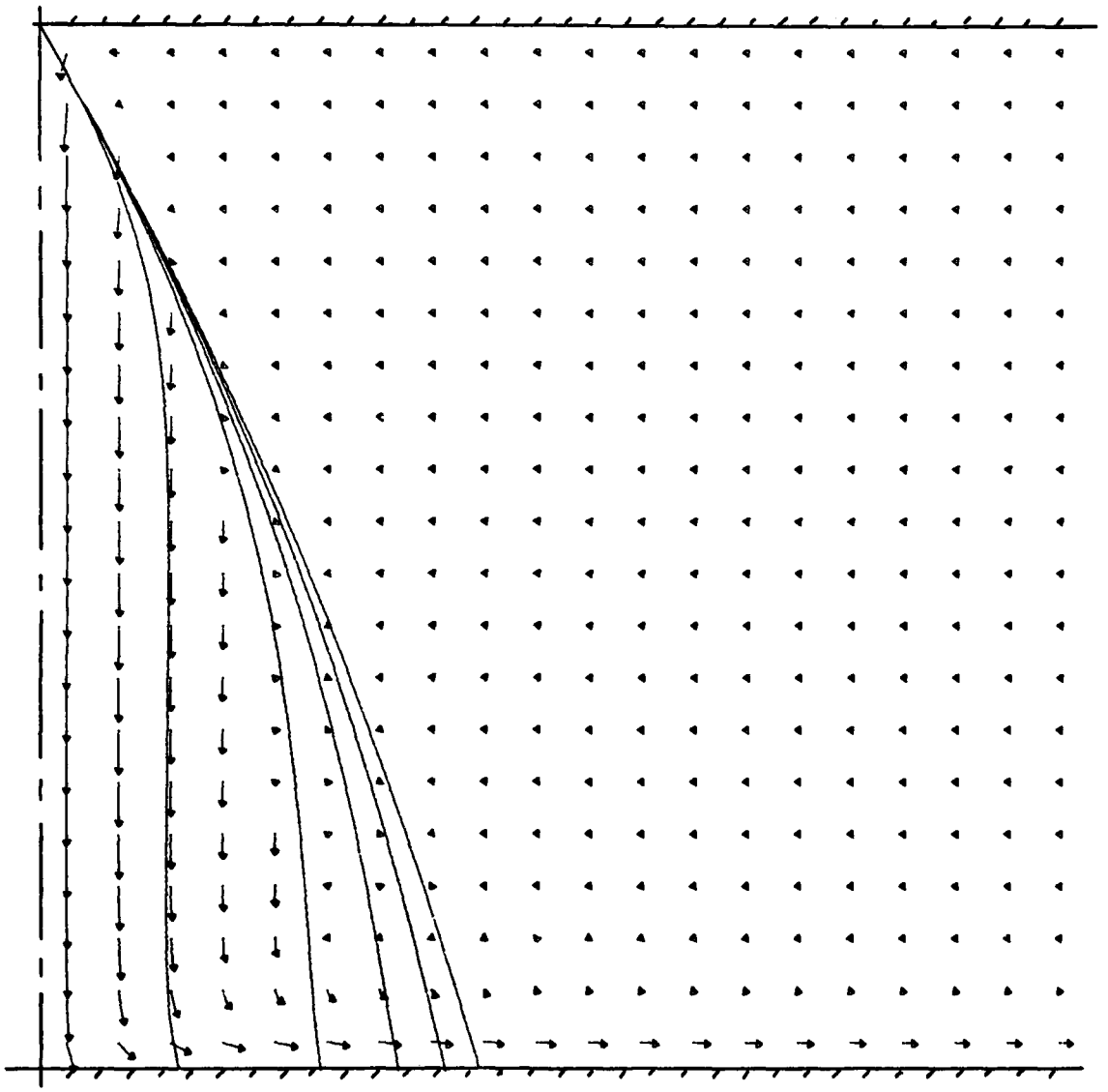

→ CORRESPONDS TO A GAS VELOCITY = 2.20 M/S

SZ1 NOZZLE 30. DEGREE HALF ANGLE
VOLUME FLOW OF WATER = 6.6 LITERS PER MINUTE
DROPLET INJECTION VELOCITY = 7.2 M/S
MEAN DROP SIZE = .83 MM HEIGHT OF NOZZLE = 2.0 M

FIGURE 4-1-2 -FLOW FIELD DUE TO A SPRAY

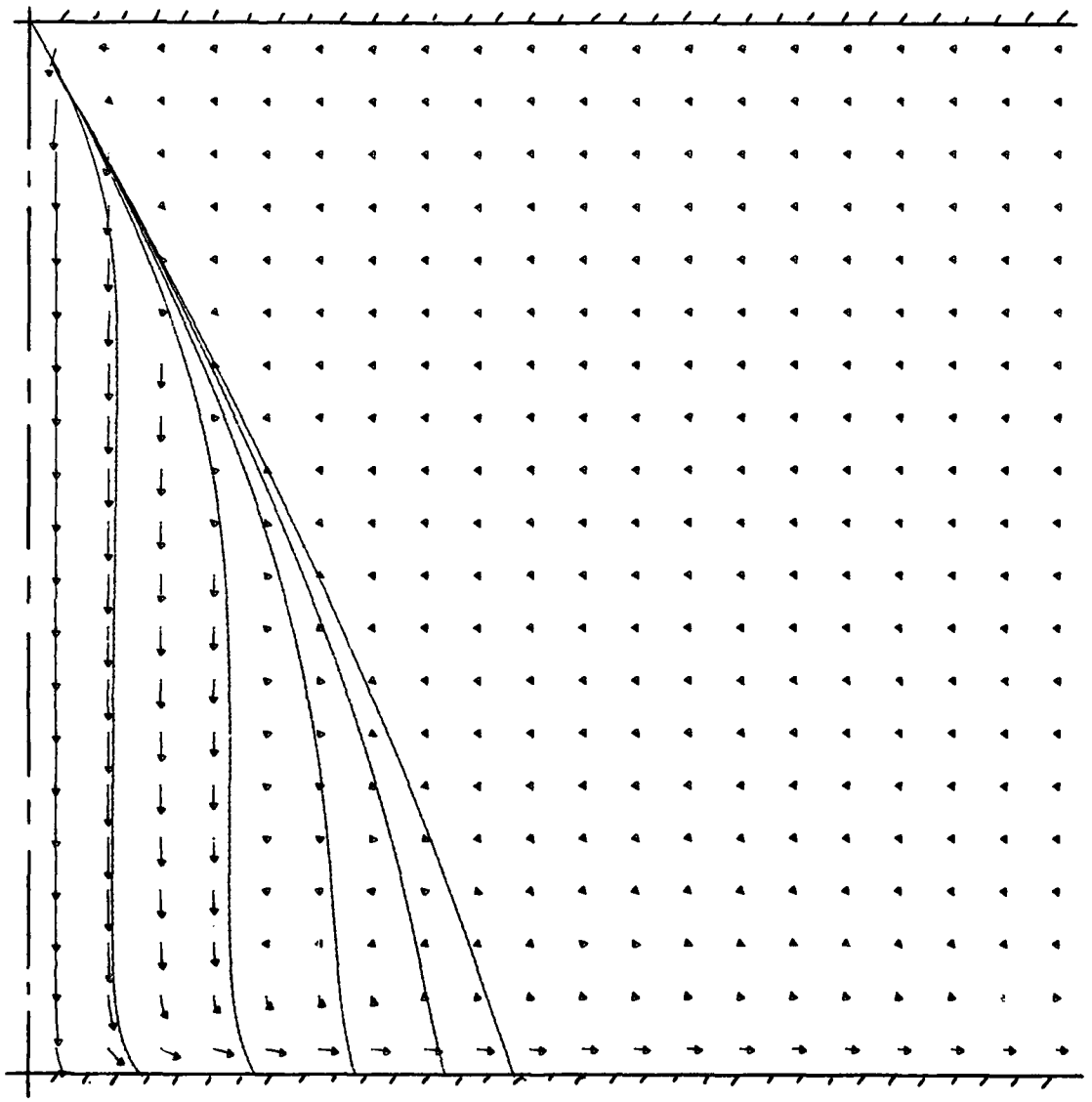

⟶ CORRESPONDS TO A GAS VELOCITY = 5.00 M/S

SZ1 NOZZLE 30. DEGREE HALF ANGLE
VOLUME FLOW OF WATER = 13.3 LITERS PER MINUTE
DROPLET INJECTION VELOCITY = 14.6 M/S
MEAN DROP SIZE = .48 MM HEIGHT OF NOZZLE = 2.0 M

FIGURE **4-1-3** -FLOW FIELD DUE TO A SPRAY

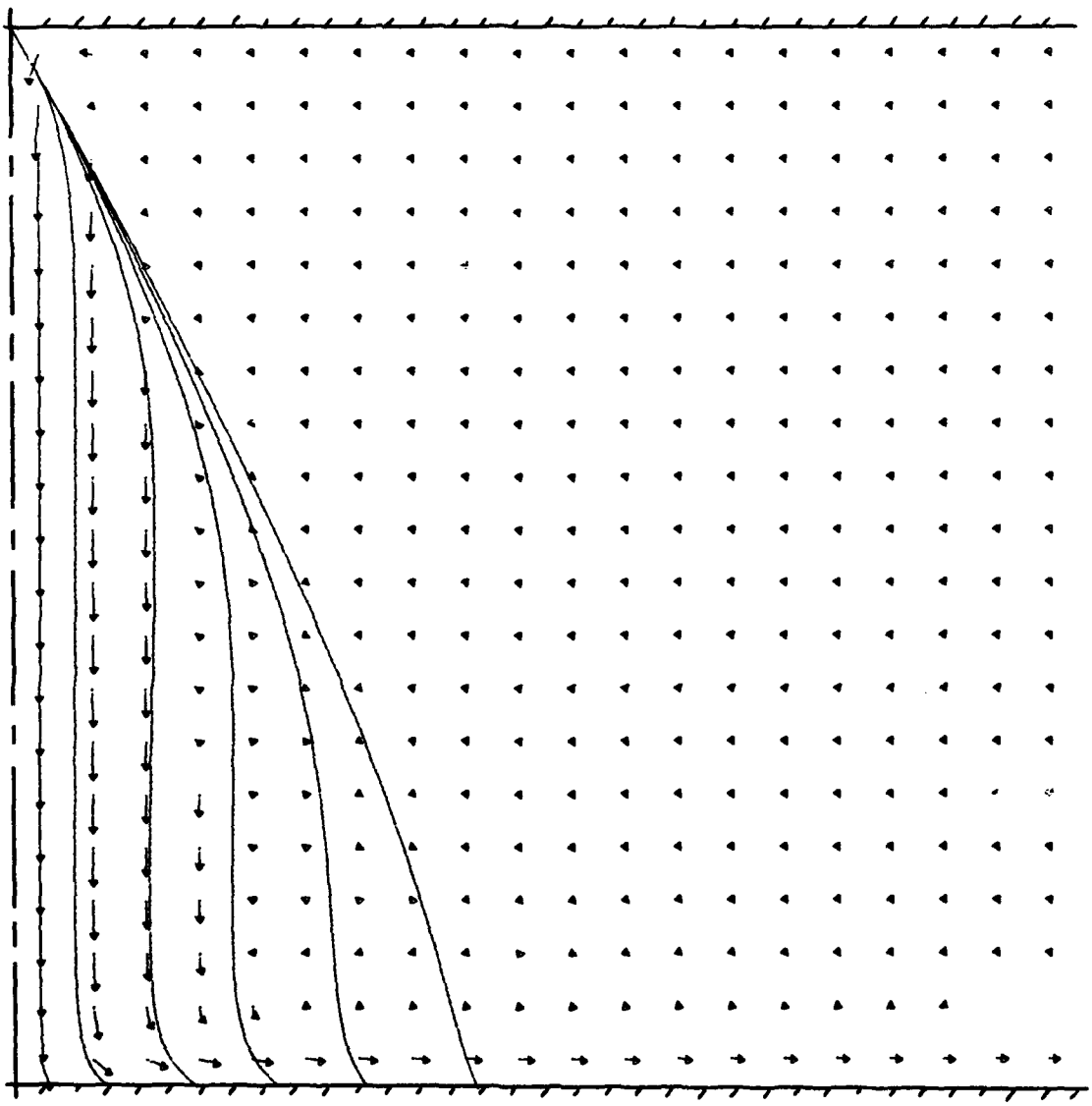

→ CORRESPONDS TO A GAS VELOCITY = 8.00 M/S

SZ1 NOZZLE 30. DEGREE HALF ANGLE
VOLUME FLOW OF WATER = 21.1 LITERS PER MINUTE
DROPLET INJECTION VELOCITY = 23.2 M/S
MEAN DROP SIZE = .32 MM HEIGHT OF NOZZLE = 2.0 M

FIGURE 4-1-4 -FLOW FIELD DUE TO A SPRAY

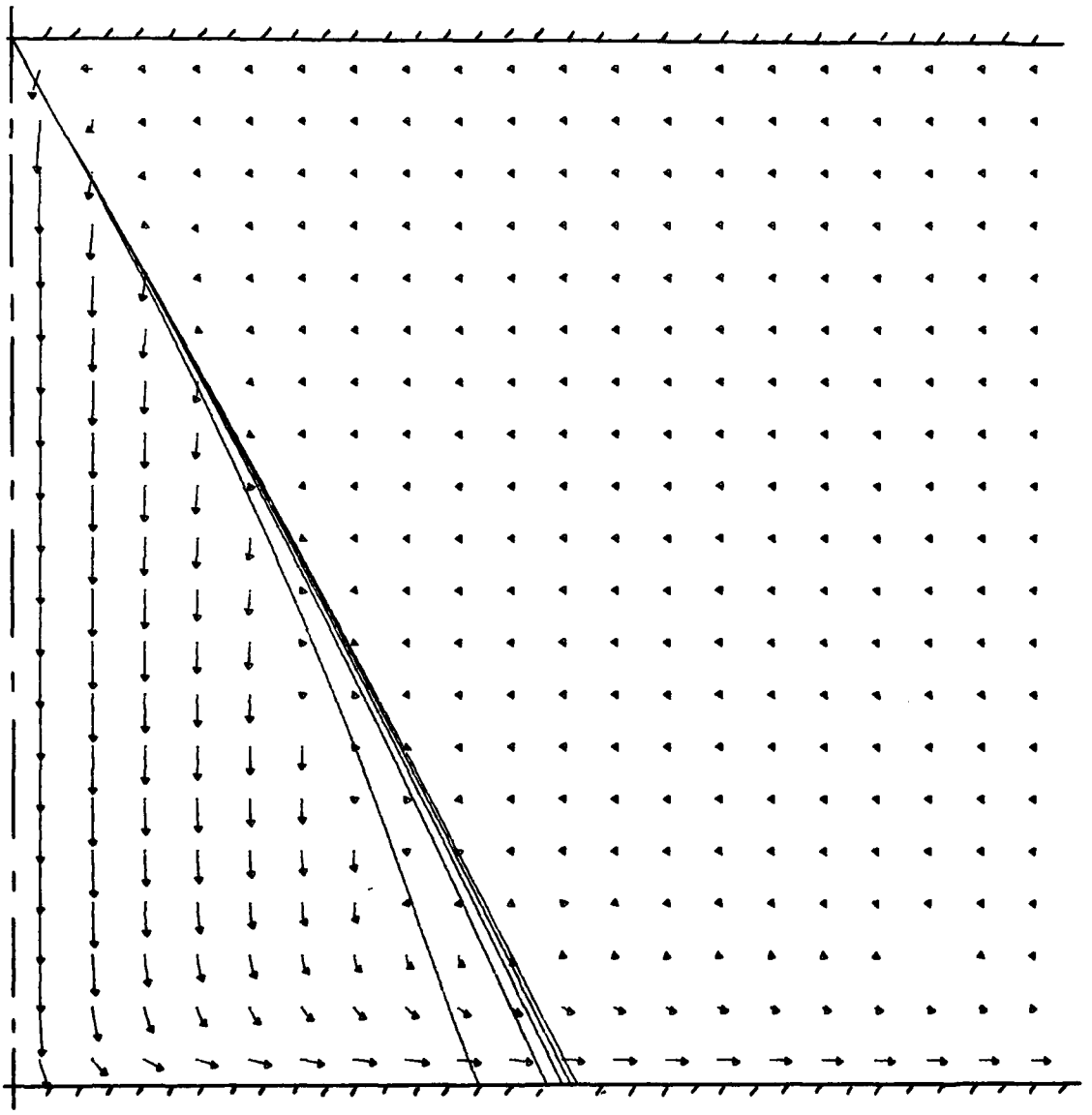

⟶ CORRESPONDS TO A GAS VELOCITY = 4.10 M/S

SZ1 NOZZLE 30. DEGREE HALF ANGLE
VOLUME FLOW OF WATER = 6.6 LITERS PER MINUTE
DROPLET INJECTION VELOCITY = 7.2 M/S
MEAN DROP SIZE = .83 MM HEIGHT OF NOZZLE = 0.4 M

FIGURE 4-1-5 -FLOW FIELD DUE TO A SPRAY

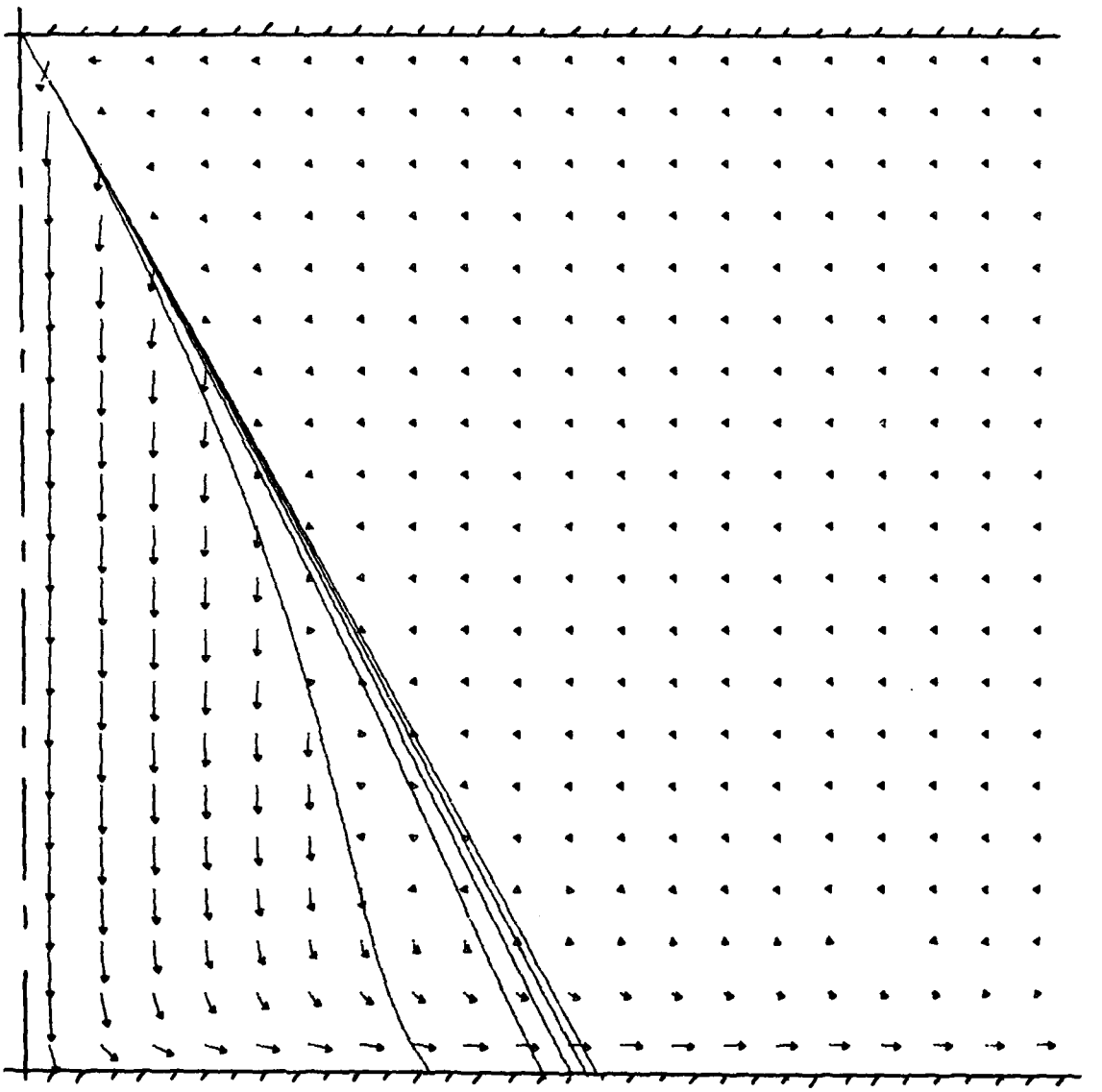

→ CORRESPONDS TO A GAS VELOCITY = 9.50 M/S

SZ1 NOZZLE 30. DEGREE HALF ANGLE
VOLUME FLOW OF WATER = 13.3 LITERS PER MINUTE
DROPLET INJECTION VELOCITY = 14.6 M/S
MEAN DROP SIZE = .48 MM HEIGHT OF NOZZLE = 0.4 M

FIGURE 4-1-6 -FLOW FIELD DUE TO A SPRAY

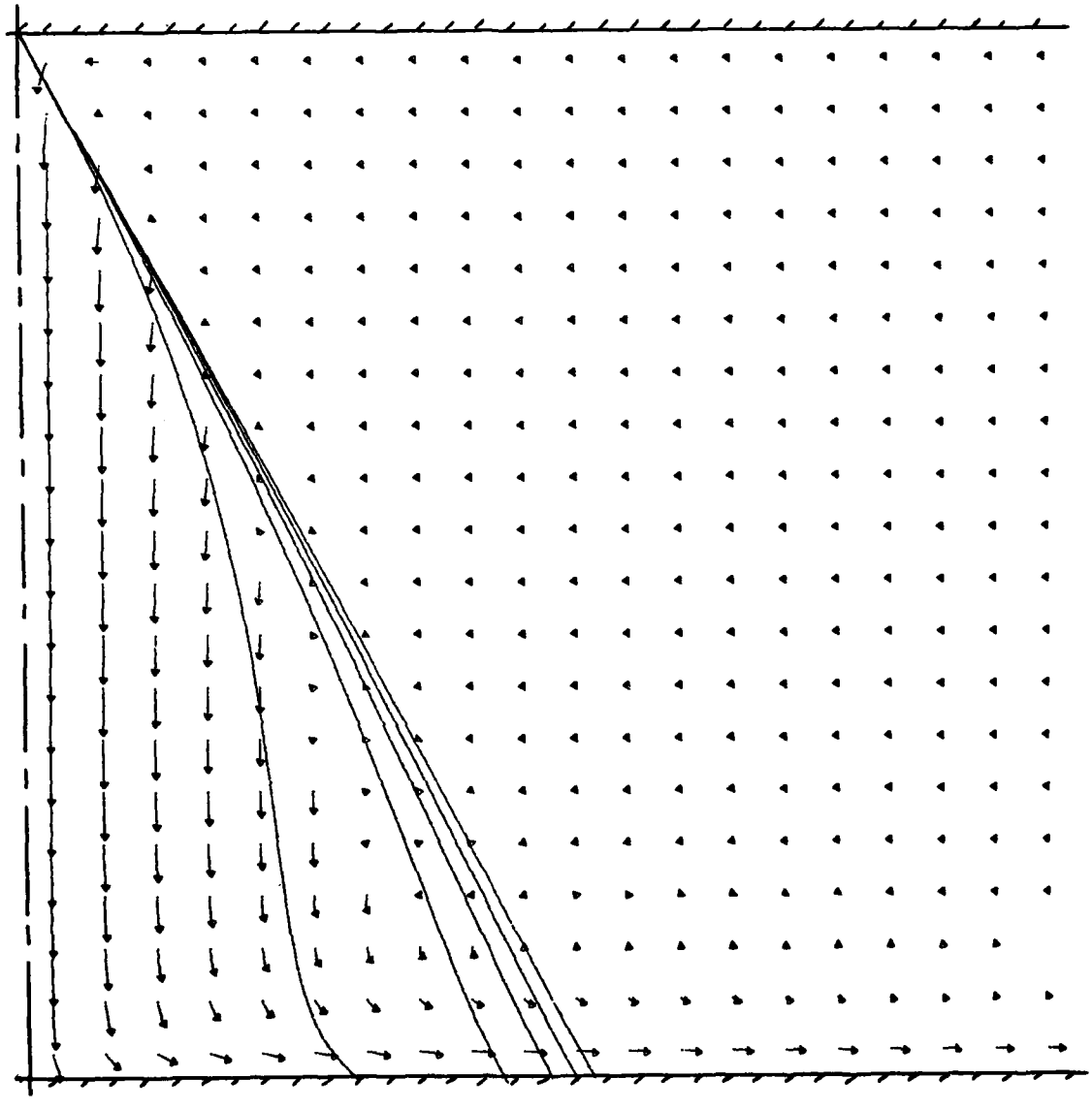

→ CORRESPONDS TO A GAS VELOCITY = 17.00 M/S

SZ1 NOZZLE 30. DEGREE HALF ANGLE
VOLUME FLOW OF WATER = 21.1 LITERS PER MINUTE
DROPLET INJECTION VELOCITY = 23.2 M/S
MEAN DROP SIZE = .32 MM HEIGHT OF NOZZLE = 2.0 M

FIGURE 4-1-7 -FLOW FIELD DUE TO A SPRAY

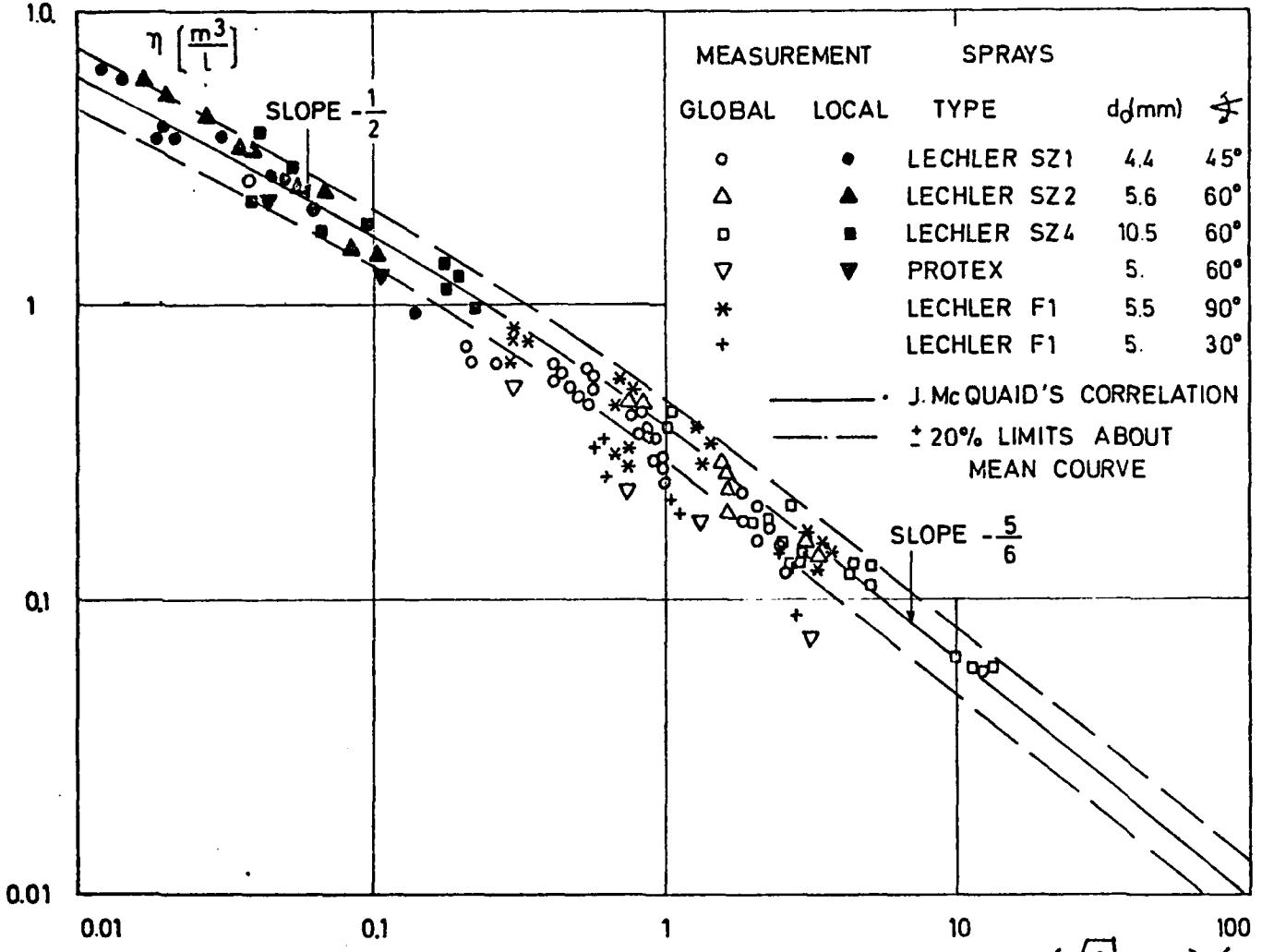

FIG. 4-1-8 -PERFORMANCES DATA FOR SPRAYS

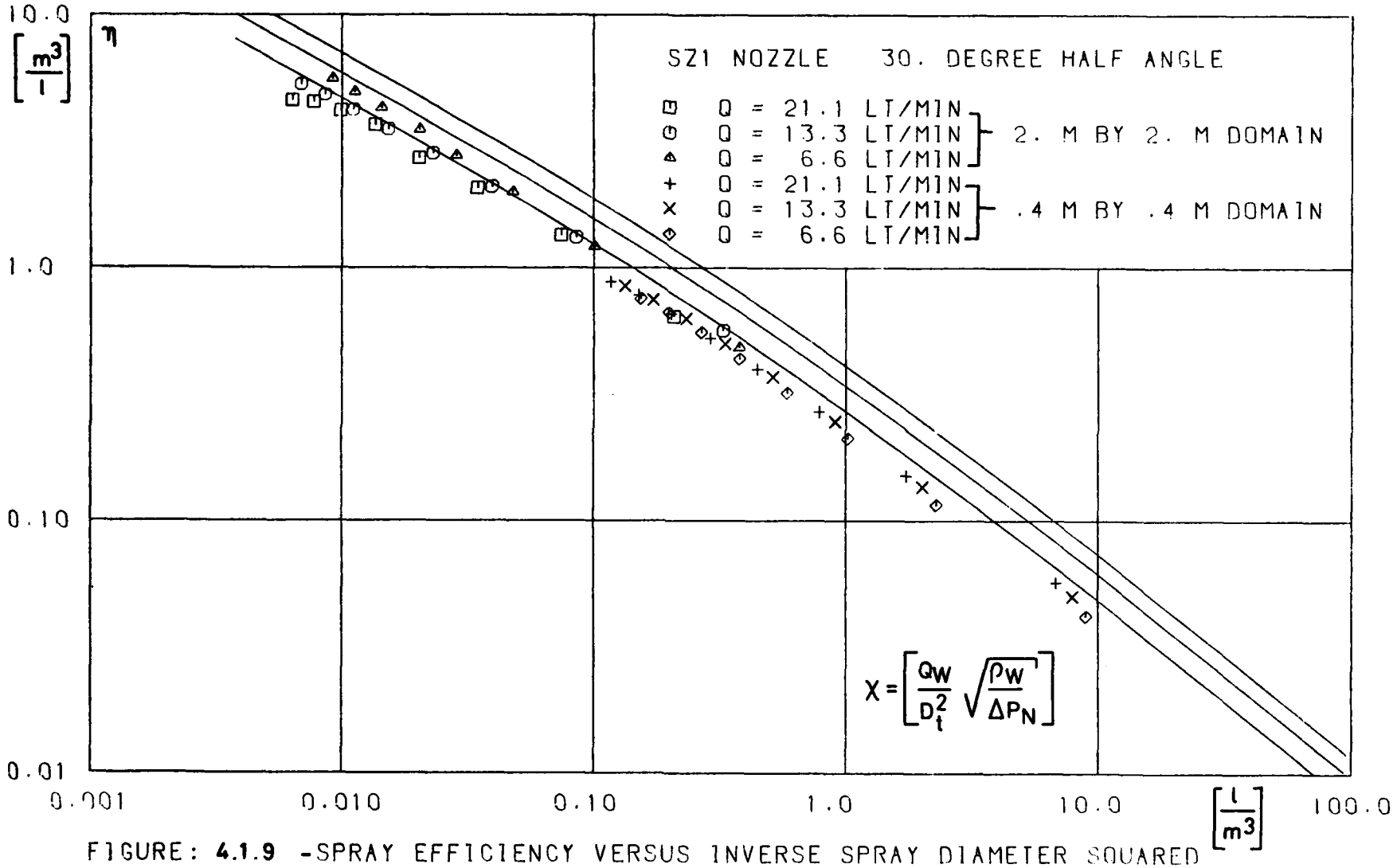

FIGURE: **4.1.9** -SPRAY EFFICIENCY VERSUS INVERSE SPRAY DIAMETER SQUARED

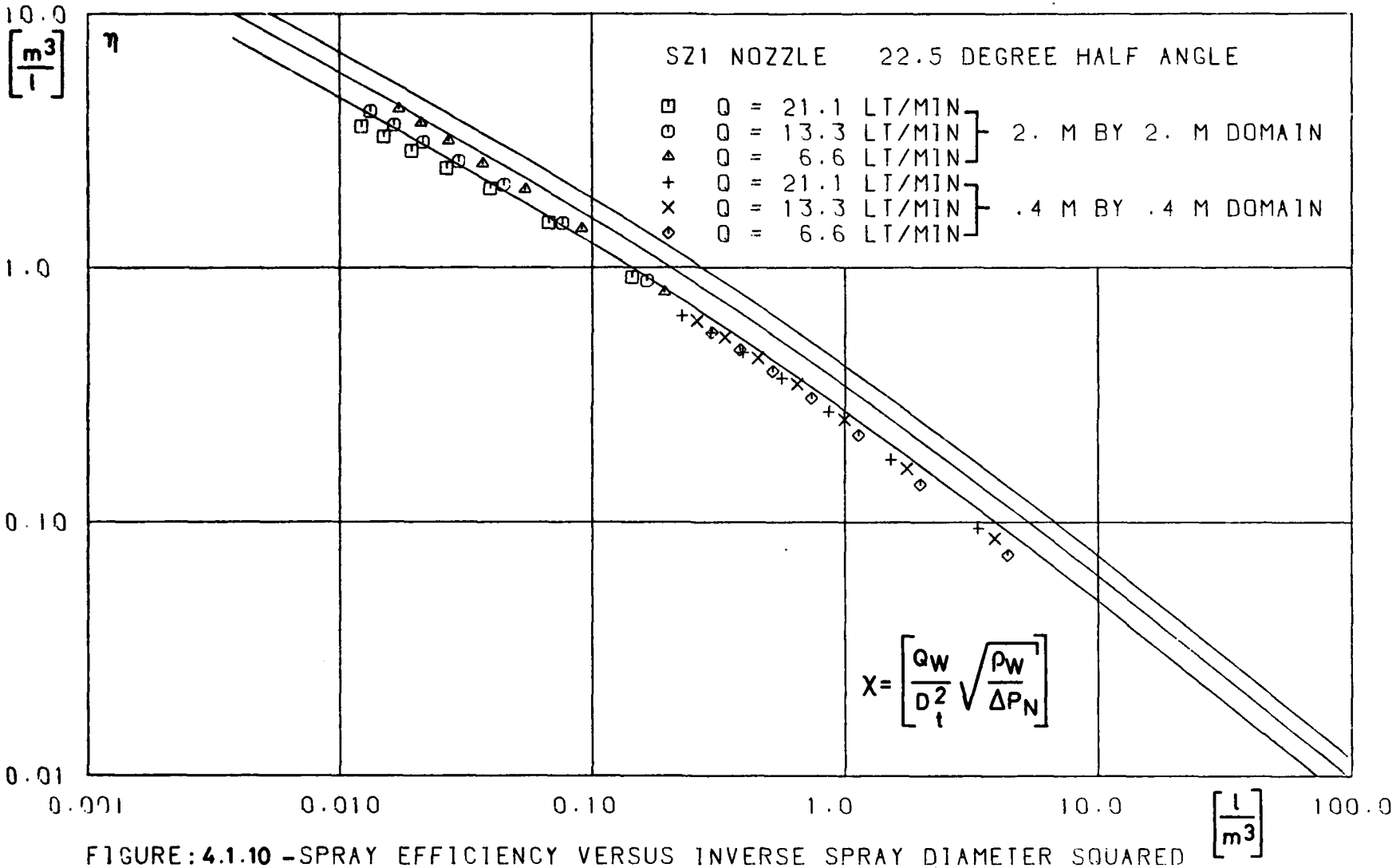

FIGURE: **4.1.10** – SPRAY EFFICIENCY VERSUS INVERSE SPRAY DIAMETER SQUARED

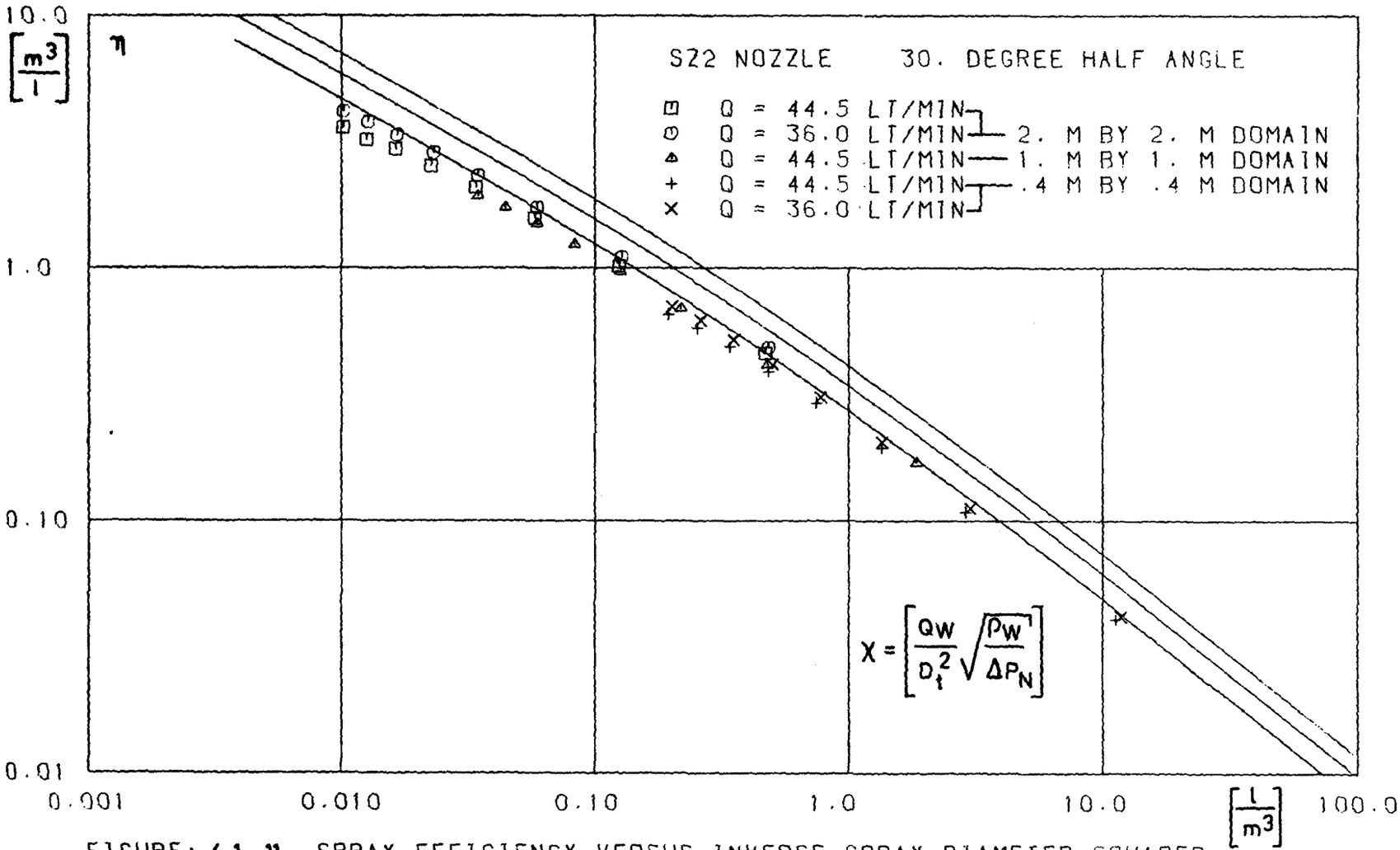

FIGURE: 4.1.11 -SPRAY EFFICIENCY VERSUS INVERSE SPRAY DIAMETER SQUARED

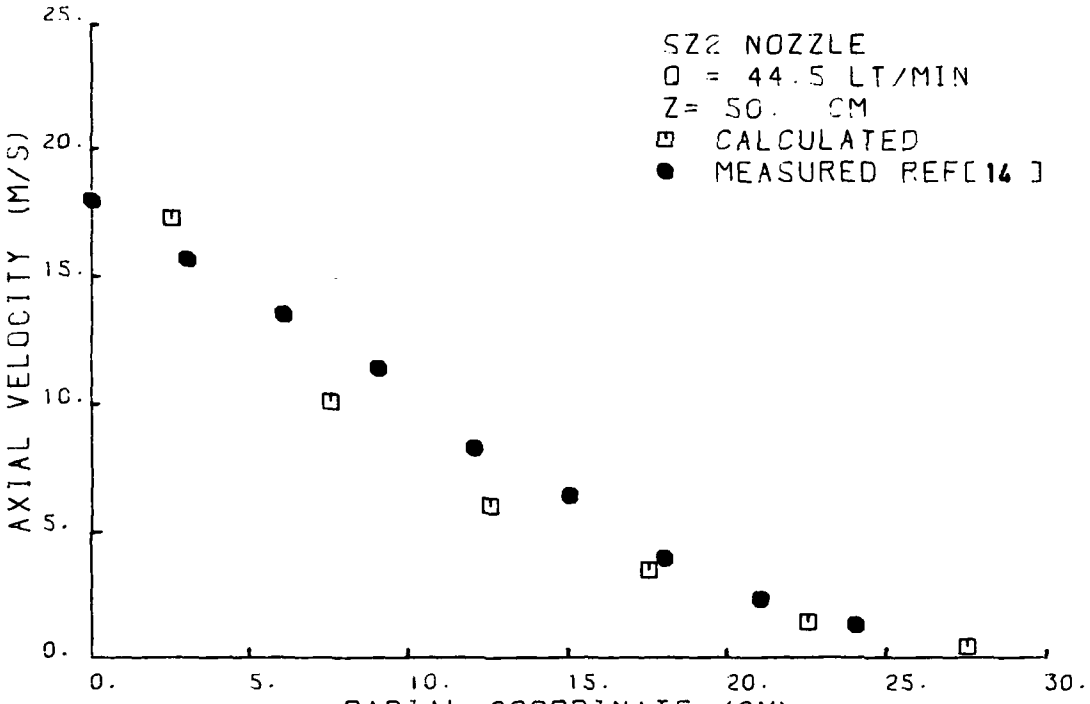

FIGURE 4-1-12 -PREDICTED AND MEASURED VELOCITIES INSIDE THE SPRAY

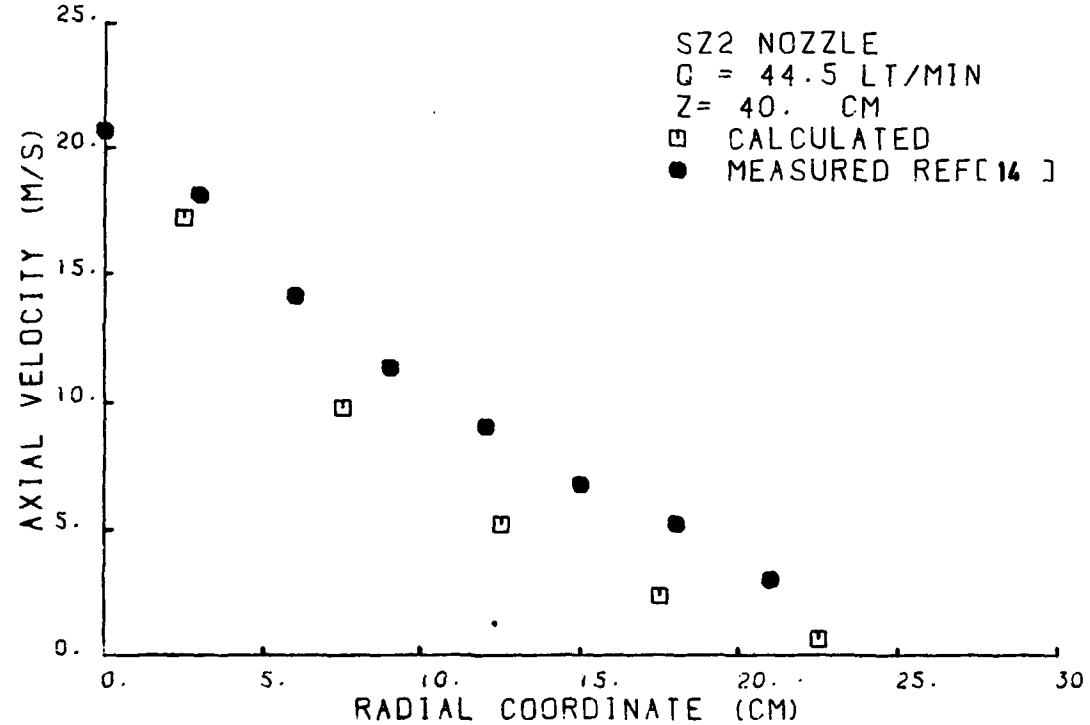

FIGURE 4-1-13 -PREDICTED AND MEASURED VELOCITIES INSIDE THE SPRAY

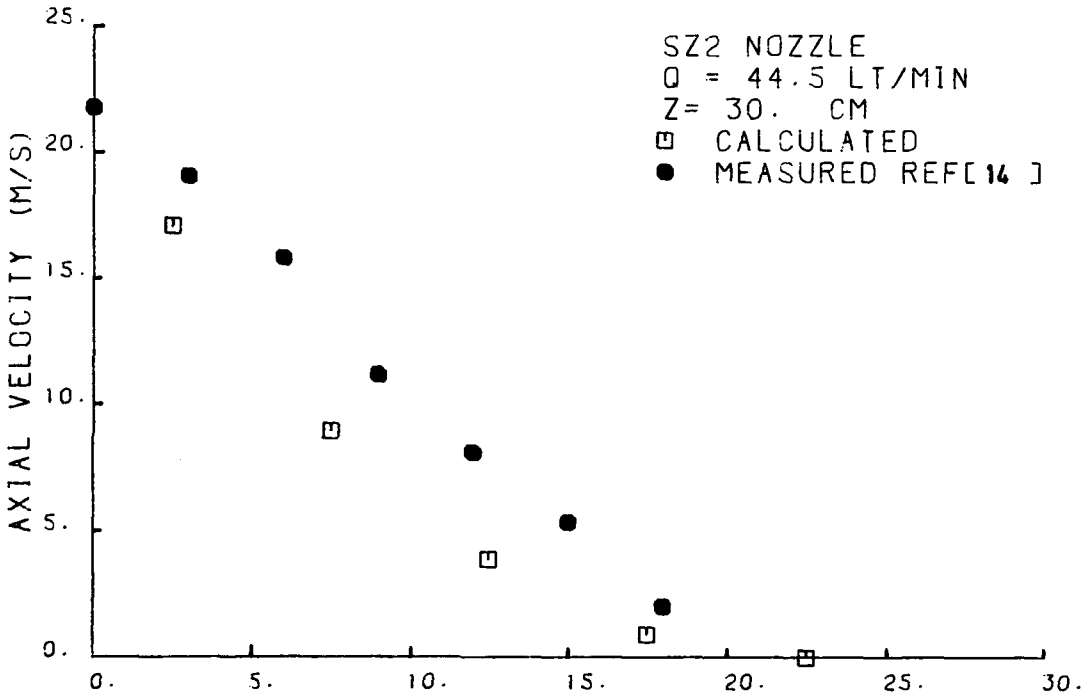

FIGURE 4.1.14 -PREDICTED AND MEASURED VELOCITIES INSIDE THE SPRAY

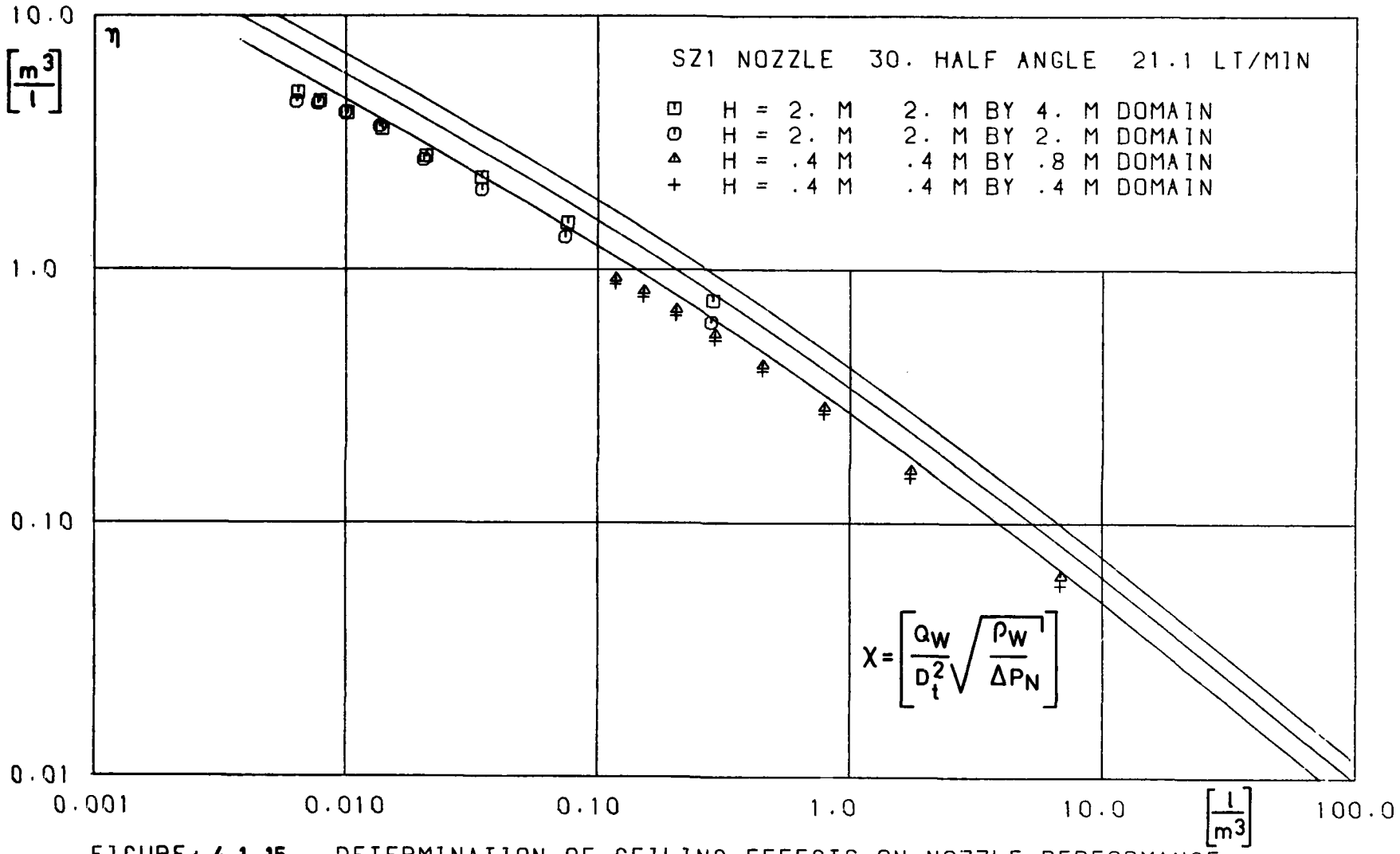

FIGURE: **4.1.15** - DETERMINATION OF CEILING EFFECTS ON NOZZLE PERFORMANCE

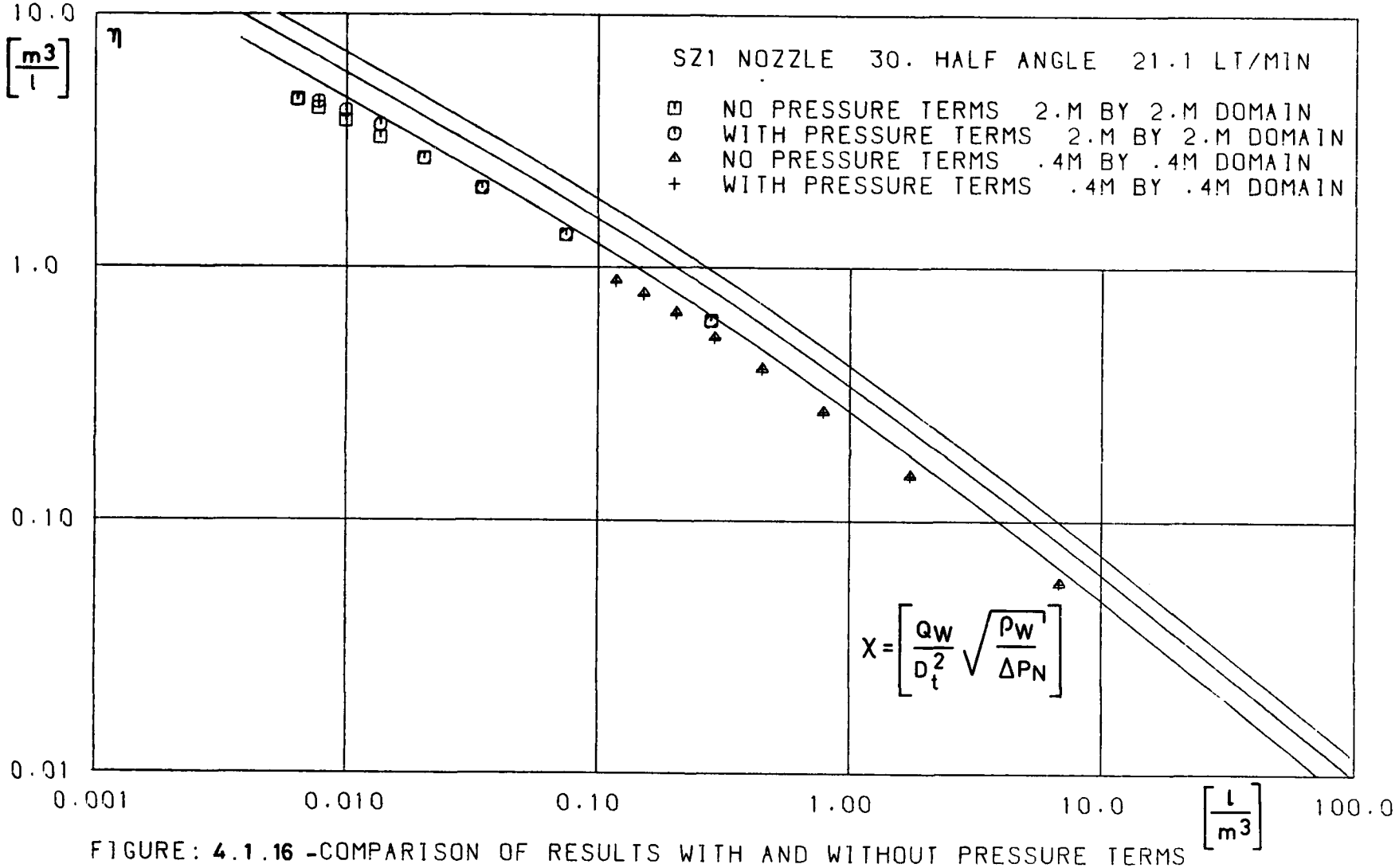

FIGURE: **4.1.16** -COMPARISON OF RESULTS WITH AND WITHOUT PRESSURE TERMS

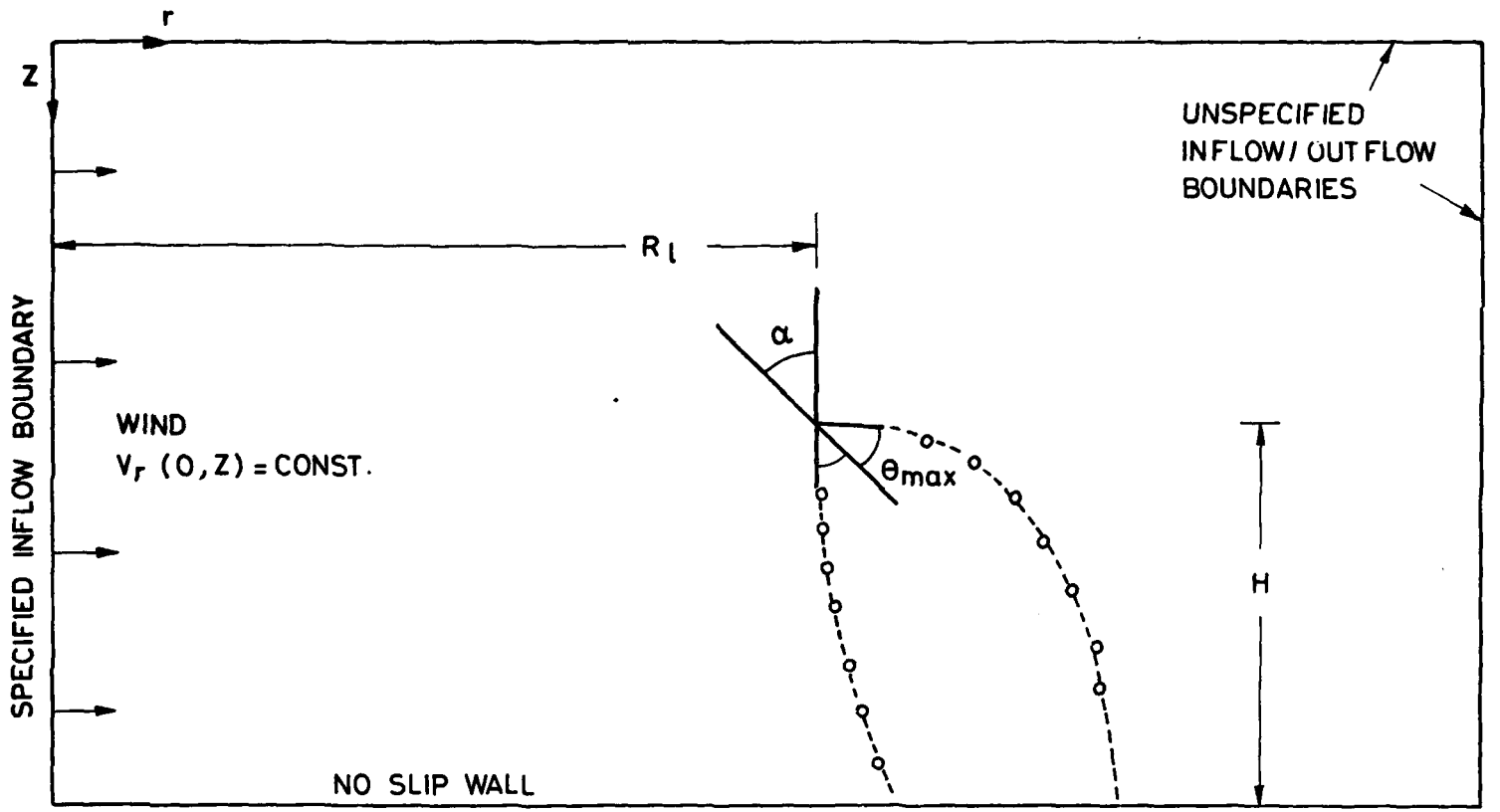

FIG. 4.2.1 - COMPUTATIONAL DOMAIN FOR PLANAR SPRAY CURTAIN

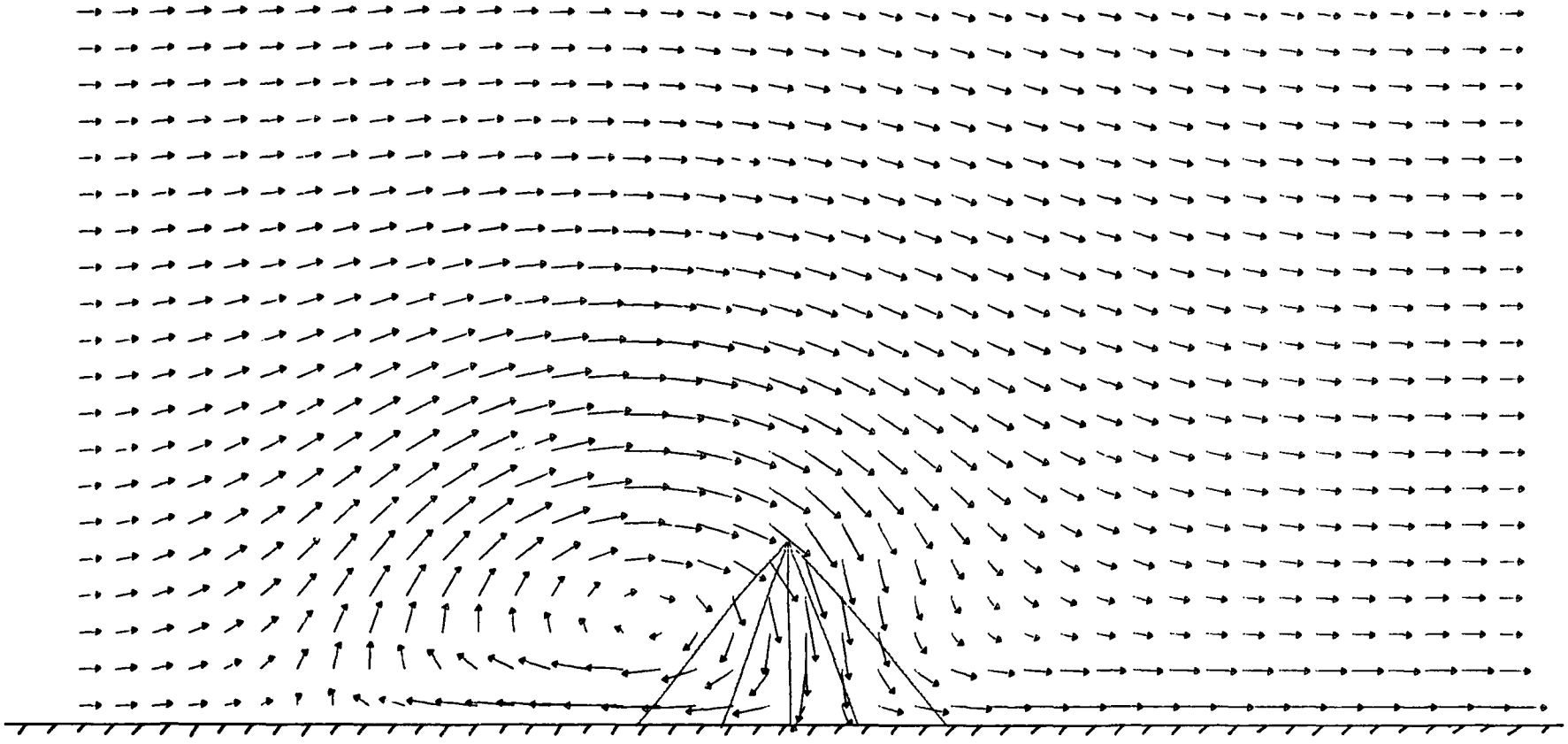

—→ CORRESPONDS TO A GAS VELOCITY = 3.00 M/S
WIND SPEED = 2.0 M/S HEIGHT OF NOZZLE = 2.5 METERS
VOLUME FLOW OF WATER = 3.0 LITERS PER SECOND PER METER
DROPLET INJECTION VELOCITY = 23.68 M/S DROPLET SIZE = 1.1 MM
CONE ANGLE OF SPRAY = 90. DEGREES TILT ANGLE = 0. DEGREES

FIGURE **4.2.2** -EFFECT OF WIND ON THE PERFORMANCE OF A SPRAY CURTAIN

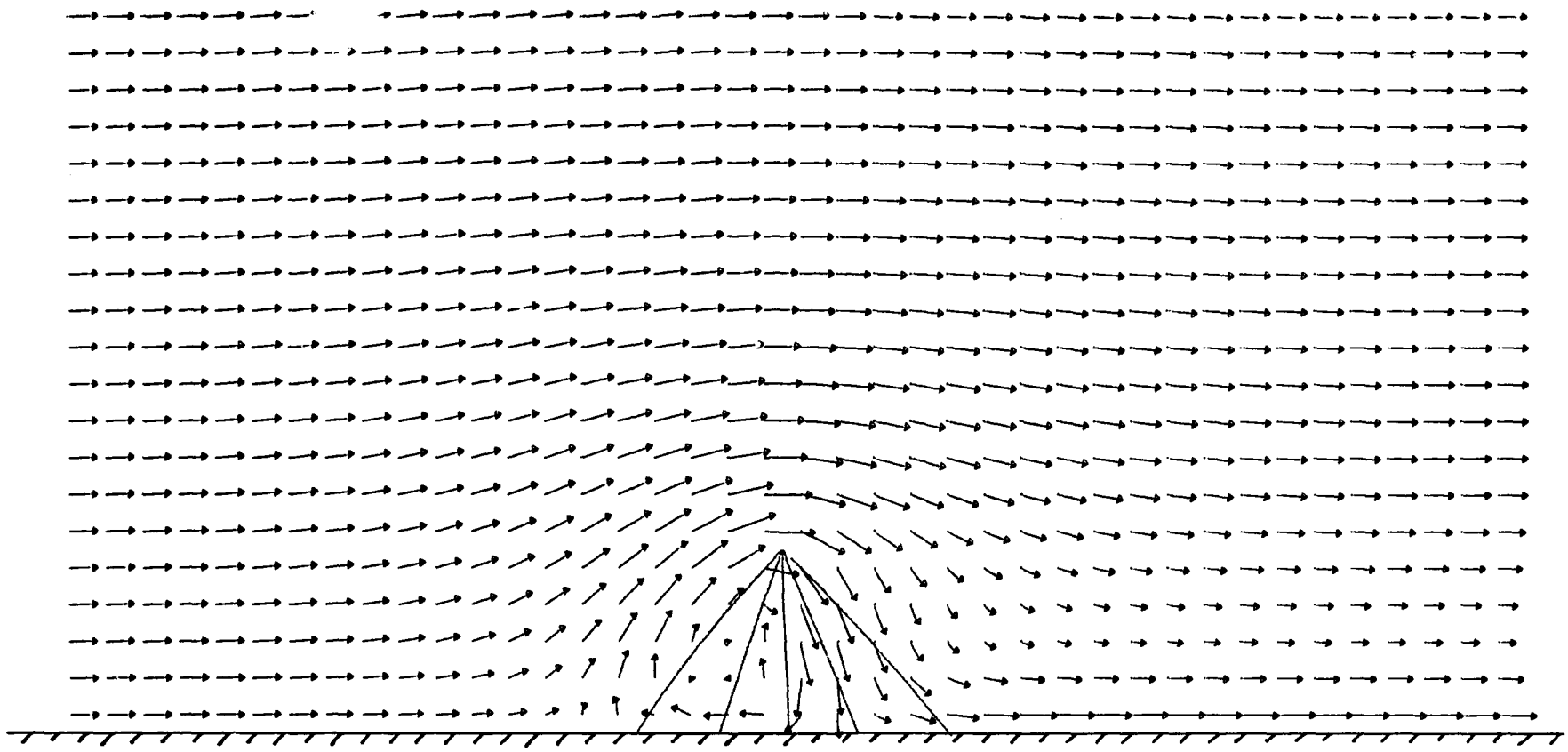

→ CORRESPONDS TO A GAS VELOCITY = 3.00 M/S
WIND SPEED = 2.5 M/S HEIGHT OF NOZZLE = 2.5 METERS
VOLUME FLOW OF WATER = 3.0 LITERS PER SECCND PER METER
DROPLET INJECTION VELOCITY = 23.68 M/S DROPLET SIZE = 1.1 MM
CONE ANGLE OF SPRAY = 90. DEGREES TILT ANGLE = 0. DEGREES

FIGURE **4.2.3** -EFFECT OF WIND ON THE PERFORMANCE OF A SPRAY CURTAIN

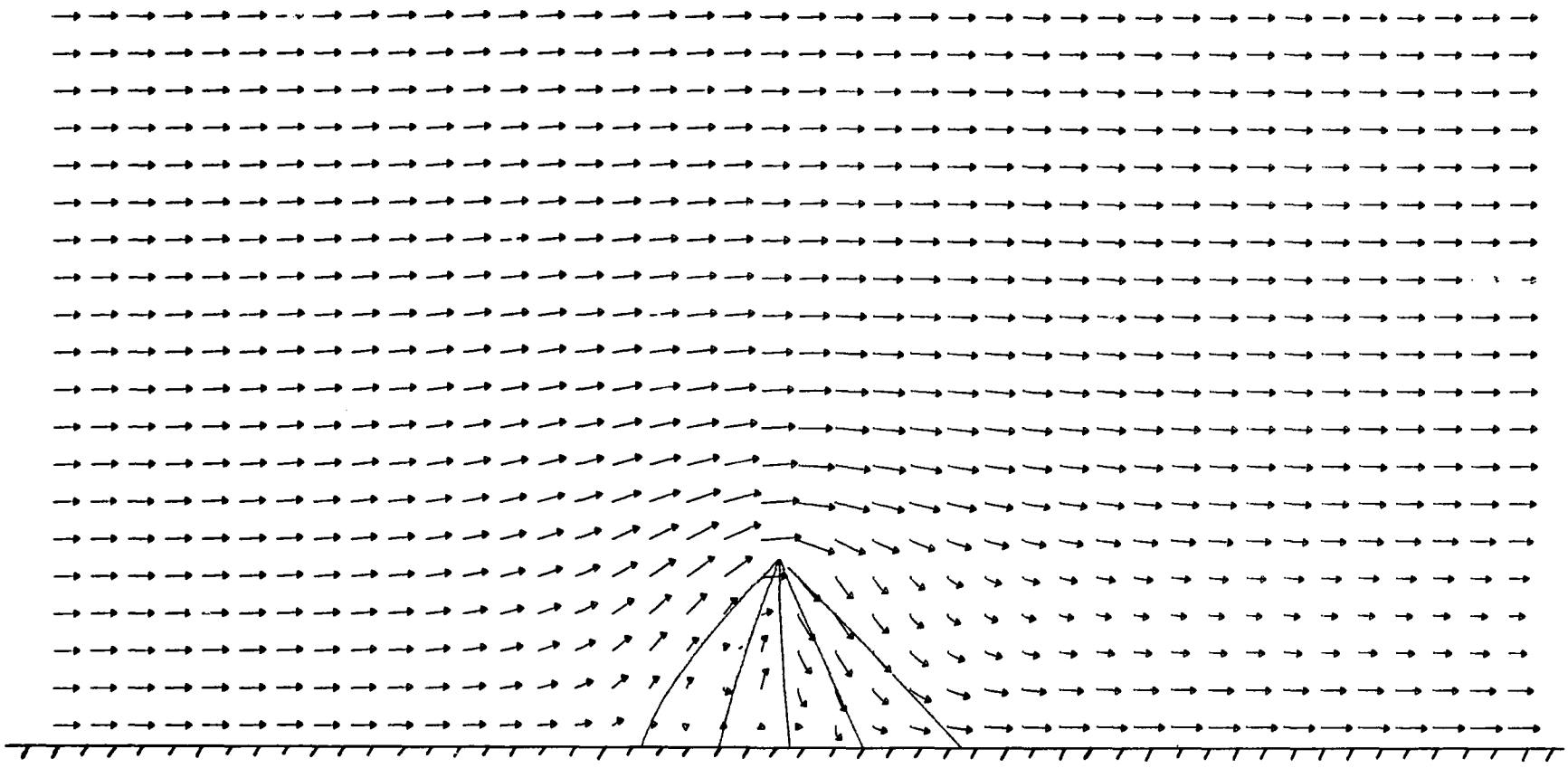

→ CORRESPONDS TO A GAS VELOCITY = 4.00 M/S
WIND SPEED = 3.0 M/S HEIGHT OF NOZZLE = 2.5 METERS
VOLUME FLOW OF WATER = 3.0 LITERS PER SECOND PER METER
DROPLET INJECTION VELOCITY = 23.68 M/S DROPLET SIZE = 1.1 MM
CONE ANGLE OF SPRAY = 90. DEGREES TILT ANGLE = 0. DEGREES

FIGURE 4.2.4 -EFFECT OF WIND ON THE PERFORMANCE OF A SPRAY CURTAIN

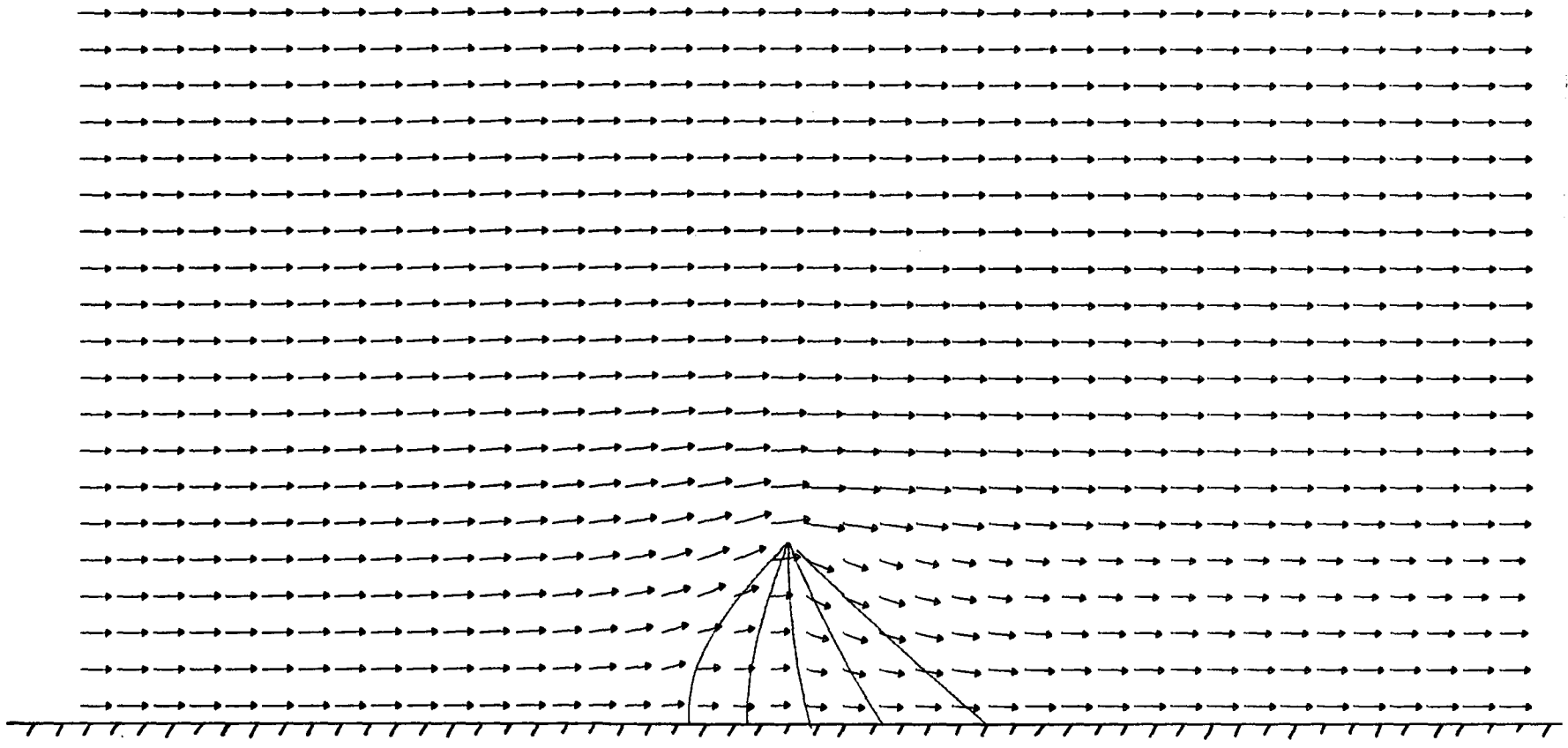

→ CORRESPONDS TO A GAS VELOCITY = 5.00 M/S
WIND SPEED = 4.5 M/S HEIGHT OF NOZZLE = 2.5 METERS
VOLUME FLOW OF WATER = 3.0 LITERS PER SECOND PER METER
DROPLET INJECTION VELOCITY = 23.68 M/S DROPLET SIZE = 1.1 MM
CONE ANGLE OF SPRAY = 90. DEGREES TILT ANGLE = 0. DEGREES

FIGURE **4.2.5** -EFFECT OF WIND ON THE PERFORMANCE OF A SPRAY CURTAIN

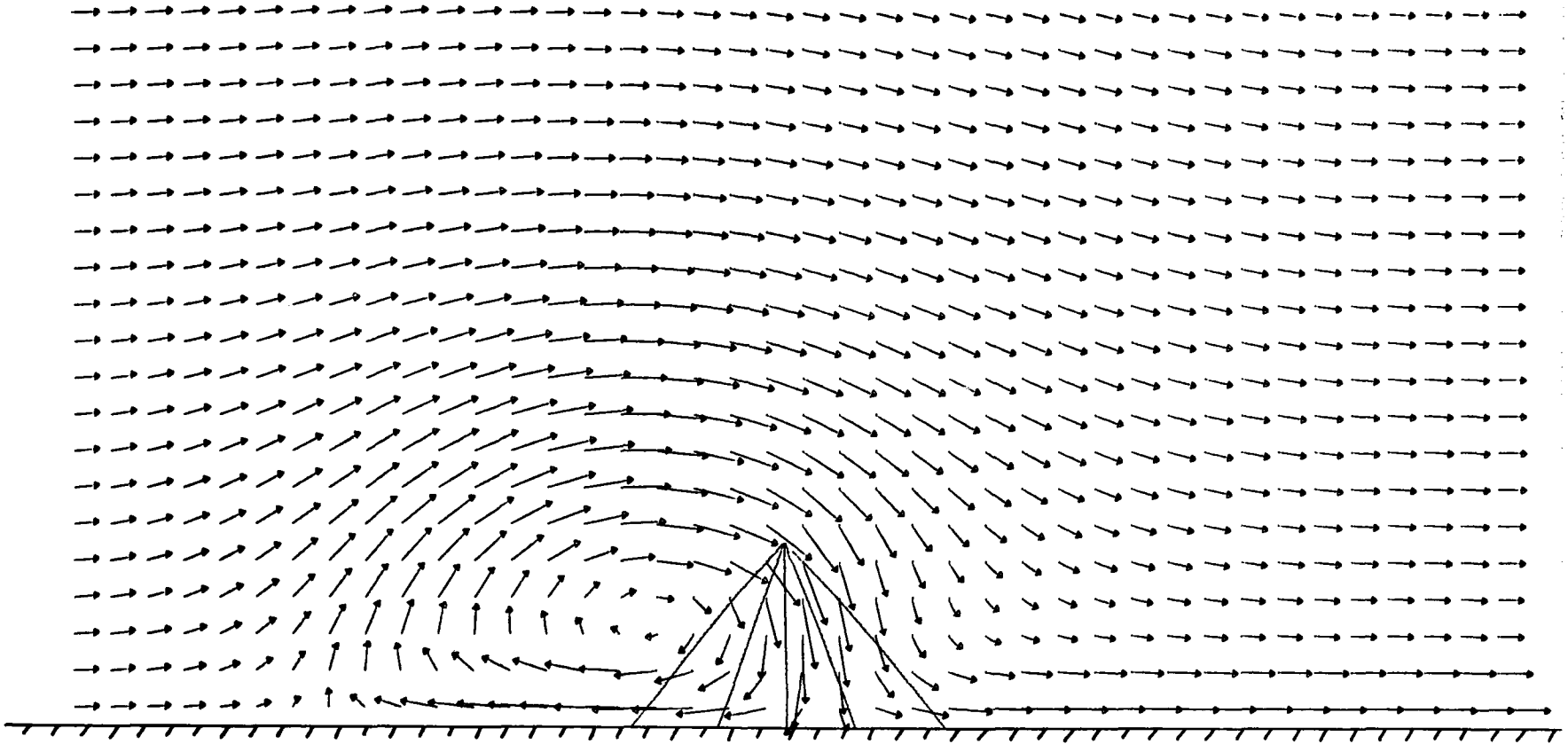

→ CORRESPONDS TO A GAS VELOCITY = 2.00 M/S
WIND SPEED = 1.5 M/S HEIGHT OF NOZZLE = 2.5 METERS
VOLUME FLOW OF WATER = 1.5 LITERS PER SECOND PER METER
DROPLET INJECTION VELOCITY = 23.68 M/S DROPLET SIZE = 1.1 MM
CONE ANGLE OF SPRAY = 90. DEGREES TILT ANGLE = 0. DEGREES

FIGURE **4.2.6** -EFFECT OF WIND ON THE PERFORMANCE OF A SPRAY CURTAIN

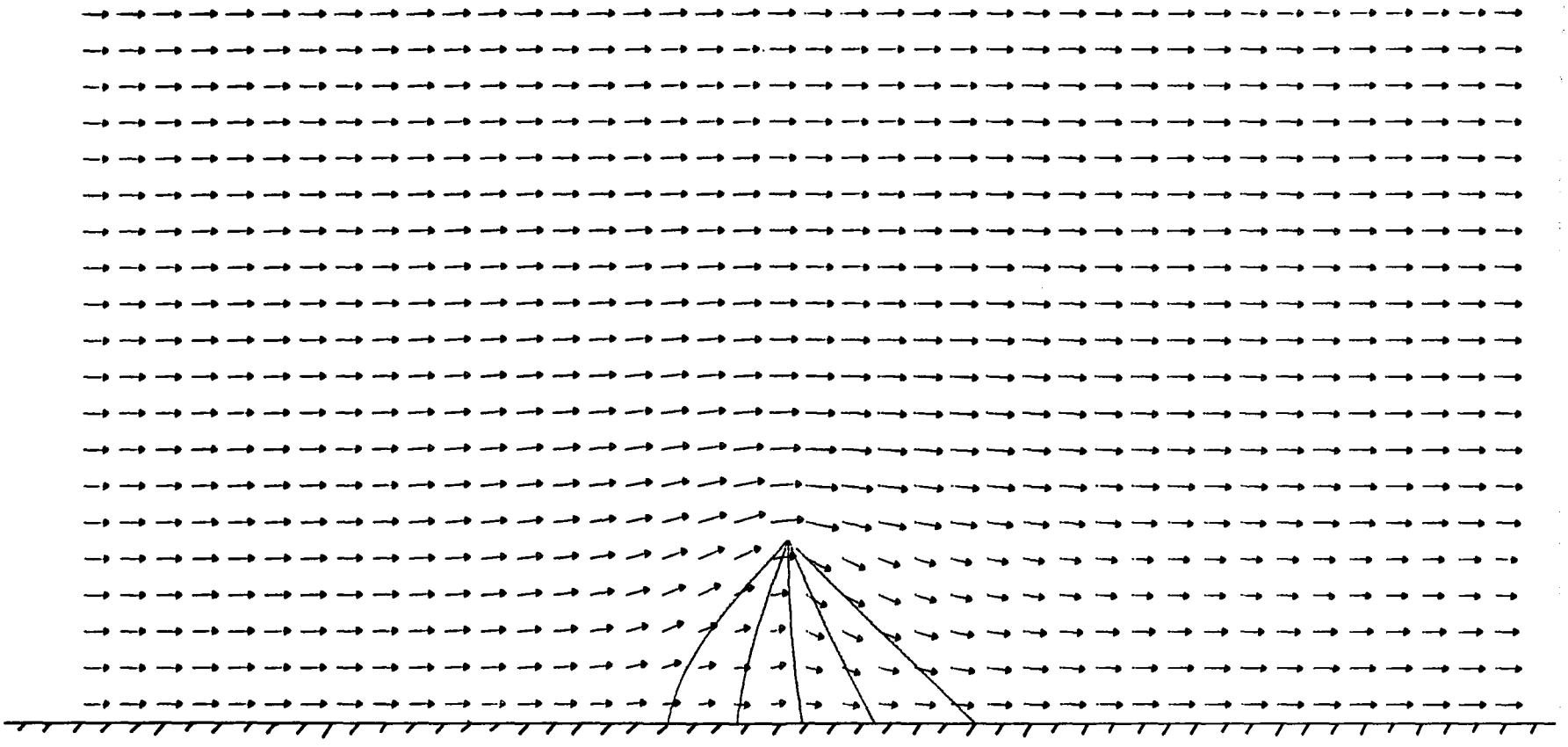

→ CORRESPONDS TO A GAS VELOCITY = 4.00 M/S
WIND SPEED = 3.0 M/S HEIGHT OF NOZZLE = 2.5 METERS
VOLUME FLOW OF WATER = 1.5 LITERS PER SECOND PER METER
DROPLET INJECTION VELOCITY = 23.68 M/S DROPLET SIZE = 1.1 MM
CONE ANGLE OF SPRAY = 90. DEGREES TILT ANGLE = 0. DEGREES

FIGURE 4.2.7 -EFFECT OF WIND ON THE PERFORMANCE OF A SPRAY CURTAIN

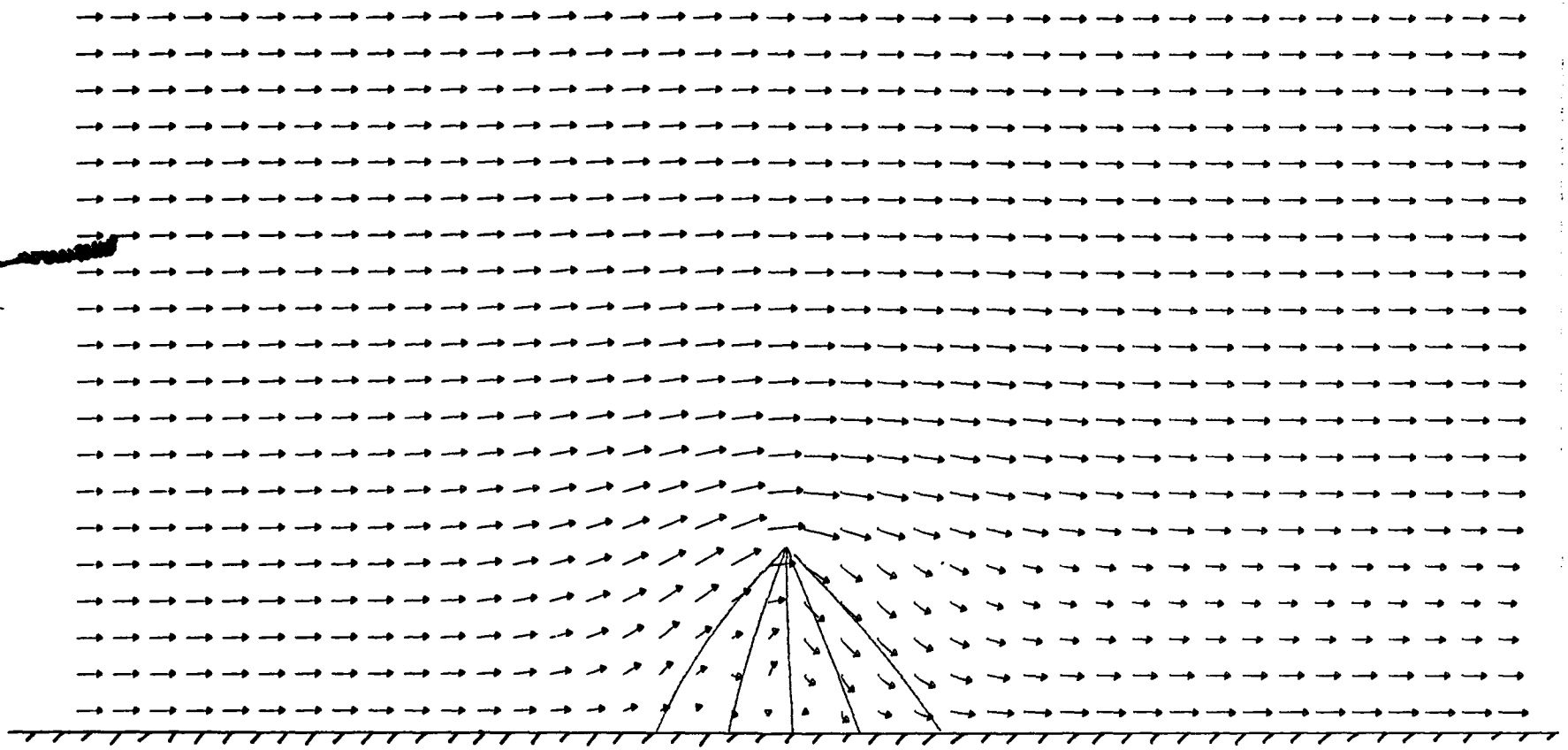

→ CORRESPONDS TO A GAS VELOCITY = 2.00 M/S
WIND SPEED = 1.5 M/S HEIGHT OF NOZZLE = 2.5 METERS
VOLUME FLOW OF WATER = 1.5 LITERS PER SECOND PER METER
DROPLET INJECTION VELOCITY = 11.85 M/S DROPLET SIZE = 1.75 MM
CONE ANGLE OF SPRAY = 90. DEGREES TILT ANGLE = 0. DEGREES

FIGURE 4.2.8 -EFFECT OF WIND ON THE PERFORMANCE OF A SPRAY CURTAIN

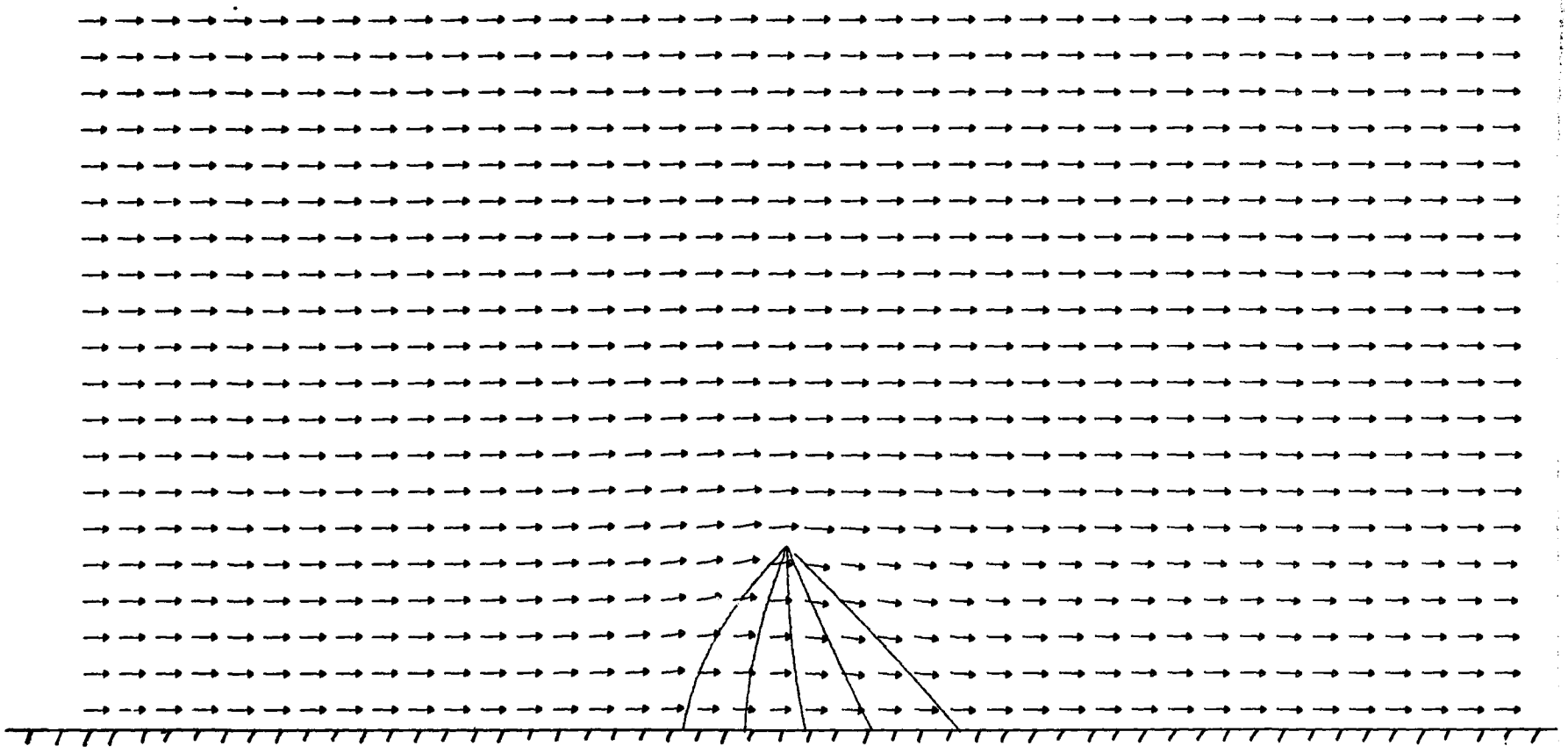

→ CORRESPONDS TO A GAS VELOCITY = 4.00 M/S
WIND SPEED = 3.0 M/S HEIGHT OF NOZZLE = 2.5 METERS
VOLUME FLOW OF WATER = 1.5 LITERS PER SECOND PER METER
DROPLET INJECTION VELOCITY = 11.85 M/S DROPLET SIZE = 1.75 MM
CONE ANGLE OF SPRAY = 90. DEGREES TILT ANGLE = 0. DEGREES

FIGURE 4.2.9 -EFFECT OF WIND ON THE PERFORMANCE OF A SPRAY CURTAIN

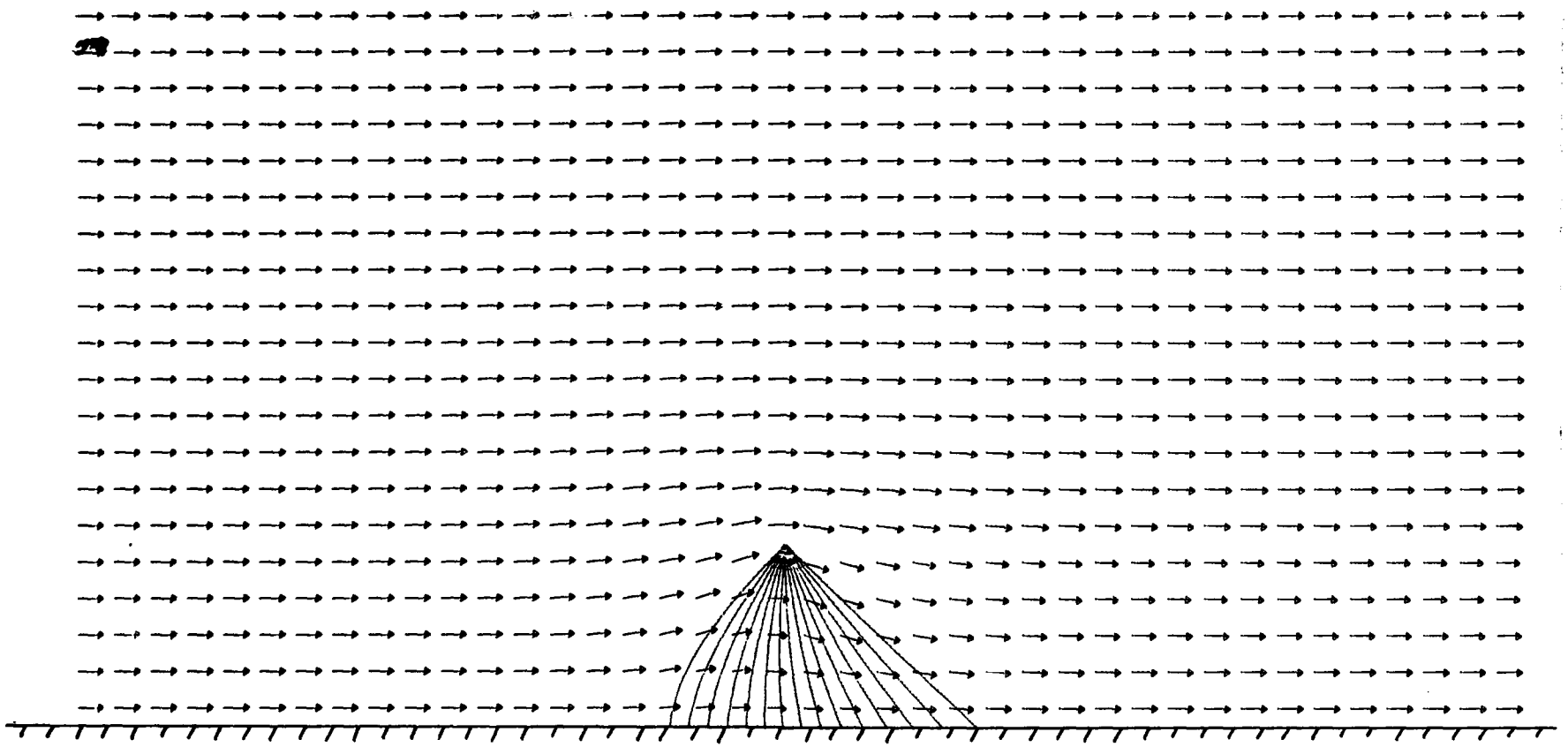

→ CORRESPONDS TO A GAS VELOCITY = 4.00 M/S
WIND SPEED = 3.0 M/S HEIGHT OF NOZZLE = 2.5 METERS
VOLUME FLOW OF WATER = 1.0 LITERS PER SECOND PER METER
DROPLET INJECTION VELOCITY = 23.68 M/S DROPLET SIZE = 1.1 MM
CONE ANGLE OF SPRAY = 90. DEGREES TILT ANGLE = 0. DEGREES

FIGURE 4.2.10 -EFFECT OF TILT ANGLE ON THE PERFORMANCE OF A SPRAY CURTAIN

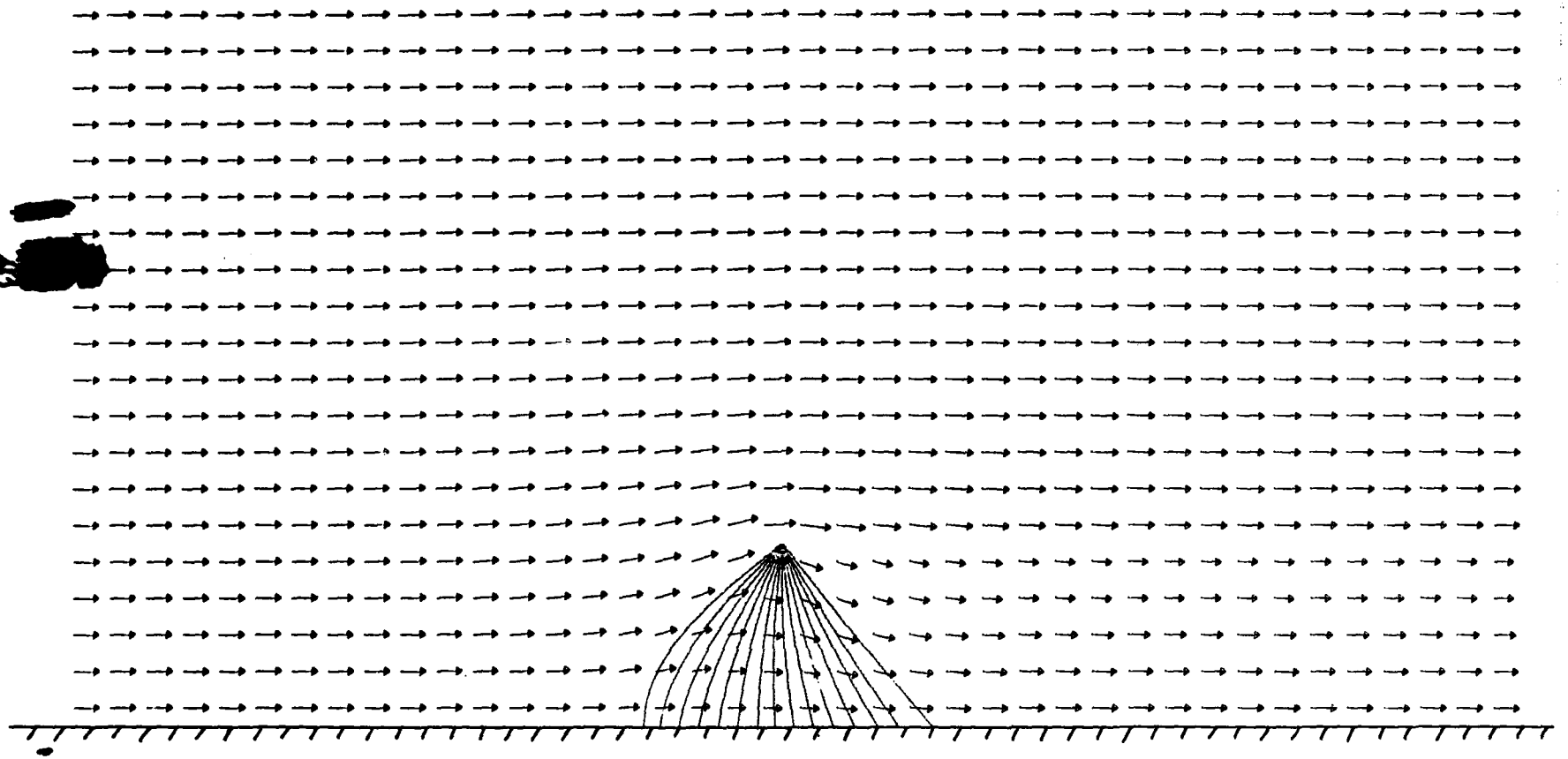

→ CORRESPONDS TO A GAS VELOCITY = 4.00 M/S
WIND SPEED = 3.0 M/S HEIGHT OF NOZZLE = 2.5 METERS
VOLUME FLOW OF WATER = 1.0 LITERS PER SECOND PER METER
DROPLET INJECTION VELOCITY = 23.68 M/S DROPLET SIZE = 1.1 MM
CONE ANGLE OF SPRAY = 90. DEGREES TILT ANGLE = -7.5 DEGREES

FIGURE 4.2.11 -EFFECT OF TILT ANGLE ON THE PERFORMANCE OF A SPRAY CURTAIN

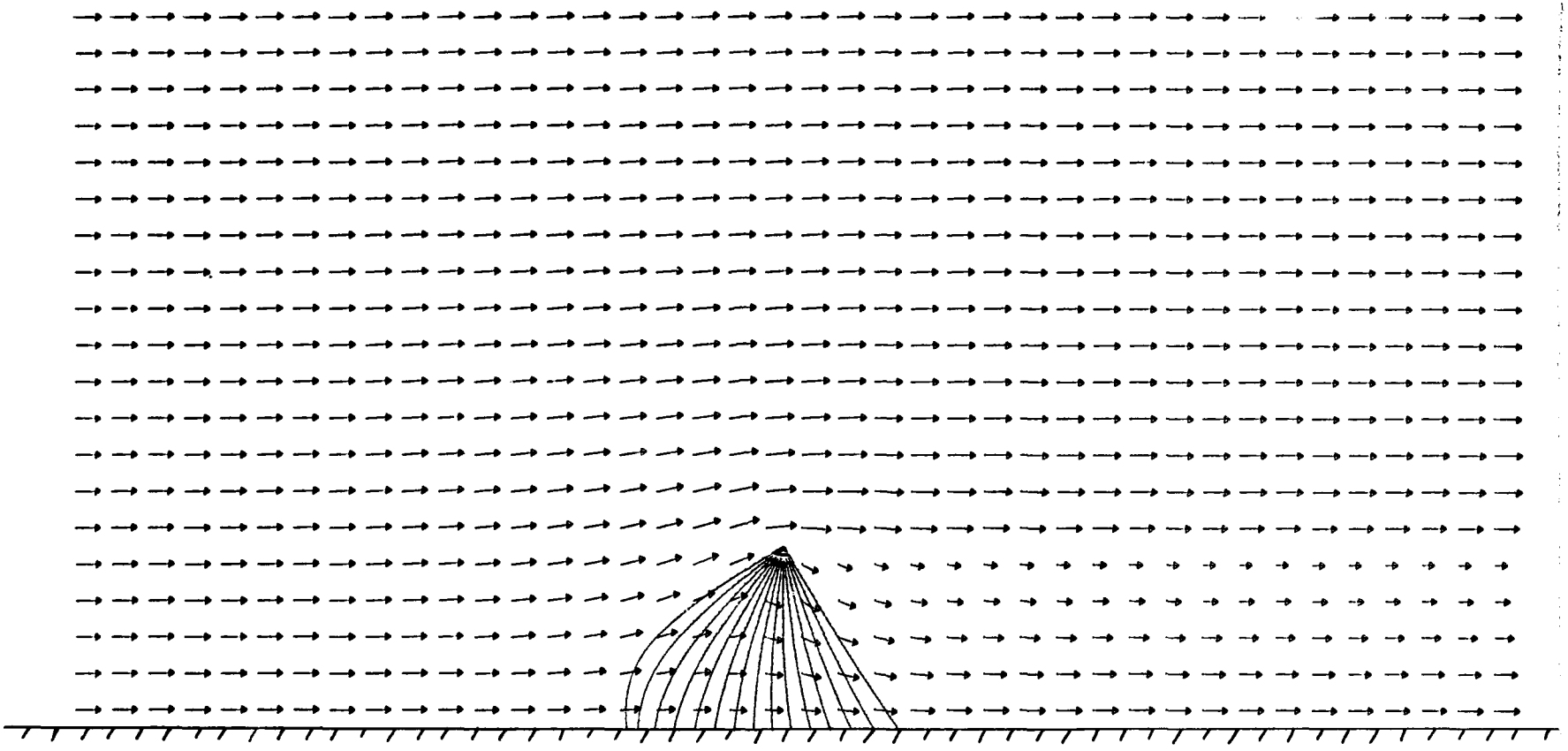

→ CORRESPONDS TO A GAS VELOCITY = 4.00 M/S
WIND SPEED = 3.0 M/S HEIGHT OF NOZZLE = 2.5 METERS
VOLUME FLOW OF WATER = 1.0 LITERS PER SECOND PER METER
DROPLET INJECTION VELOCITY = 23.68 M/S DROPLET SIZE = 1.1 MM
CONE ANGLE OF SPRAY = 90. DEGREES TILT ANGLE = -15. DEGREES

FIGURE 4.2.12 -EFFECT OF TILT ANGLE ON THE PERFORMANCE OF A SPRAY CURTAIN

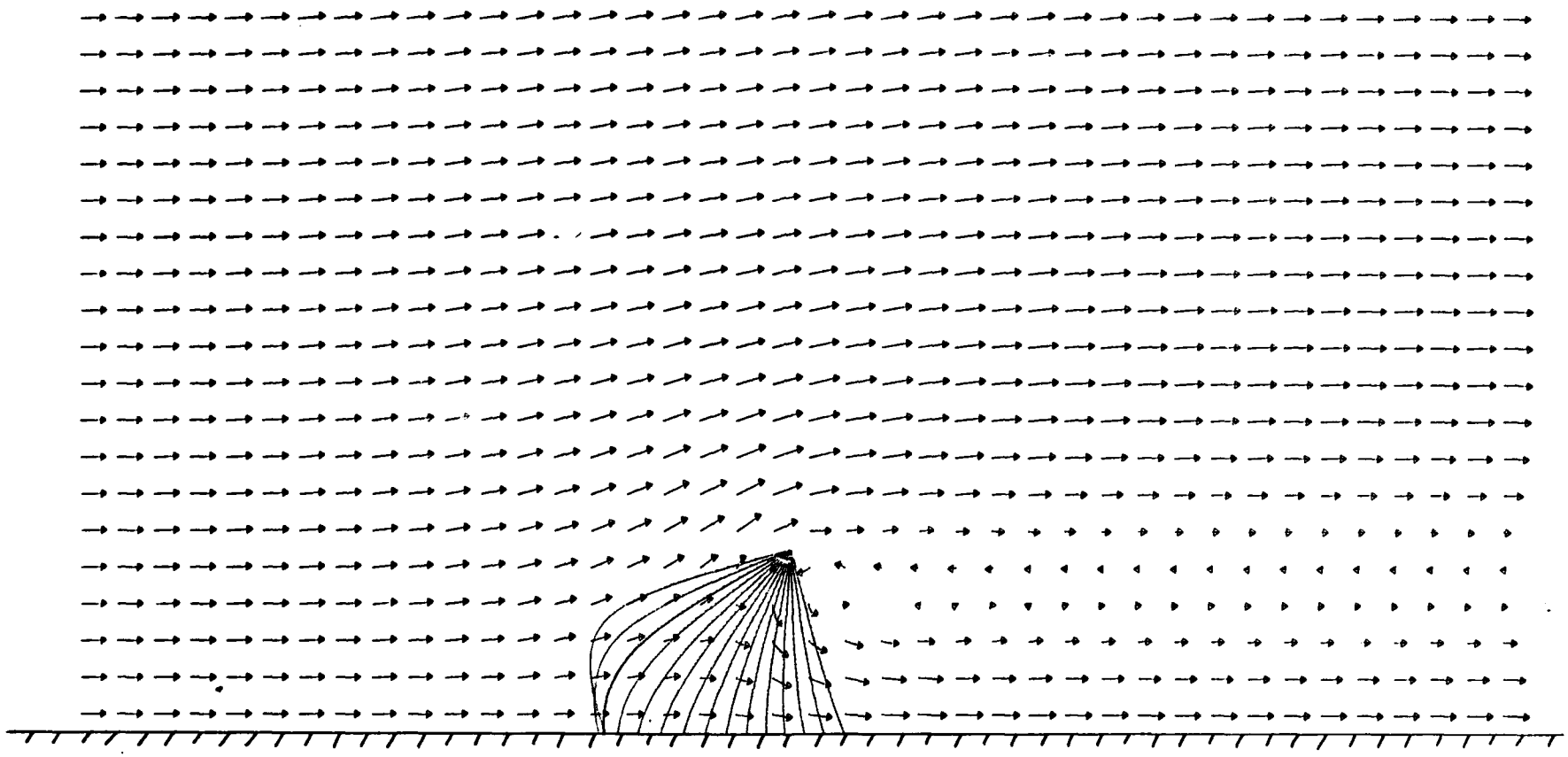

→ CORRESPONDS TO A GAS VELOCITY = 4.00 M/S
WIND SPEED = 3.0 M/S HEIGHT OF NOZZLE = 2.5 METERS
VOLUME FLOW OF WATER = 1.0 LITERS PER SECOND PER METER
DROPLET INJECTION VELOCITY = 23.68 M/S DROPLET SIZE = 1.1 MM
CONE ANGLE OF SPRAY = 90. DEGREES TILT ANGLE = -30. DEGREES

FIGURE **4.2.13**-EFFECT OF TILT ANGLE ON THE PERFORMANCE OF A SPRAY CURTAIN

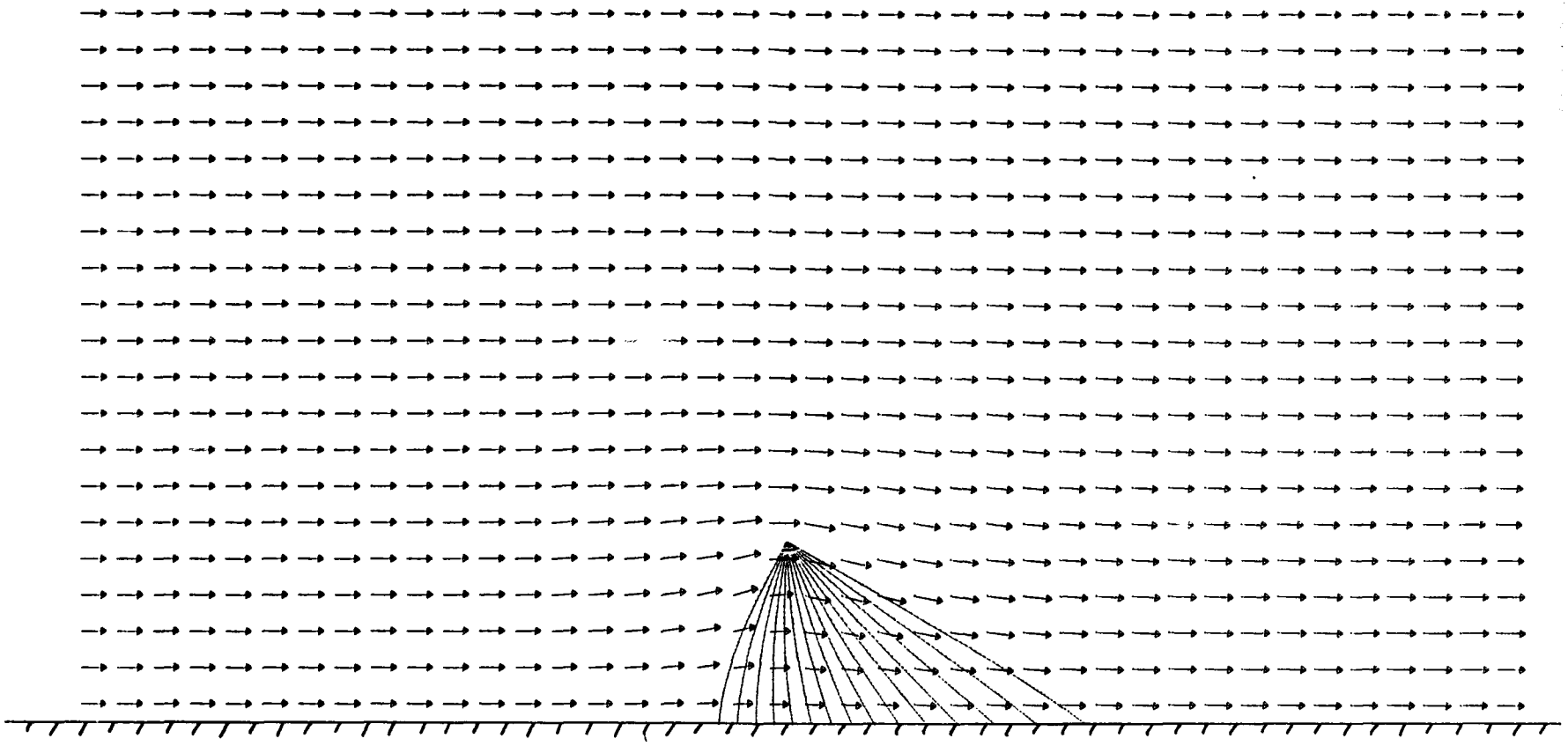

→ CORRESPONDS TO A GAS VELOCITY = 4.00 M/S
WIND SPEED = 3.0 M/S HEIGHT OF NOZZLE = 2.5 METERS
VOLUME FLOW OF WATER = 1.0 LITERS PER SECOND PER METER
DROPLET INJECTION VELOCITY = 23.68 M/S DROPLET SIZE = 1.1 MM
CONE ANGLE OF SPRAY = 90. DEGREES TILT ANGLE = +15. DEGREES

FIGURE 4.2.14 -EFFECT OF TILT ANGLE ON THE PERFORMANCE OF A SPRAY CURTAIN

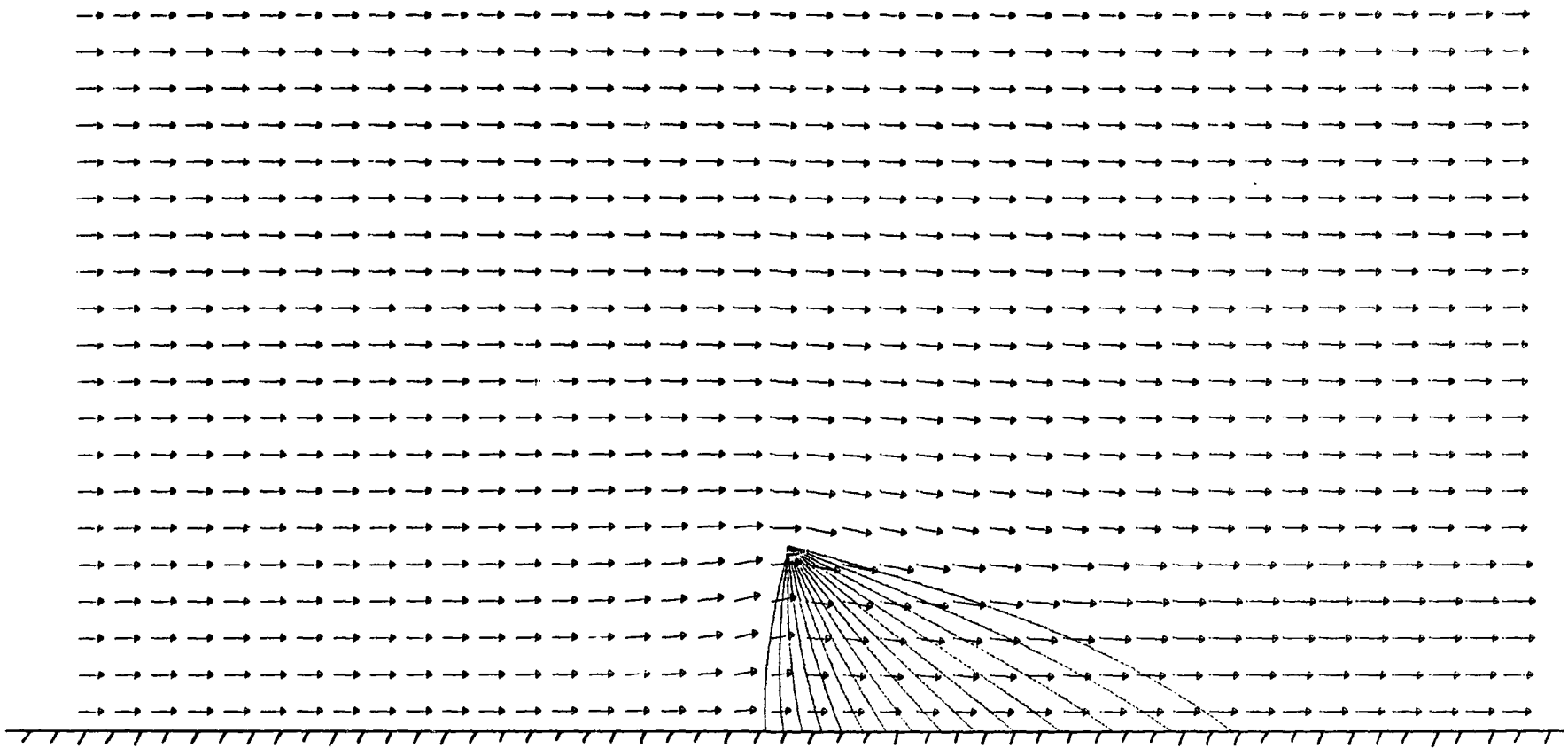

CORRESPONDS TO A GAS VELOCITY = 4.00 M/S
WIND SPEED = 3.0 M/S HEIGHT OF NOZZLE = 2.5 METERS
VOLUME FLOW OF WATER = 1.0 LITERS PER SECOND PER METER
DROPLET INJECTION VELOCITY = 23.68 M/S DROPLET SIZE = 1.1 MM
CONE ANGLE OF SPRAY = 90. DEGREES TILT ANGLE = +30. DEGREES

FIGURE 4.2.15 -EFFECT OF TILT ANGLE ON THE PERFORMANCE OF A SPRAY CURTAIN

AD-A128 717 A NUMERICAL MODEL FOR GAS-DROPLET FLOW APPLICATION TO LIQUID SPRAY AND CO..(U) VON KARMAN INST FOR FLUID DYNAMICS RHODE-SAINT-GENESE (BELGIU..

2/2

UNCLASSIFIED P WEINACHT ET AL. FEB 83 EOARD-TR-83-5 F/G 20/4 NL

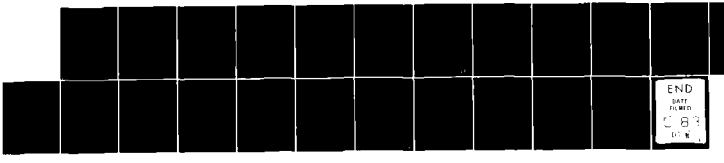

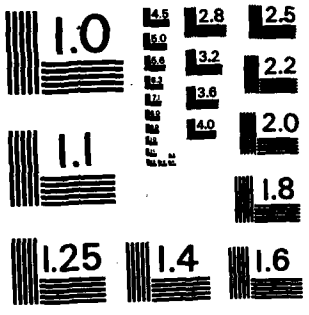

MICROCOPY RESOLUTION TEST CHART
NATIONAL BUREAU OF STANDARDS-1963-A

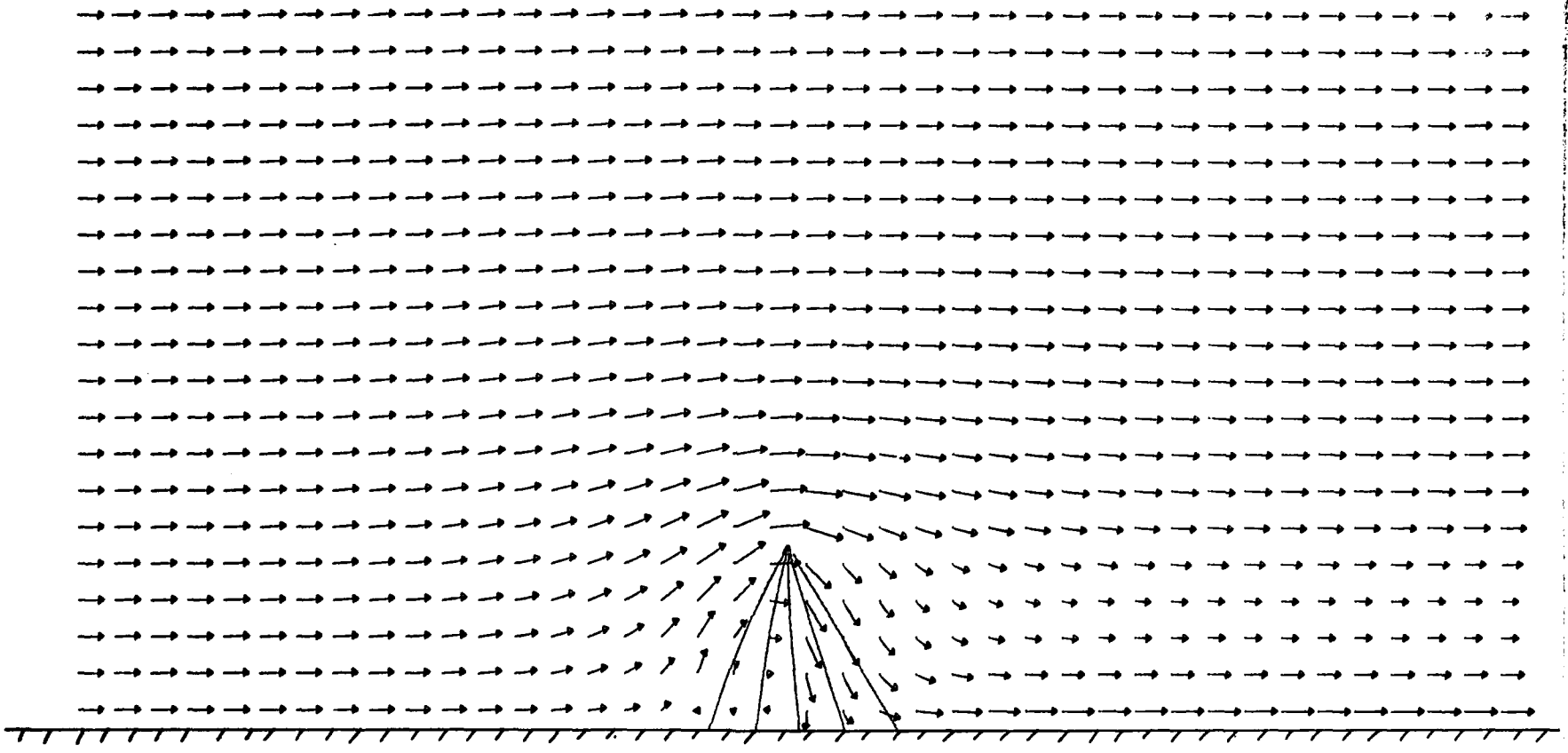

→ CORRESPONDS TO A GAS VELOCITY = 4.00 M/S
WIND SPEED = 3.0 M/S HEIGHT OF NOZZLE = 2.5 METERS
VOLUME FLOW OF WATER = 3.0 LITERS PER SECOND PER METER
DROPLET INJECTION VELOCITY = 23.68 M/S DROPLET SIZE = 1.1 MM
CONE ANGLE OF SPRAY = 60. DEGREES TILT ANGLE = 0. DEGREES

FIGURE 4.2.16-EFFECT OF WIND ON THE PERFORMANCE OF A SPRAY CURTAIN

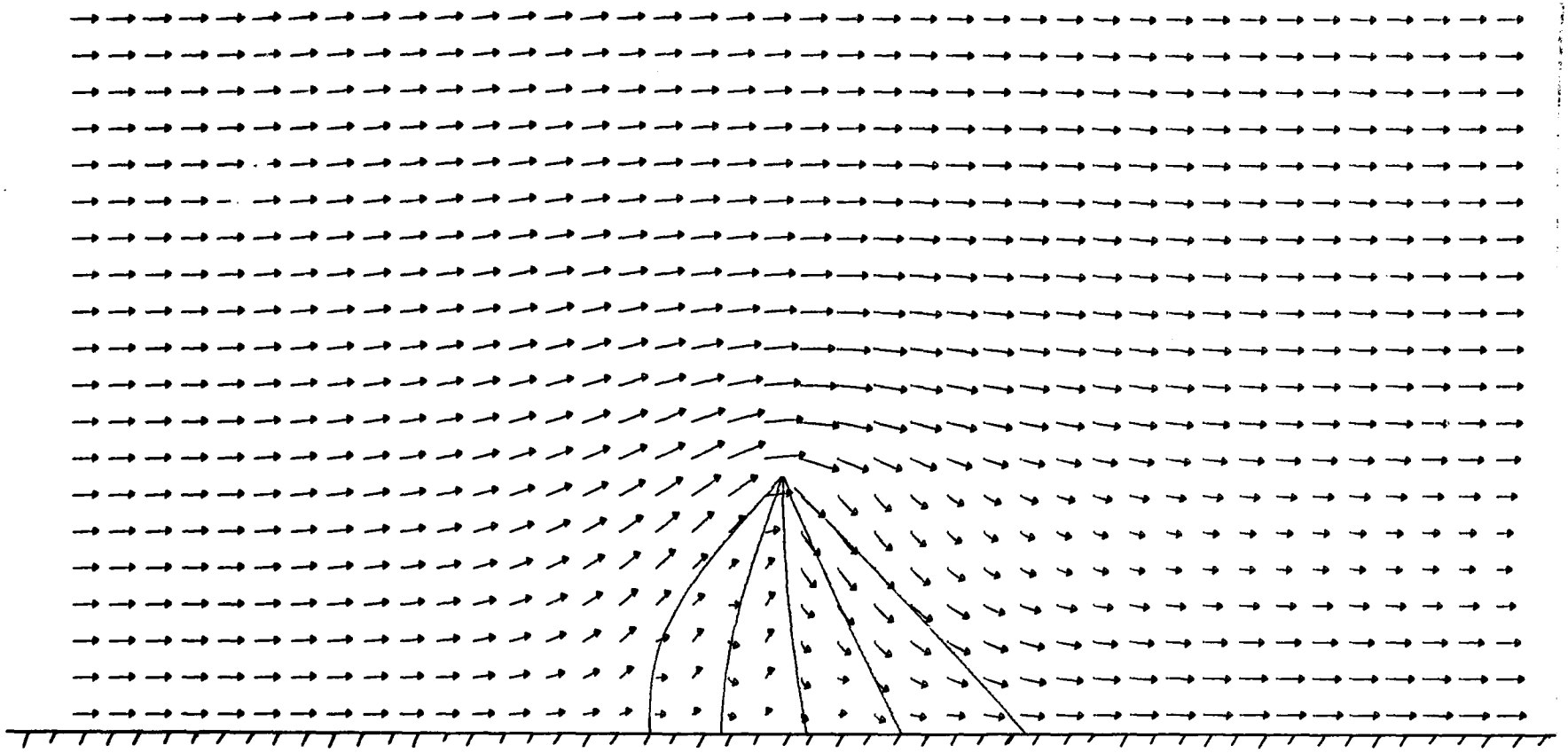

→ CORRESPONDS TO A GAS VELOCITY = 4.00 M/S
WIND SPEED = 3.0 M/S HEIGHT OF NOZZLE = 3.5 METERS
VOLUME FLOW OF WATER = 3.0 LITERS PER SECOND PER METER
DROPLET INJECTION VELOCITY = 23.68 M/S DROPLET SIZE = 1.1 MM
CONE ANGLE OF SPRAY = 90. DEGREES TILT ANGLE = 0. DEGREES

FIGURE 4.2.17 -EFFECT OF WIND ON THE PERFORMANCE OF A SPRAY CURTAIN

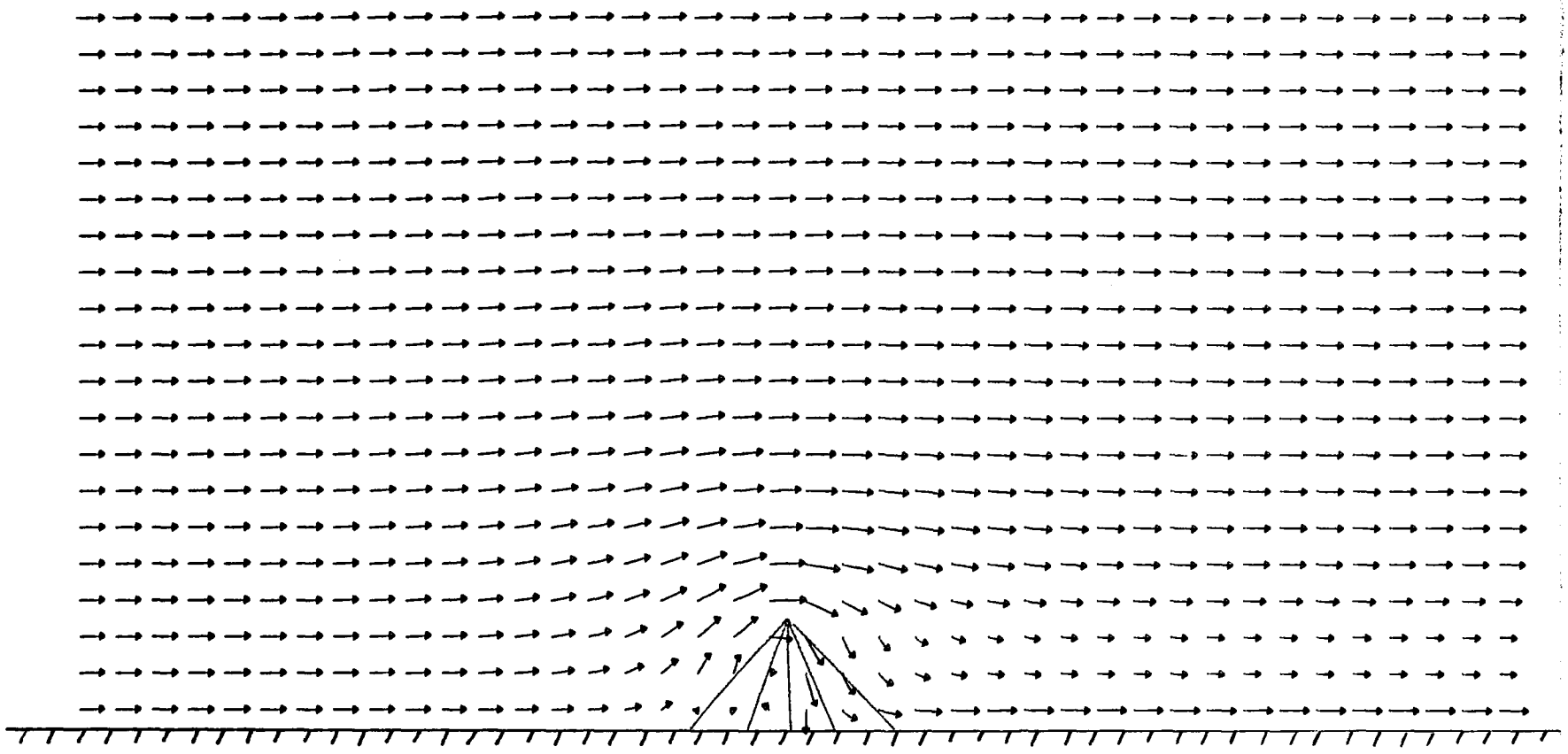

→ CORRESPONDS TO A GAS VELOCITY = 4.00 M/S
WIND SPEED = 3.0 M/S HEIGHT OF NOZZLE = 1.5 METERS
VOLUME FLOW OF WATER = 3.0 LITERS PER SECOND PER METER
DROPLET INJECTION VELOCITY = 23.68 M/S DROPLET SIZE = 1.1 MM
CONE ANGLE OF SPRAY = 90. DEGREES TILT ANGLE = 0. DEGREES

FIGURE **4.2.18**-EFFECT OF WIND ON THE PERFORMANCE OF A SPRAY CURTAIN

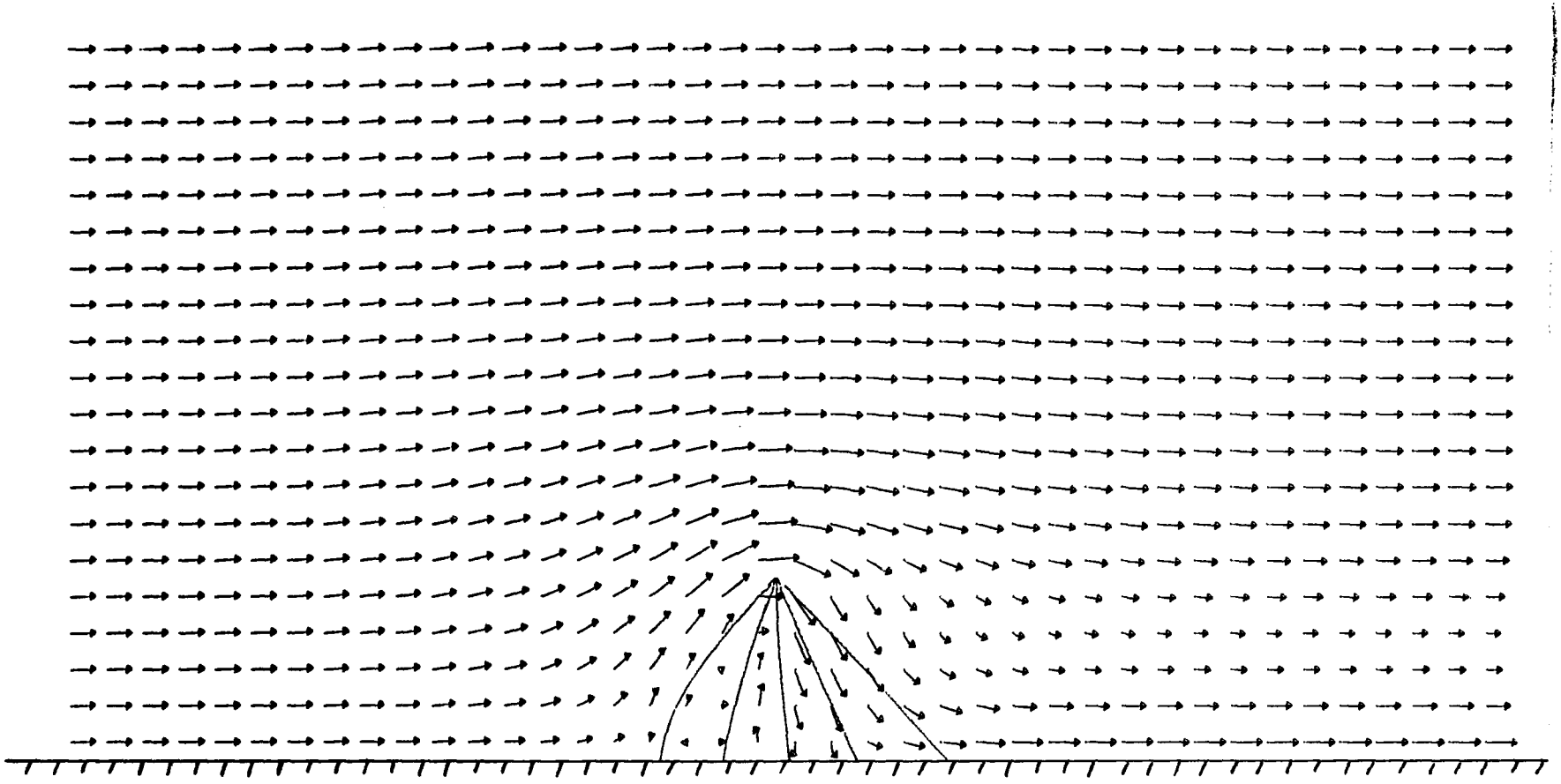

→ CORRESPONDS TO A GAS VELOCITY = 4.00 M/S
WIND SPEED = 3.0 M/S HEIGHT OF NOZZLE = 2.5 METERS
VOLUME FLOW OF WATER = 3.0 LITERS PER SECOND PER METER
DROPLET INJECTION VELOCITY = 23.68 M/S DROPLET SIZE = .88 MM
CONE ANGLE OF SPRAY = 90. DEGREES TILT ANGLE = 0. DEGREES

FIGURE **4.2.19** -EFFECT OF WIND ON THE PERFORMANCE OF A SPRAY CURTAIN

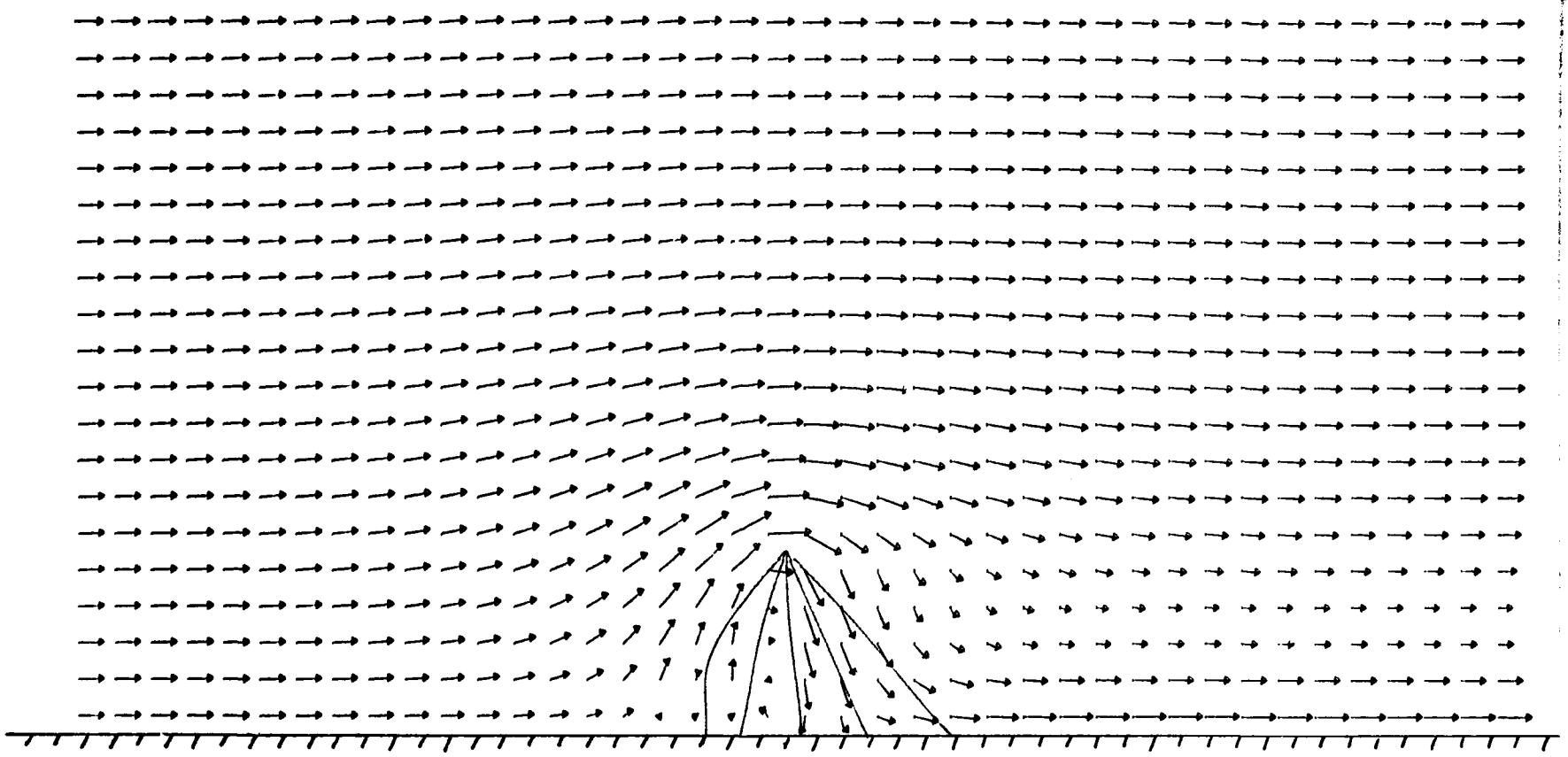

→ CORRESPONDS TO A GAS VELOCITY = 4.00 M/S
WIND SPEED = 3.0 M/S HEIGHT OF NOZZLE = 2.5 METERS
VOLUME FLOW OF WATER = 3.0 LITERS PER SECOND PER METER
DROPLET INJECTION VELOCITY = 23.68 M/S DROPLET SIZE = .66 MM
CONE ANGLE OF SPRAY = 90. DEGREES TILT ANGLE = 0. DEGREES

FIGURE **4.2.20**-EFFECT OF WIND ON THE PERFORMANCE OF A SPRAY CURTAIN

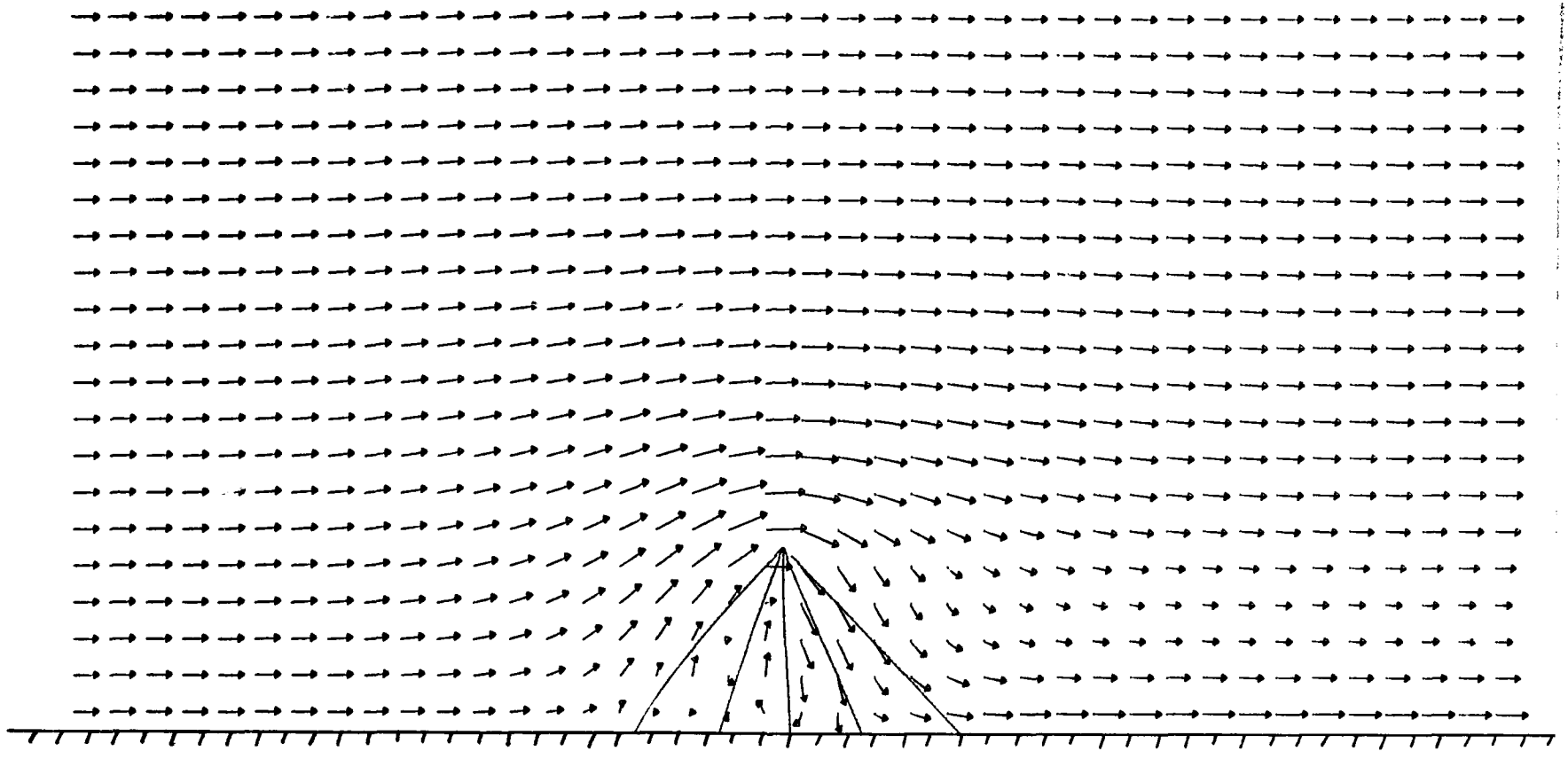

→ CORRESPONDS TO A GAS VELOCITY = 4.00 M/S
WIND SPEED = 3.0 M/S HEIGHT OF NOZZLE = 2.5 METERS
VOLUME FLOW OF WATER = 3.0 LITERS PER SECOND PER METER
DROPLET INJECTION VELOCITY = 28.42 M/S DROPLET SIZE = 1.1 MM
CONE ANGLE OF SPRAY = 90. DEGREES TILT ANGLE = 0. DEGREES

FIGURE **4.2.21**-EFFECT OF WIND ON THE PERFORMANCE OF A SPRAY CURTAIN

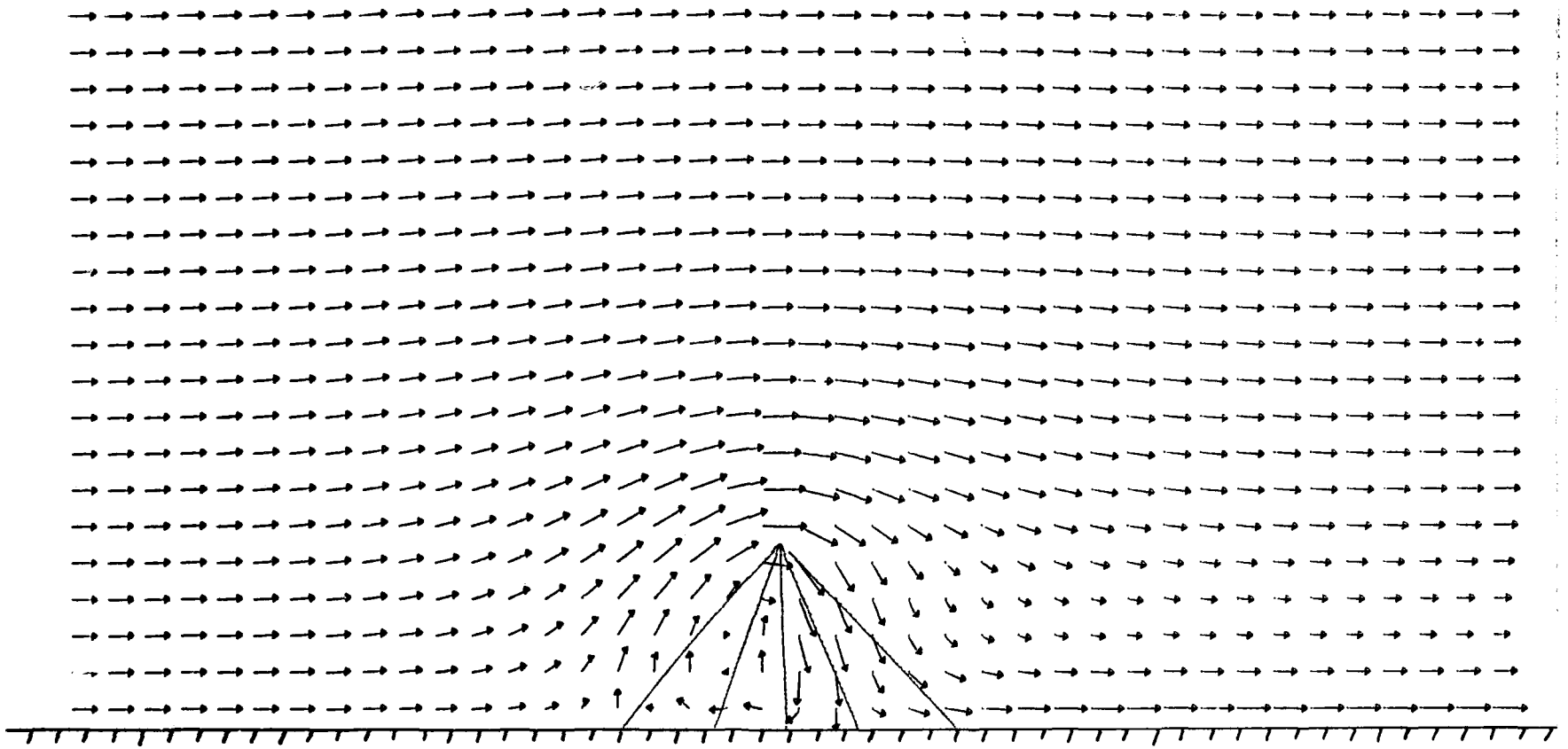

→ CORRESPONDS TO A GAS VELOCITY = 4.00 M/S
WIND SPEED = 3.0 M/S HEIGHT OF NOZZLE = 2.5 METERS
VOLUME FLOW OF WATER = 3.0 LITERS PER SECOND PER METER
DROPLET INJECTION VELOCITY = 33.15 M/S DROPLET SIZE = 1.1 MM
CONE ANGLE OF SPRAY = 90. DEGREES TILT ANGLE = 0. DEGREES

FIGURE **4.2.22.** EFFECT OF WIND ON THE PERFORMANCE OF A SPRAY CURTAIN

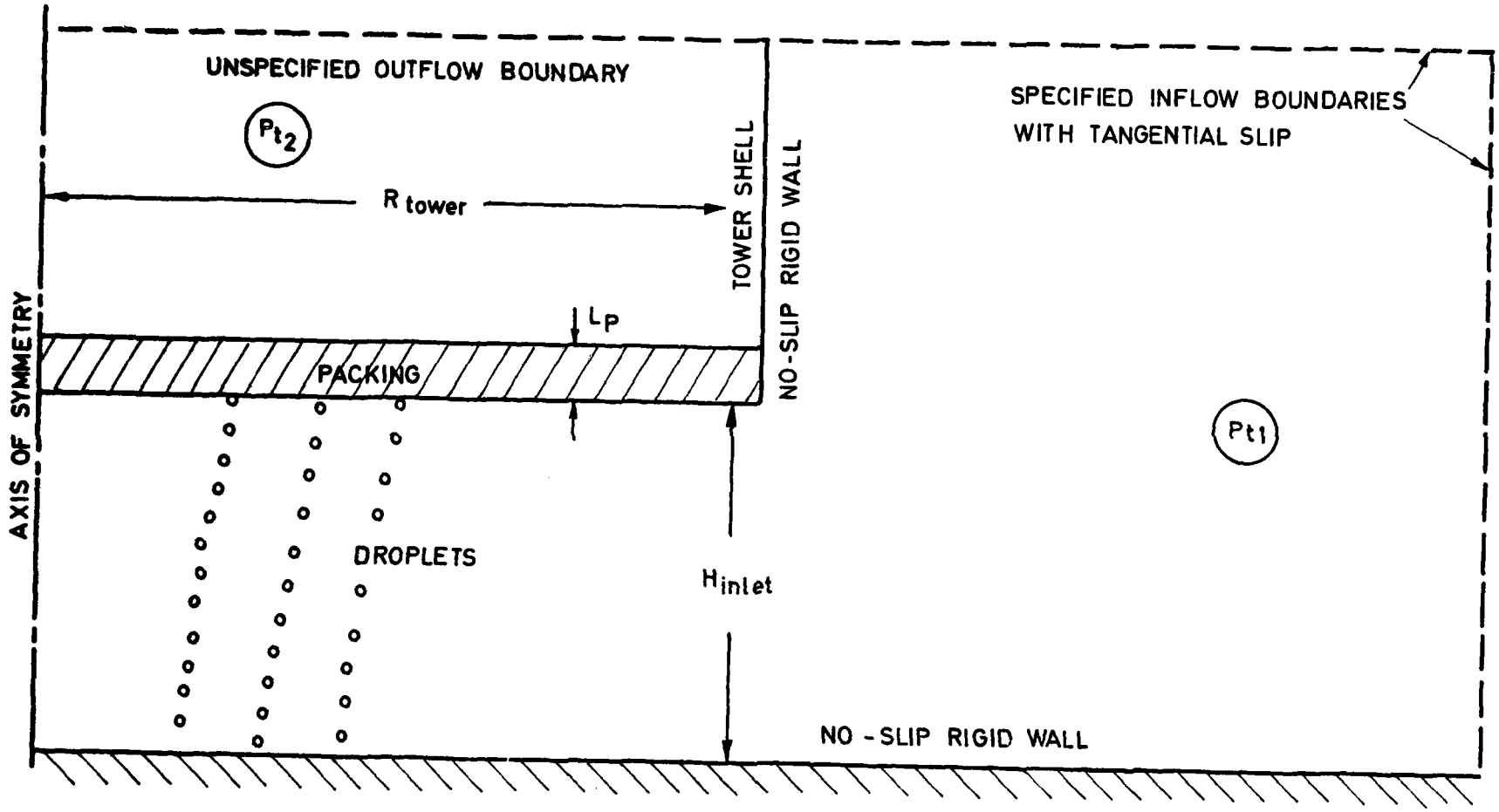

FIG. 4.3.1 - COMPUTATIONAL DOMAIN FOR COOLING TOWER.

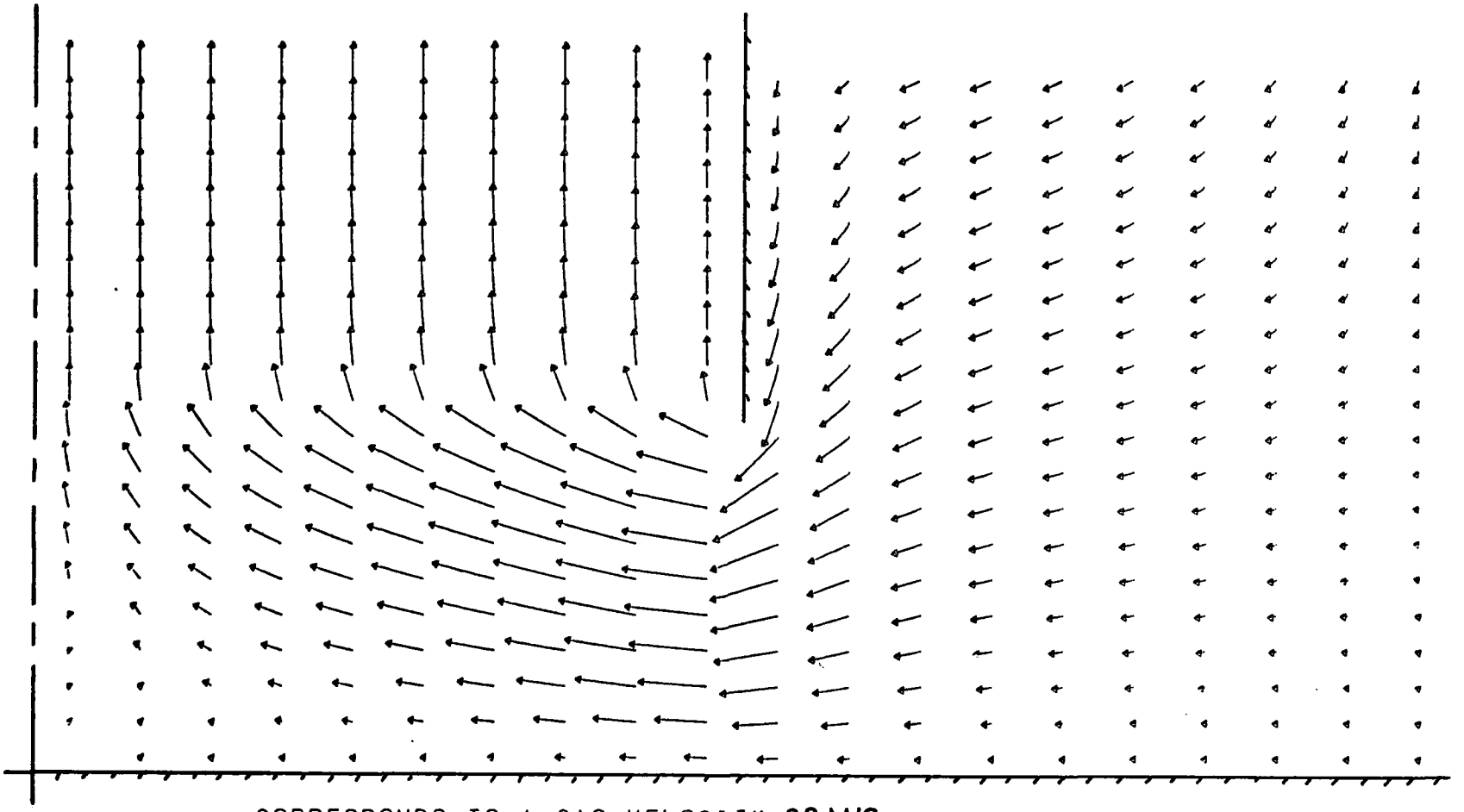

→ CORRESPONDS TO A GAS VELOCITY=3.0 M/S
TOWER RADIUS = 60. METERS HEIGHT OF INLET = 10. METERS
VERTICAL COORDINATE STRETCHED BY A FACTOR OF 3.
VOLUME FLOW OF AIR THROUGH THE TOWER = 22619. M**3/S
WITH PACKING - NO DROPLETS

FIG. 4.3.2 -FLOW FIELD IN A COOLING TOWER

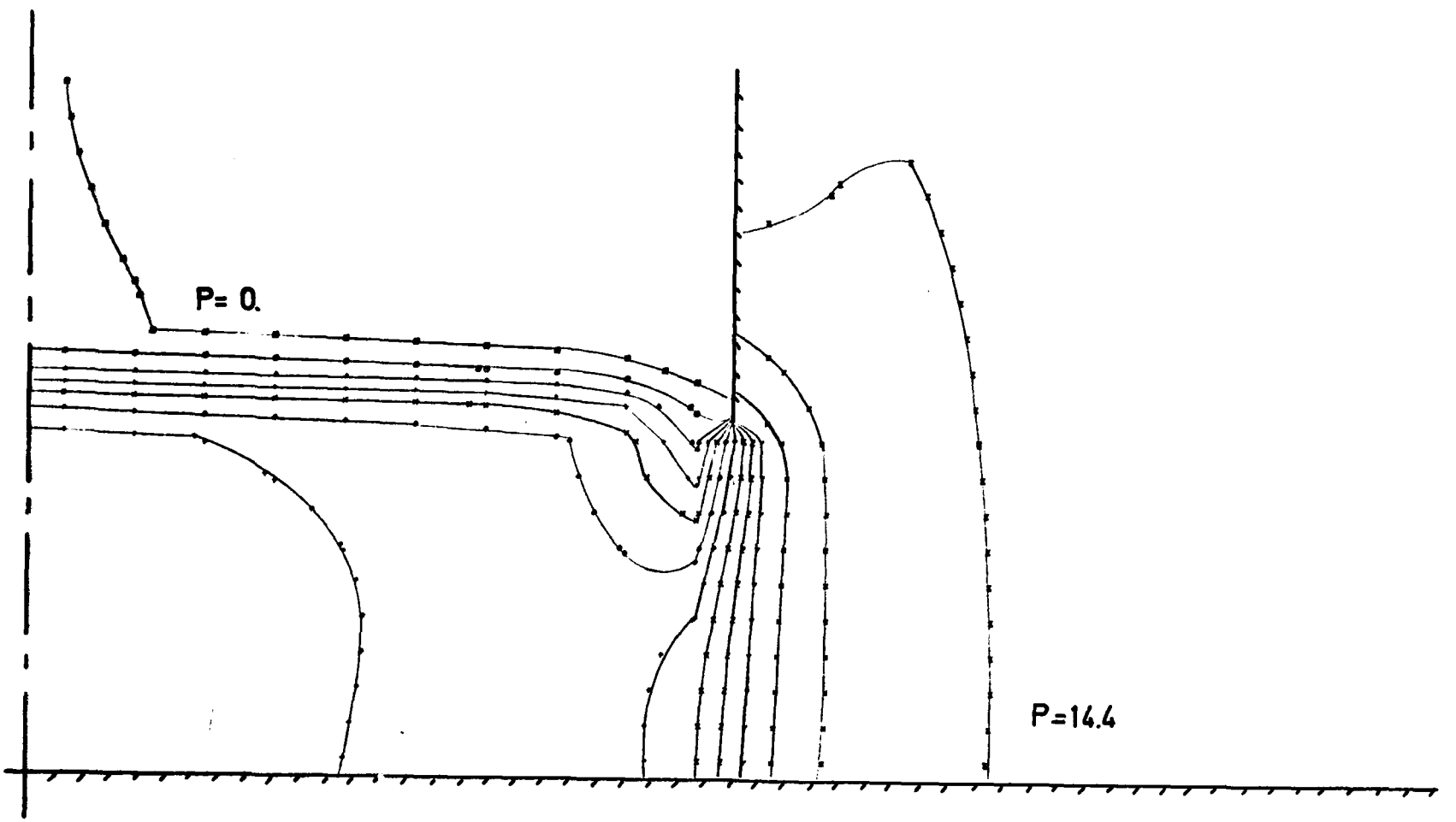

STATIC PRESSURE ISOBARS ARE IN INCREMENTS OF 1.2
VOLUME FLOW OF AIR THROUGH THE TOWER = 22619. M**3/S
WITH PACKING - NO DROPLETS
VERTICAL COORDINATE STRETCHED BY A FACTOR OF 3.

FIGURE 4.3.3-STATIC PRESSURE ISOBARS FOR FLOW THROUGH COOLING TOWER

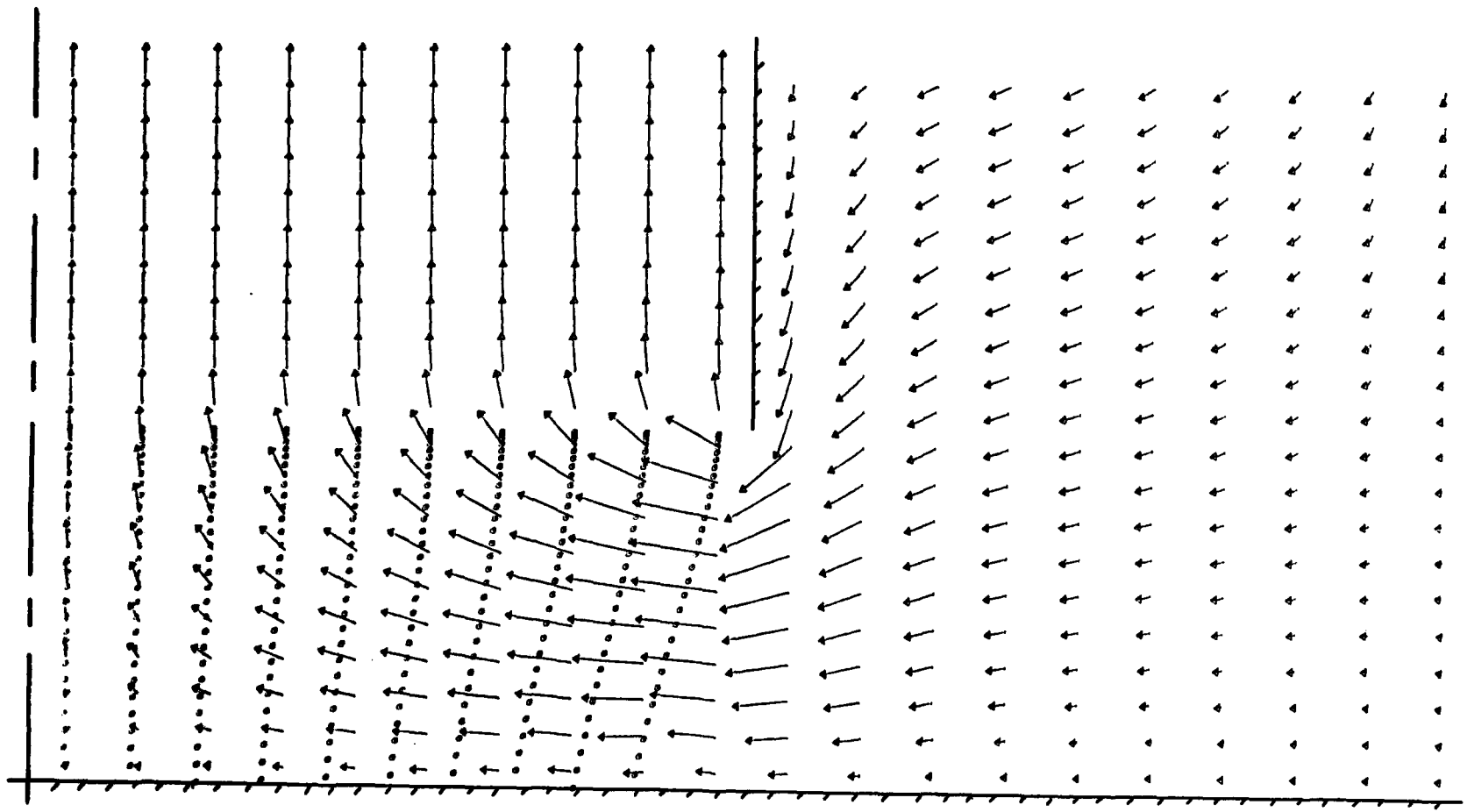

→ CORRESPONDS TO A GAS VELOCITY=3.0 M/S
TOWER RADIUS = 60. METERS HEIGHT OF INLET = 10. METERS
VERTICAL COORDINATE IS STRETCHED BY A FACTOR OF 3.
VOLUME FLOW OF AIR = 22619. M**3/S VOLUME FLOW OF WATER = 31.4 M**3/S
WITH PACKING - WITH DROPLETS (DIAMETER = 3. MM)

FIGURE 4.3.4-FLOW FIELD IN A COOLING TOWER

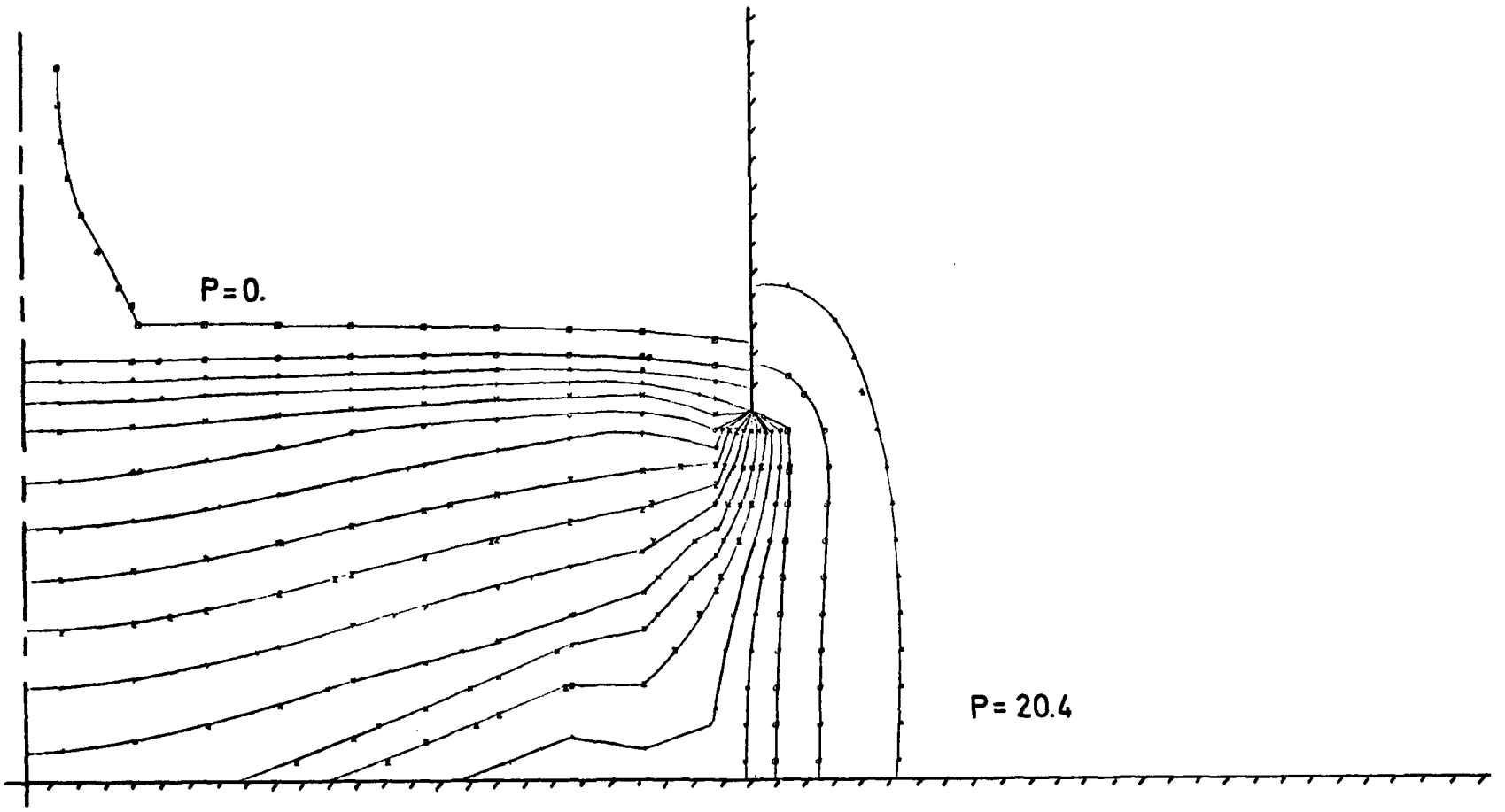

STATIC PRESSURE ISOBARS ARE IN INCREMENTS OF 1.2
VOLUME FLOW OF AIR = 22619. M**3/S VOLUME FLOW OF WATER = 31.4 M**3/S
WITH PACKING - WITH DROPLETS (DIAMETER 3. MM)
VERTICAL COORDINATE STRETCHED BY A FACTOR OF 3.

FIG. **4.3.5** - STATIC PRESSURE ISOBARS FOR FLOW THROUGH A COOLING TOWER

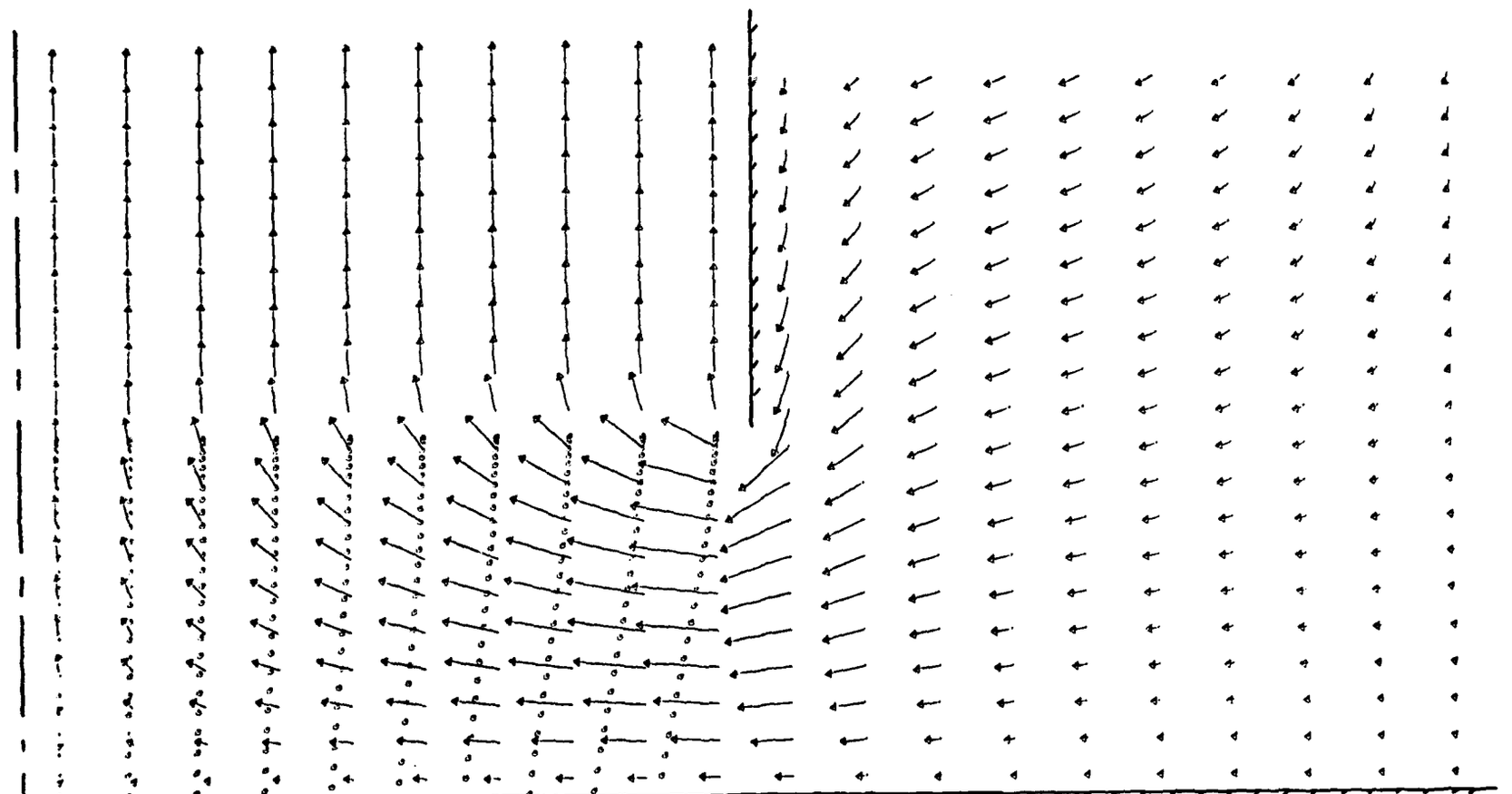

→ CORRESPONDS TO A GAS VELOCITY=3.0 M/S
TOWER RADIUS = 60. METERS HEIGHT OF INLET = 10. METERS
VERTICAL COORDINATE STRETCHED BY A FACTOR OF 3.
VOLUME FLOW OF AIR = 22619. M**3/S VOLUME FLOW OF WATER = 31.4 M**3/S
WITH PACKING - WITH DROPLETS (DIAMETER 4. MM)

FIGURE 4.3.6-FLOW FIELD IN A COOLING TOWER

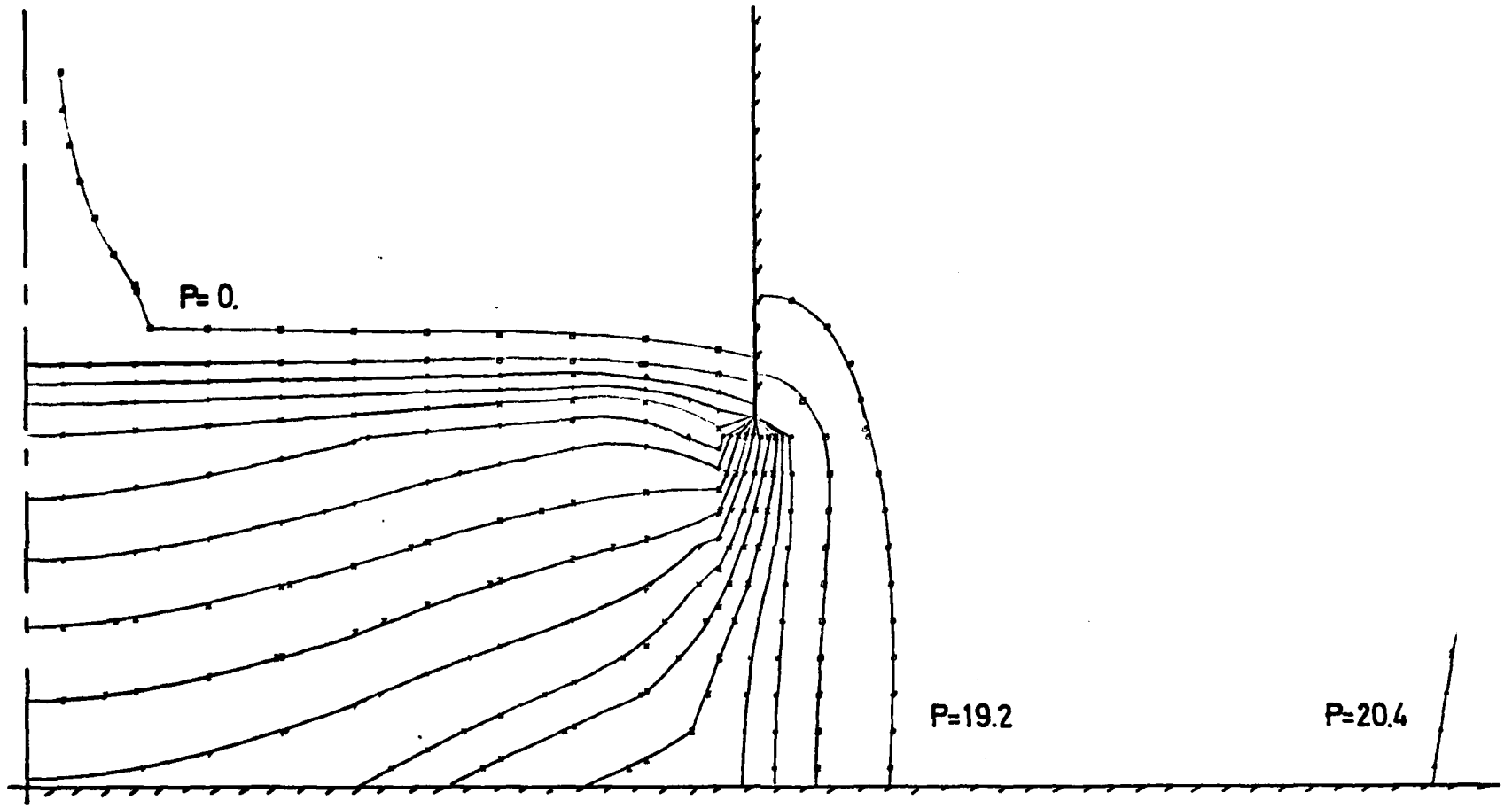

STATIC PRESSURE ISOBARS ARE IN INCREMENTS OF 1.2
VOLUME FLOW OF AIR = 22619. M**3/S VOLUME FLOW OF WATER = 31.4 M**3/S
WITH PACKING - WITH DROPLETS (DIAMETER 4. MM)
VERTICAL COORDINATE STRETCHED BY A FACTOR OF 3.

FIG. 4.3.7 - STATIC PRESSURE ISOBARS FOR FLOW THROUGH A COOLING TOWER

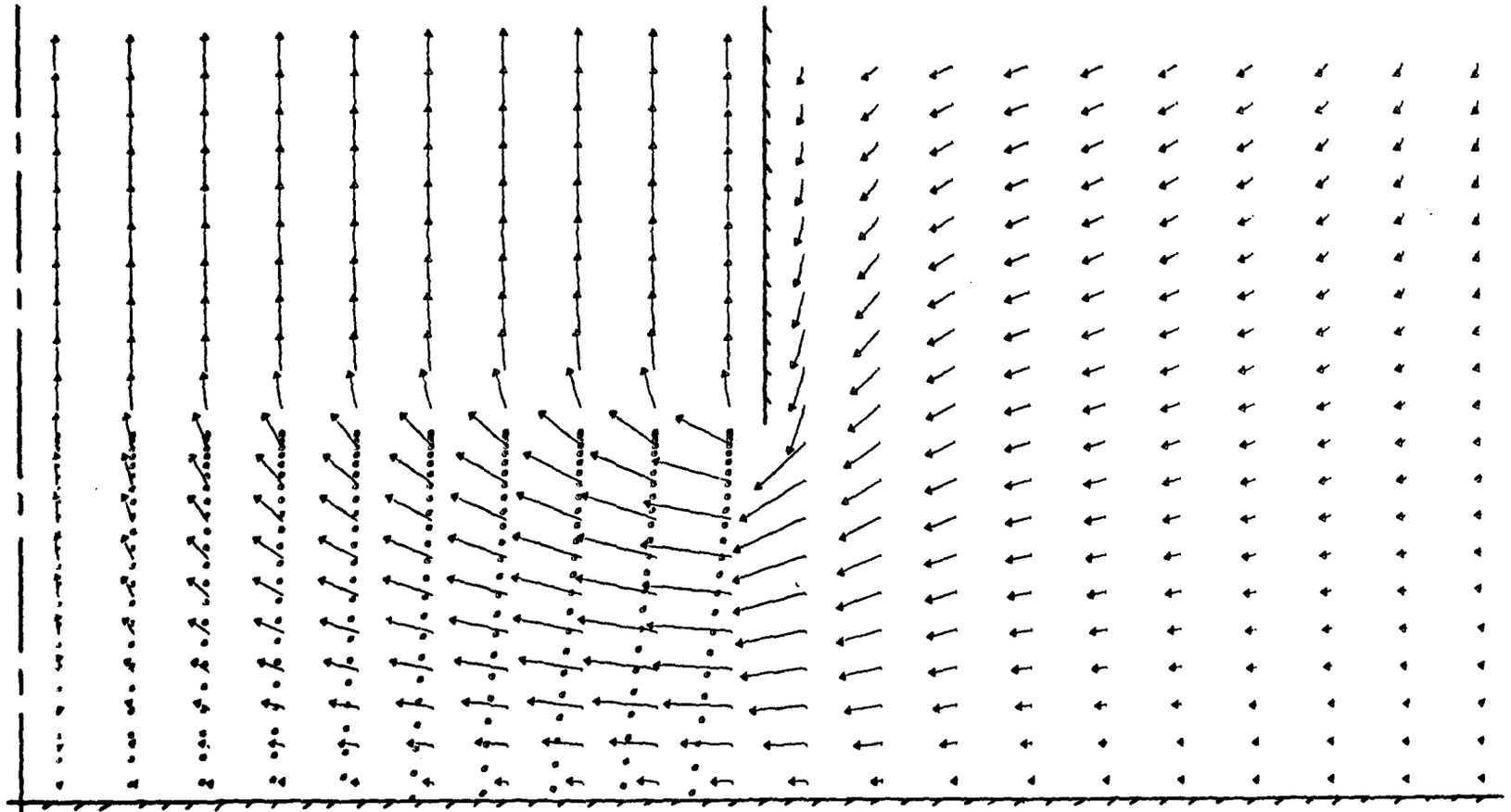

→ CORRESPONDS TO A GAS VELOCITY=3.0 M/S
TOWER RADIUS = 60. METERS HEIGHT OF INLET = 10. METERS
VERTICAL COORDINATE STRETCHED BY A FACTOR OF 3.
VOLUME FLOW OF AIR = 22619. M**3/S VOLUME FLOW OF WATER = 31.4 M**3/S
WITH PACKING - WITH DROPLETS (DIAMETER = 6. MM)

FIG. 4.3.8 -FLOW FIELD IN A COOLING TOWER

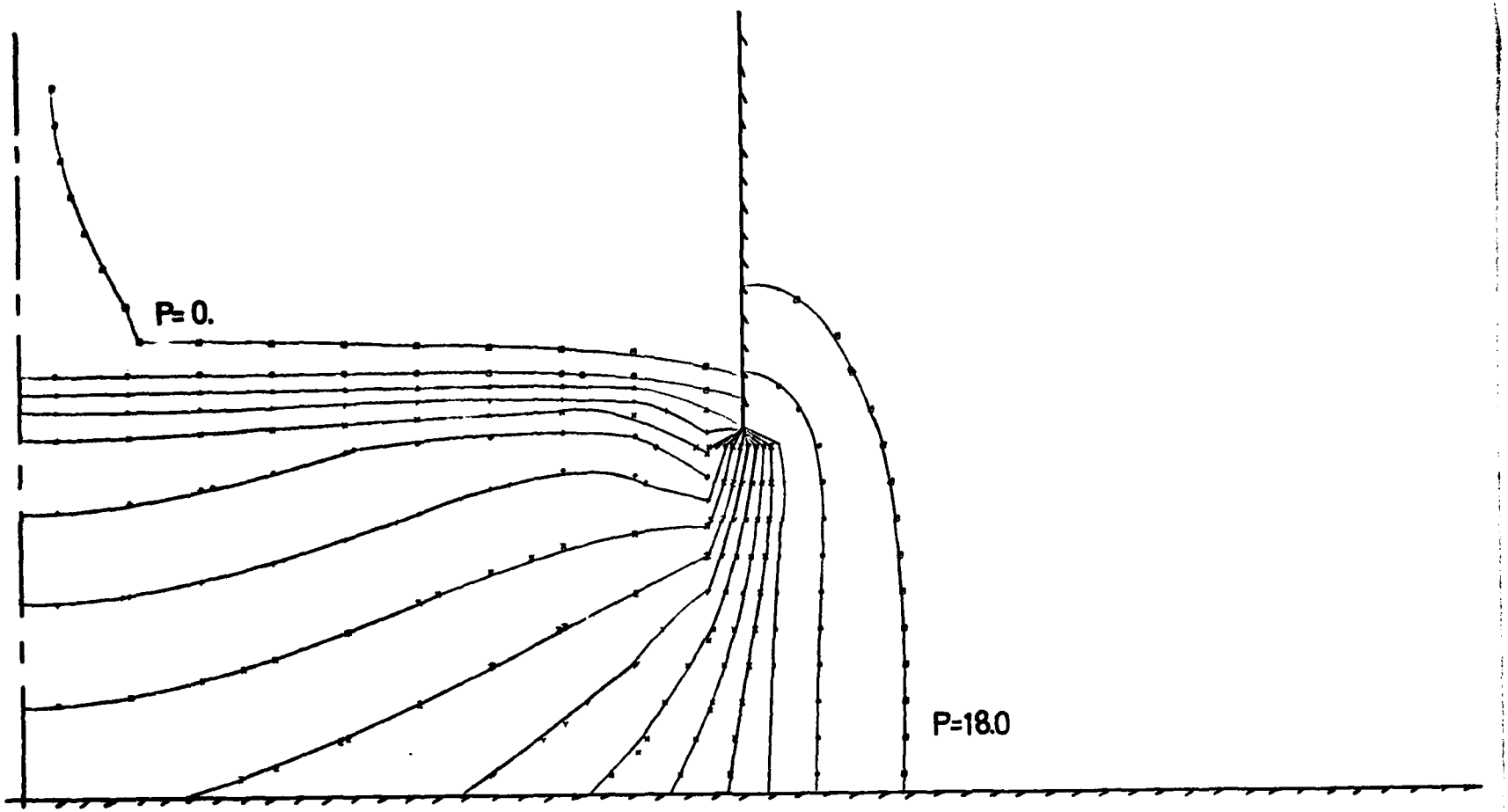

STATIC PRESSURE ISOBARS ARE IN INCREMENTS OF 1.2
VOLUME FLOW OF AIR = 22619. M**3/S VOLUME FLOW OF WATER = 31.4 M**3/S
WITH PACKING - WITH DROPLETS (DIAMETER 6. MM)
VERTICAL COORDINATE STRETCHED BY A FACTOR OF 3.

FIG. 4.3.9-STATIC PRESSURE ISOBARS FOR FLOW THROUGH A COOLING TOWER

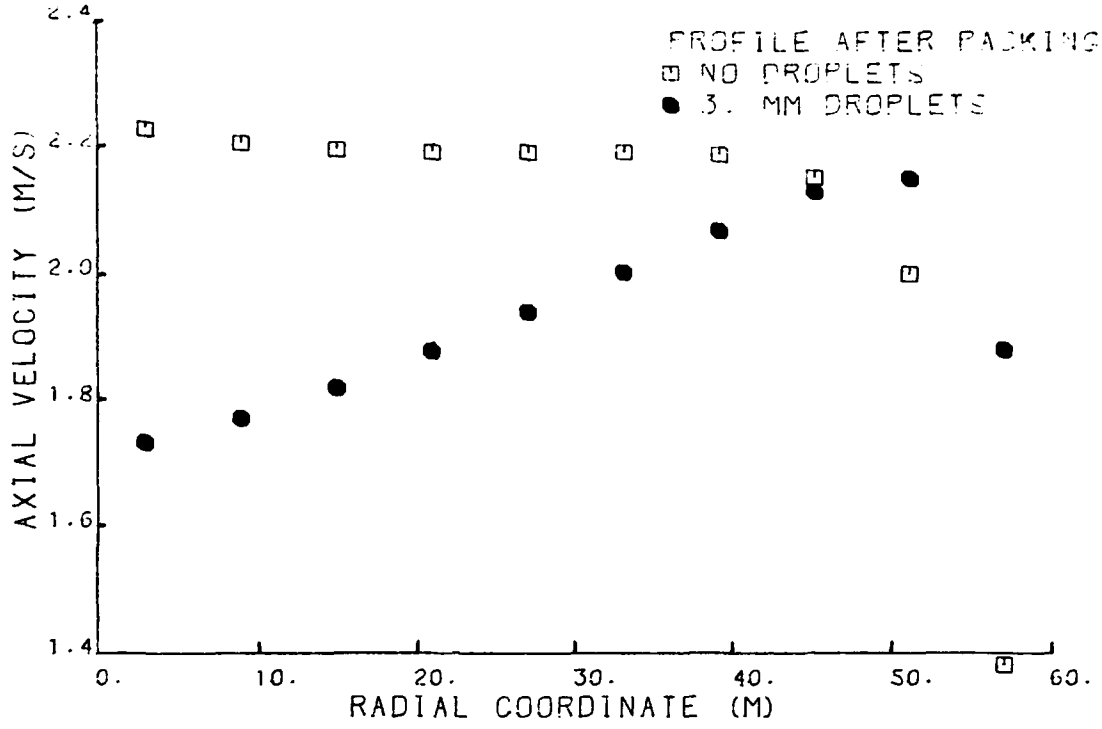

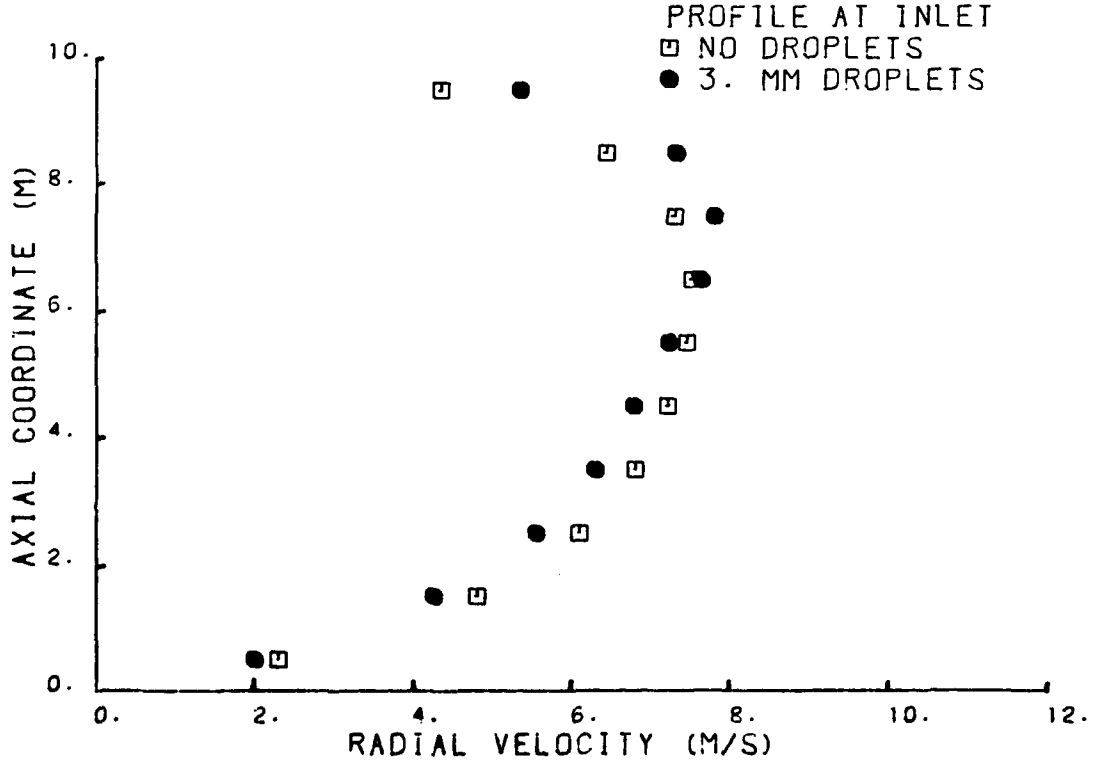

FIGURE **4.3.10-** COMPARISON OF VELOCITY PROFILES AT INLET AND AFTER PACKING

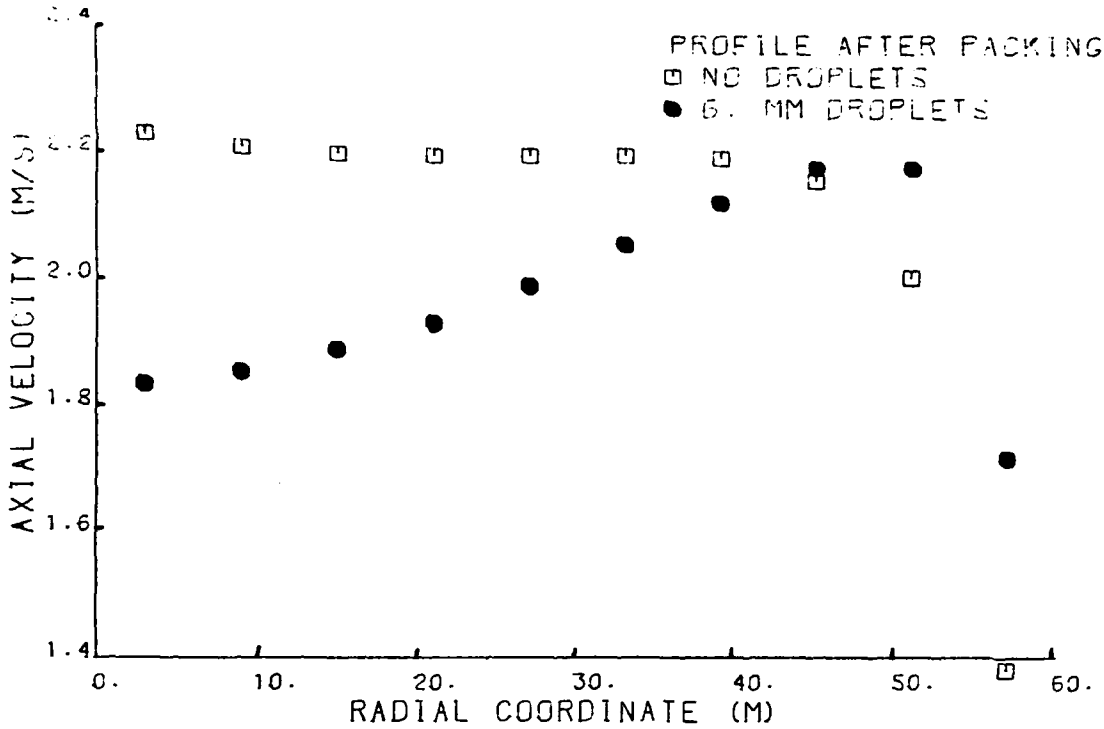

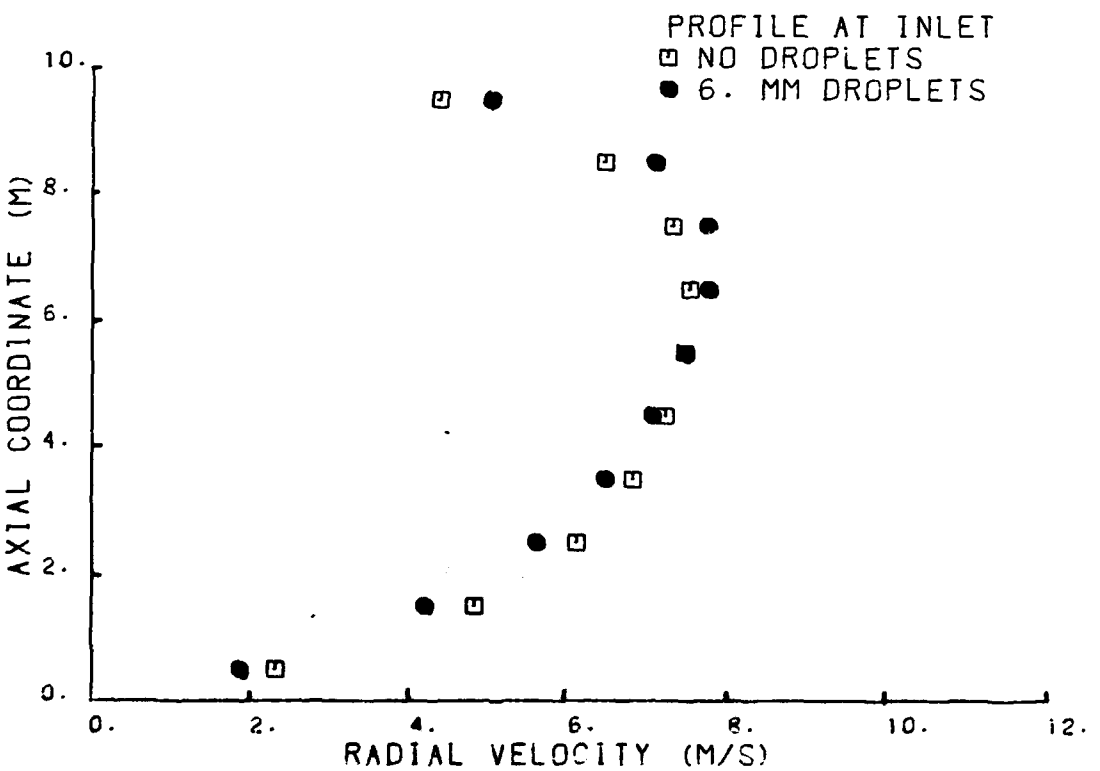

FIGURE 4.3.11 - COMPARISON OF VELOCITY PROFILES AT INLET AND AFTER PACKING

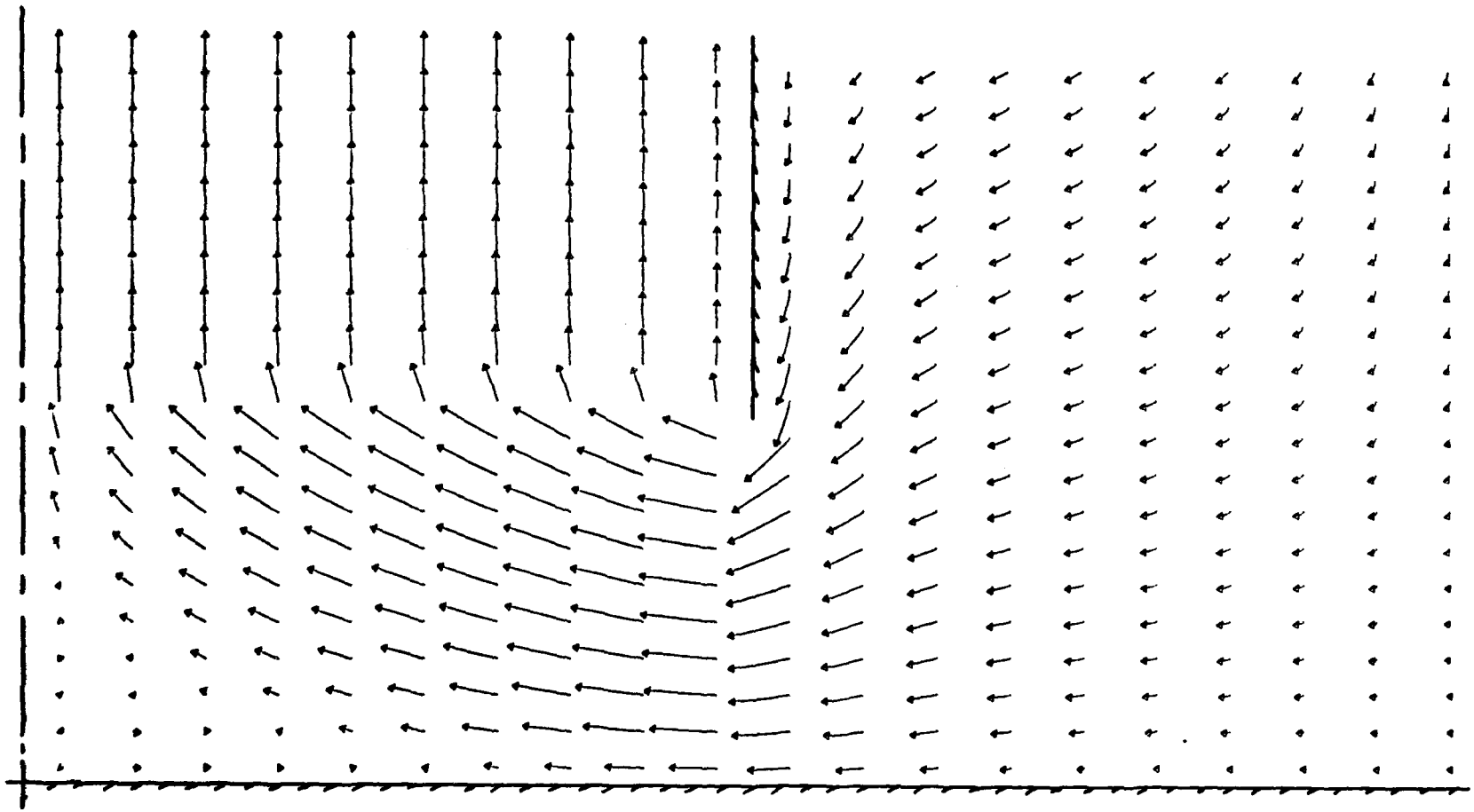

→ CORRESPONDS TO A GAS VELOCITY=3.00 M/S
TOWER RADIUS = 60. METERS HEIGHT OF INLET = 10. METERS
VERTICAL COORDINATE STRETCHED BY A FACTOR OF 3.
VOLUME FLOW OF AIR = 22619. M**3/S VOLUME FLOW OF WATER = 31.4 M**3/S
WITH PACKING - NO DROPLETS EFFECTIVE VISCOSITY DECREASED BY 10.

FIGURE **4.3.12**-FLOW FIELD IN A COOLING TOWER

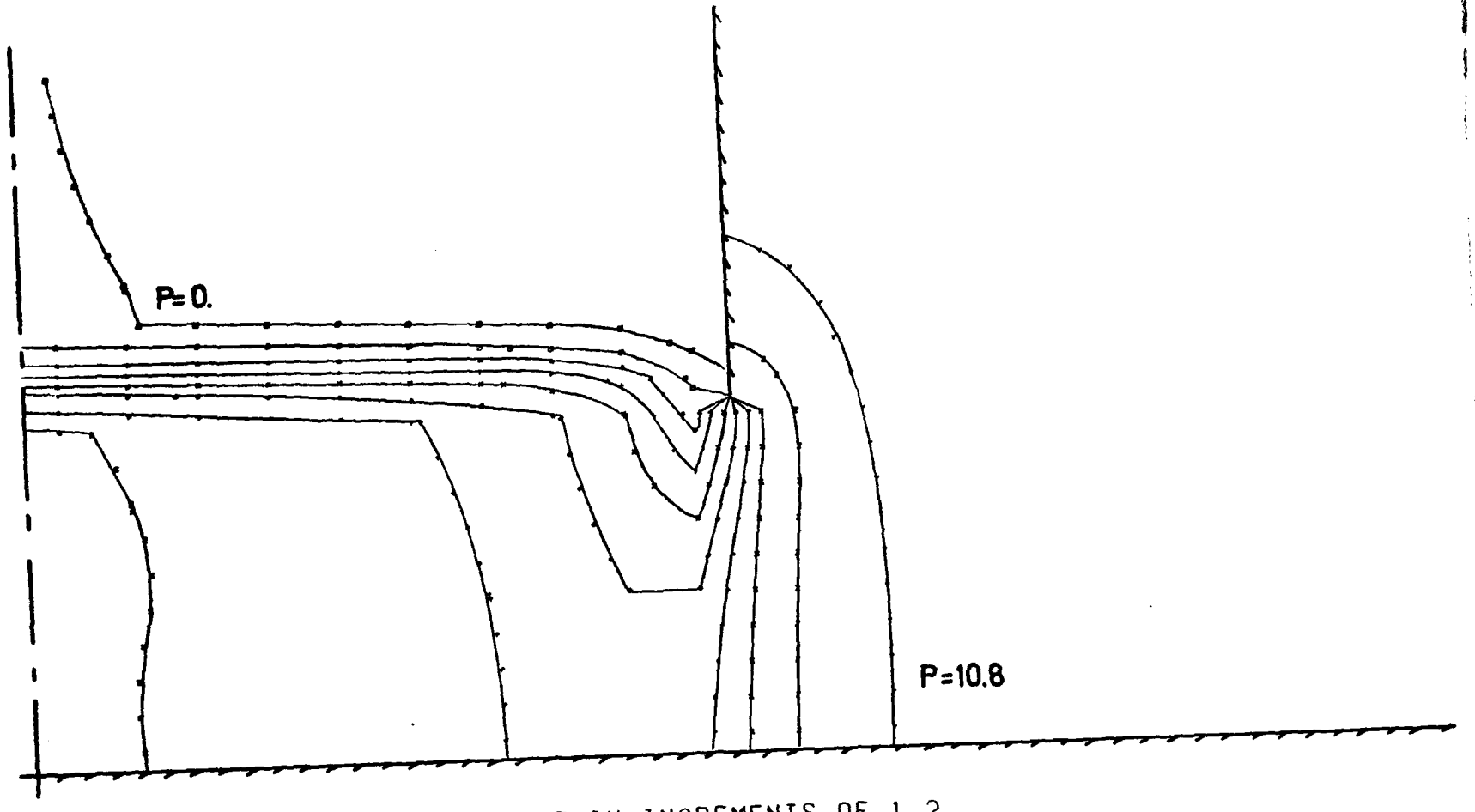

STATIC PRESSURE ISOBARS ARE IN INCREMENTS OF 1.2
VOLUME FLOW OF AIR = 22619. M**3/S VOLUME FLOW OF WATER = 31.4 M**3/S
WITH PACKING - NO DROPLETS EFFECTIVE VISCOSITY DECREASED BY 10.
VERTICAL COORDINATE STRETCHED BY A FACTOR OF 3.

FIGURE **4.3.13** - STATIC PRESSURE ISOBARS FOR FLOW THROUGH A COOLING TOWER

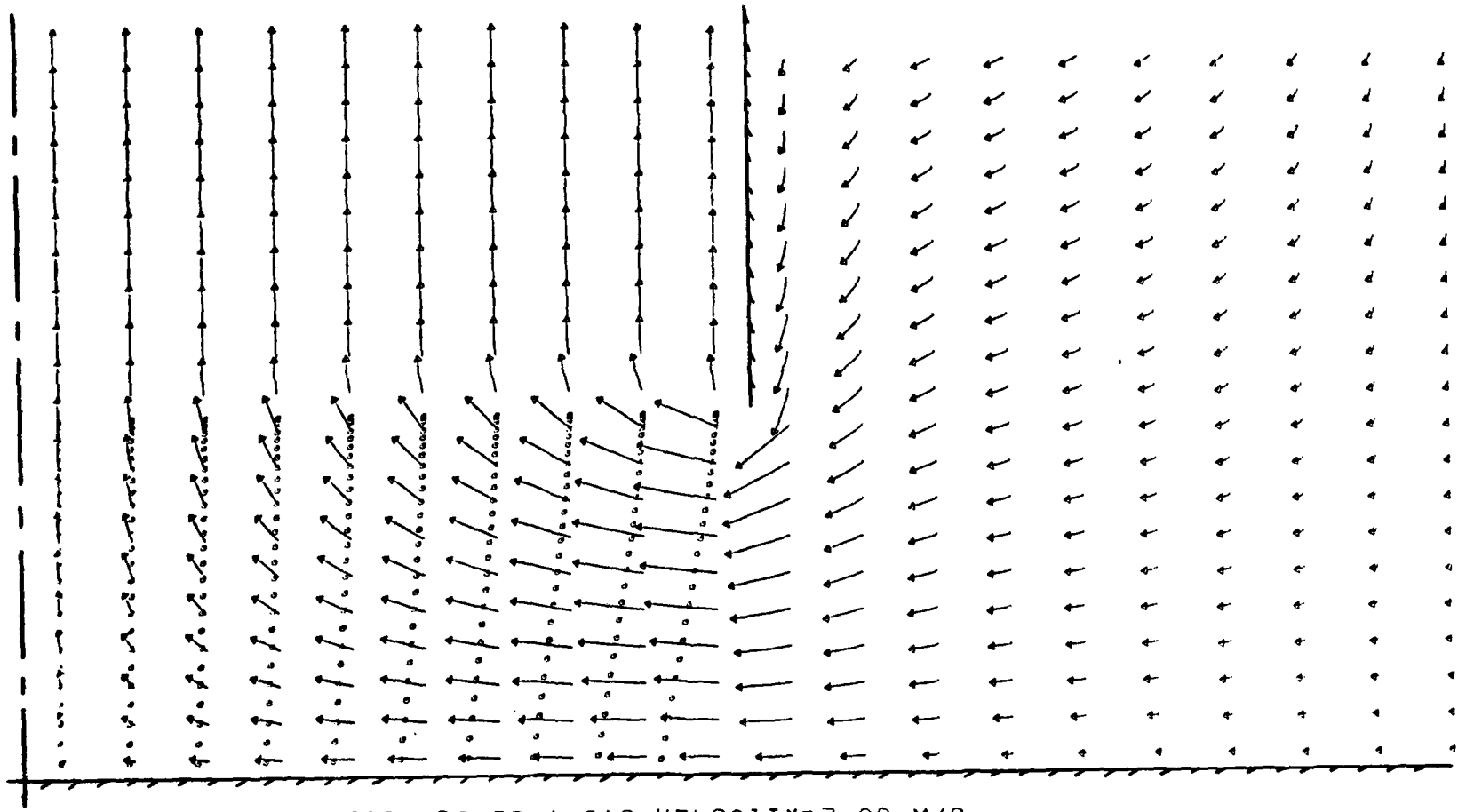

→ CORRESPONDS TO A GAS VELOCITY=3.00 M/S
TOWER RADIUS = 60. METERS HEIGHT OF INLET = 10. METERS
VERTICAL COORDINATE STRETCHED BY A FACTOR OF 3.
VOLUME FLOW OF AIR = 22619. M**3/S VOLUME FLOW OF WATER = 31.4 M**3/S
WITH PACKING + DROPLETS (D= 4. MM) EFFECTIVE VISCOSITY DECREASED BY 10

FIGURE 4.3.14 -FLOW FIELD IN A COOLING TOWER

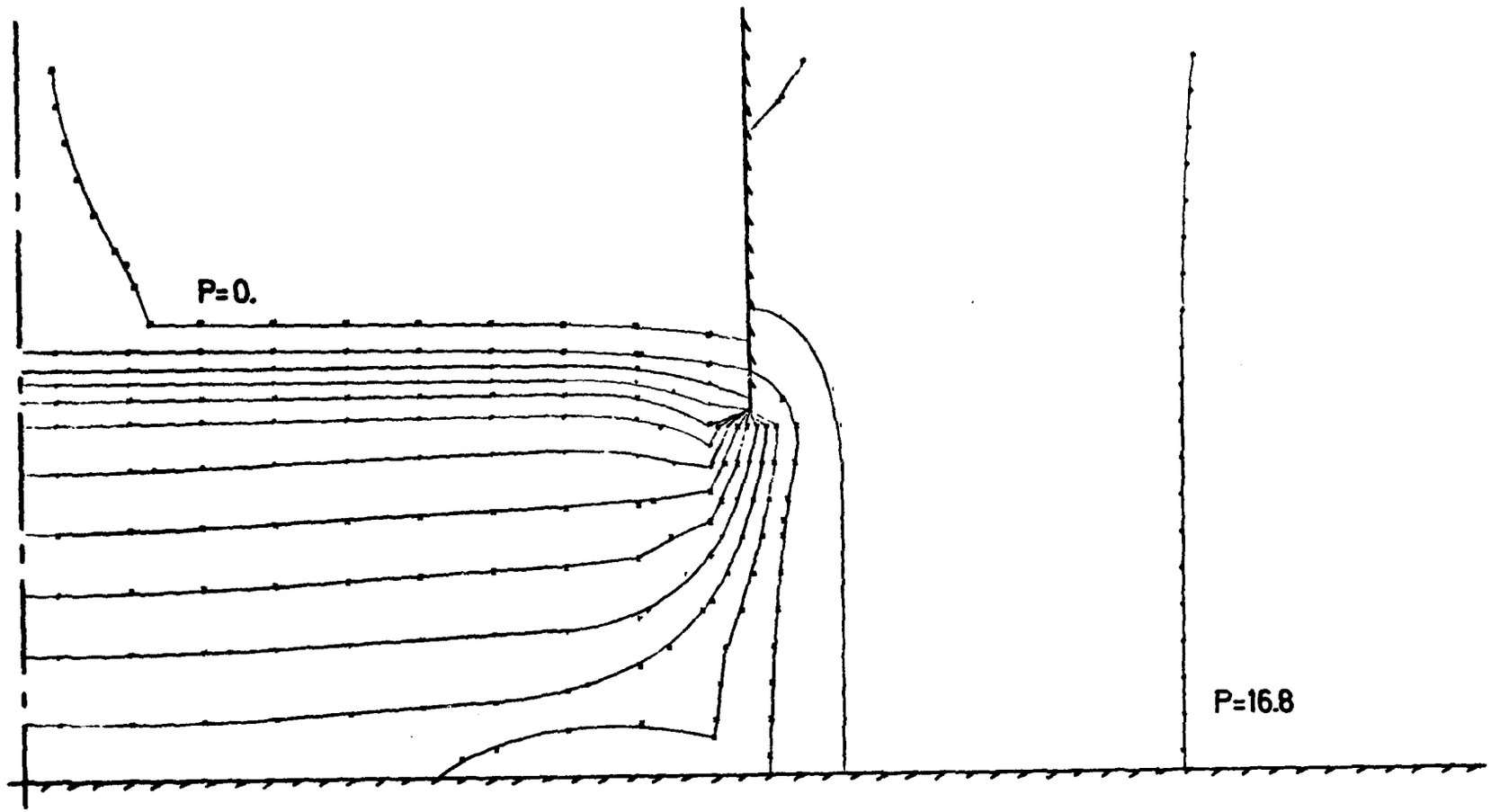

STATIC PRESSURE ISOBARS ARE IN INCREMENTS OF 1.2
VOLUME FLOW OF AIR = 22619. M**3/S VOLUME FLOW OF WATER = 31.4 M**3/S
WITH PACKING + DROPLETS (D= 4. MM) EFFECTIVE VISCOSITY DECREASED BY 10
VERTICAL COORDINATE STRETCHED BY A FACTOR OF 3.

FIGURE **4.3.15**-STATIC PRESSURE ISOBARS FOR FLOW THROUGH A COOLING TOWER

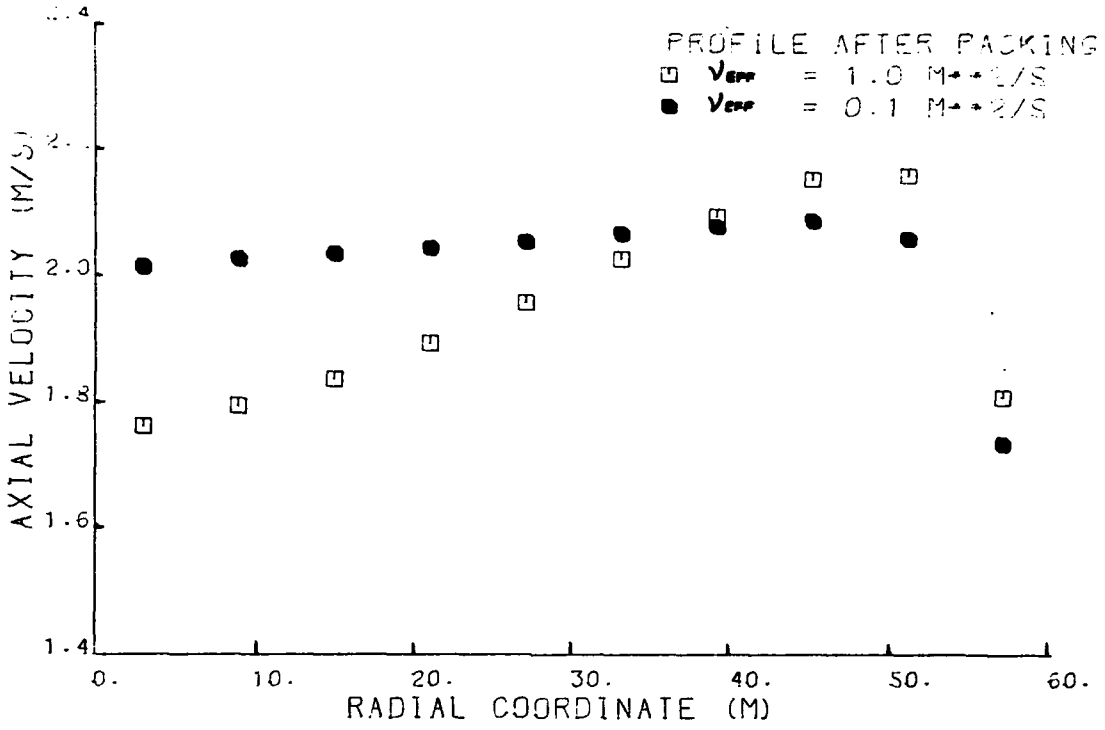

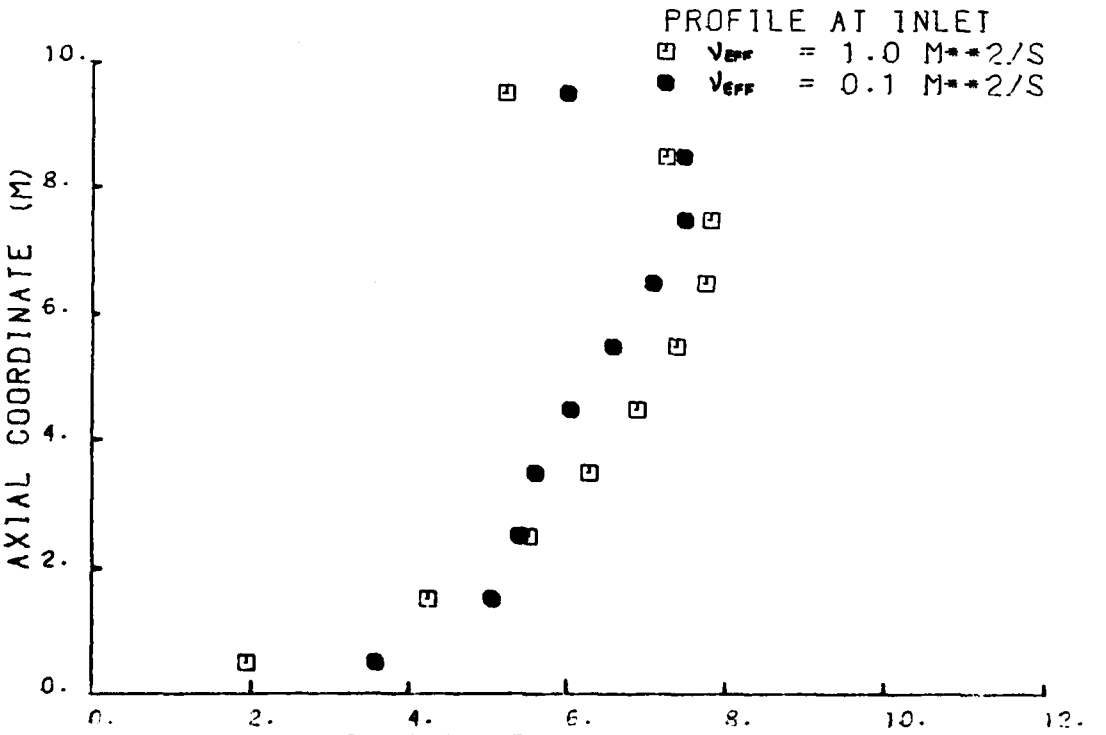

FIGURE 4.3.16. COMPARISON OF VELOCITY PROFILES AT INLET AND AFTER PACKING

END

DATE
FILMED

5 83

DTIC